PALACKY UNIVERSITY
FACULTY OF MEDICINE AND DENTISTRY
Doctoral program: Pediatrics

Nucleolar structure and the role of BYSL protein in ribosomopathies

Zuzana Macečková, M.Sc.

DISSERTATION THESIS

Olomouc, 2022

Statement:

I declare that this thesis has been written solely by myself and that all the relevant resources are cited and included in the references part. The research was carried out at the Laboratory of Experimental Medicine, Institute of Molecular and Translational Medicine, Faculty of Medicine and Dentistry, Palacky University in Olomouc and in cooperation with the University Hospital in Olomouc and other participating institutions.

Acknowledgment:

I would like to express my gratitude to all my colleagues, especially my supervisor associate professor Marián Hajdúch, M.D. Ph.D. for advice and support,Prof. Dagmar Pospíšilová M.D., Ph. D. who introduced me to clinical aspects of DBA, as well as Agáta Kubíčková, without whom my thesis would not be possible. I am also grateful to all my friends, especially Alena Kadlecová and Bára Klimovičová, who stood by me the whole time and of course to my family, which supported me unconditionally during my studies.

This work was supported by the following grants: Czech Ministry of Health (AZV16-32105A), Czech Ministry of Education, Youth and Sports (8F20005, EATRIS-CZ LM2018133, ACGT-CZ.02.1.01/0.0/0.0/16_026/0008448), Technological Agency of the Czech Republic (PerMed TACR TN 01000013), and Palacky University Olomouc (IGA UP LF_2021_019, IGA UP LF_ 2021_038, and IGA_LF_2021_004).

August 30, 2022 Zuzana Macečková, M.Sc.

Bibliographical identification:

Author´s name and surname: Zuzana Macečková

Title: Nucleolar structure and the role of BYSL protein in ribosomopathies

Type of thesis: Dissertation

Department: Laboratory of Experimental Medicine, Institute of Molecular and Translational Medicine, Faculty of Medicine and Dentistry, Palacky University Olomouc

Supervisor: Marian Hajduch, M.D., Ph.D.

The year of defense: 2022

Keywords: ribosomal stress, nucleolus, *Bystin*, glucocorticosteroids

Number of pages: 62

Language: English

Bibliografická identifikace:

Jméno a příjmení autora: Zuzana Macečková

Název práce: Struktura jadérka a role proteinu BYSL u ribosomopatií.

Typ práce: Dizertační

Pracoviště: Laboratoř experimentální medicíny, Ústav molekulární a translační medicíny, Lékařská fakulta Univerzity Palackého v Olomouci

Vedoucí práce: Doc. MUDr. Marián Hajdúch, Ph.D.

Rok obhajoby práce: 2022

Klíčová slova: ribozomální stres, jadérko, *Bystin*, glucocrticosteroidy

Počet stran: 62

Jazyk: Anglický

Abstract:

In this work, we focused on the role of the nucleolus in the cell. We explored its structure, nucleolar stress induction, and its effects. Furthermore, we have explored molecular pathogenesis of Diamond-Blackfan anemia (DBA), which is congenital anemia originating in ribosomal proteins aberration, and it is usually treated by glucocorticosteroids.

The first aspect of this study was to estimate the impact of oxaliplatin (L-OHP) and RPS7 mutation on the structure of nucleoli. We revealed that nucleoli structure is an essential factor in ribosomal stress and can be used for its evaluation. Next, we focused on the role of nucleoli structure protein BYSL (encoded by *Bystin* gene) in the DBA phenotype. We employed biochemical, molecular biology and *in silico* modelling methods and observed the details of BYSL behaviour and interaction with the other proteins and investigated bystin targeting by small molecules. In summary, we have identified *bystin* as the first disease-modifying gene in DBA. Mutation of *bystin* gene improves DBA phenotype and thus it is interesting molecular target. Furthermore, we determined that bystin improves DBA pathology through c-Myc regulation via direct interaction. We also proved that bystin is targeted by routinely used glucocorticosteroid therapy in DBA. This finding may lead to development of novel class of DBA therapies in future.

Abstrakt:

V této práci jsme se zaměřili na roli jadérka v buňce. Zkoumali jsme jeho strukturu, indukci nukleárního stresu a jeho účinky. Dále jsme se zabývali DBA, což je vrozená anémie mající původ v aberacích ribozomálních proteinů a jejíž léčba je většinou založena na kortikosteroidech.

Prvním aspektem této studie bylo popsání vlivu L-OHP a mutace v RPS7 proteinu na strukturu jadérek. Zjistili jsme, že struktura jadérek je důležitým faktorem ribozomálního stresu a může být použita pro jeho hodnocení. Dále jsme se zaměřili na roli strukturního proteinu jadérka BYSL (kódovaným genem *Bystin*) na fenotyp DBA. Identifikovali jsme *bystin* jako první možný gen modifikující onemocnění DBA. Dále jsme zjistili, že bystin řídí patologii DBA prostřednictvím regulace c-Mycu skrze přímou interakci. Dále jsme prokázali, že bystin je molekulárním cílem terapie DBA glukokortikoidy. Toto zjištění může vést k vývoji nové terapie pro DBA pacienty bez závažných vedlejších účinků glukokortikoidů.

Table of contents

1 Introduction

1.1 Nucleolus

The nucleolus is the largest membrane-free structure in the nucleus. Initially, it was thought that the nucleolus is mainly the space, where ribosome biogenesis occurs, but the increasing evidence points to the nucleolus as the main component in various cellular processes. Although control of ribosome production seems to be the most important because this step regulates overall cellular protein production, which is mandatory for cell growth and proliferation [1], other roles of nucleolus have come into the spotlight recently. Among others, the nucleolus plays an important part in metabolic maintenance, oncogene regulation, and cell cycle progression [2]. Furthermore, its emerging role in cellular stress detection and response is undeniable [3].

1.1.1 Nucleolar structure

The nucleolus is mainly composed of structural proteins and factors required for ribosomal RNA (rRNA) maturation and ribosomes production [4].

The nucleolus is organized around so-called NORs (nucleolus organizer region). NORs can be found on short arms of acentric chromosomes, specifically chromosomes 13, 14, 15, 21, and 22. Each NOR contains a highly repetitive DNA sequence encoding rRNA [5]. Three out of four mammalian rRNA are expressed in NORs by RNA polymerase I as one 47S RNA precursor, which needs to be cleaved to 18S, 5.8S, and 28S rRNA [6], while fourth rRNA – 5S rRNA is expressed in the nucleolus by RNA polymerase III [7].

We can distinguish three structural features of the nucleolus. At the nucleolar centre, there are round fibrillar centres (FC), each FC is tightly surrounded by a dense fibrillary centre (DFC), and both FC and DFC are enveloped by granular components (Gc) (Fig.1) [2]. The structures of the nucleolus reflects ribosome biogenesis. At FC, there are DNA encoding rRNAs and elements necessary for DNA transcription, mainly RNA polymerase I, DNA topoisomerases, upstream binding factors, and other components of transcriptional machinery [8]. The ribosomal RNA transcription occurs on FC/DFC borders in the form of 47S rRNA, and rRNA is further processed in DFC. Therefore, DFC contains mostly factors necessary for rRNA modification, specifically fibrillarin, which is the main element of small ribonucleoprotein particles involved in rRNA primary modifications (snoRNA) [9]. GC occupy the largest area of

the nucleolus. In the GC area, rRNA is maturated and interacts with ribosomal proteins and other factors to assemble almost mature ribosomes [10].

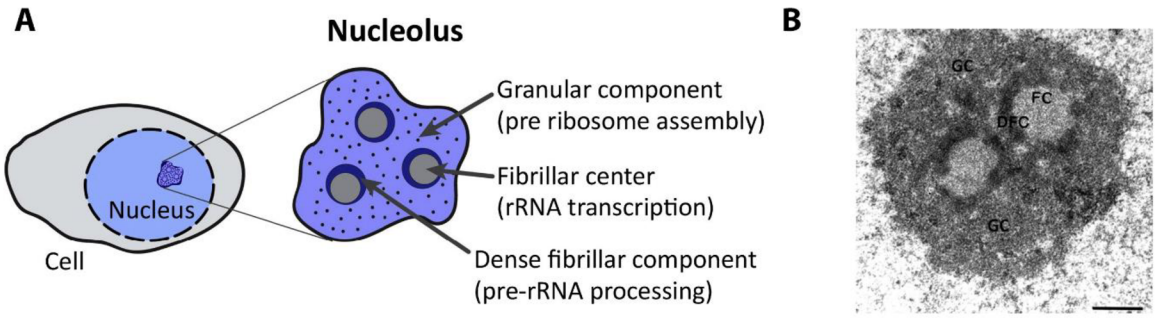

Figure 1: Nucleolus structure: A) nucleoli structure scheme (adopted from [2]), B) structure of nucleolus in electron microscope (adopted from [11]).

Furthermore, nucleoli structure is not rigid, and its size and structure reflect proliferative and metabolic state of the cell. More specifically, cells that require swift protein production for their rapid proliferation, like embryonic or cancer cells, produce a higher amount of rRNA and ribosomes, and therefore, overall nucleoli size is increased. In contrast, old or senescent cells reduce their ribosome requirement, thus decreasing their nucleolar size and metabolic activity [2]. Moreover, nucleoli size can also be affected by physiological changes or congenital disorders [3].

1.1.2 Nucleolus function

Ribosomes are multi-molecular complexes responsible for translation of the DNA code into functional proteins. The main function of the nucleolus is ribosomes production. The ribosomes translate mRNA to proteins and play an irreplaceable role in all living cells. In recent years, it has become clear that the nucleolus also plays a unique role in multiple cellular processes – from mitosis regulation to stress response and uncoupling of ribosomal function from other cellular processes may lead to multiple human pathologies.

1.1.2.1 Ribosome production

Ribosome biogenesis is a complex and highly coordinated process in which many proteins and other factors participate. Every human ribosome (the 80S) composes of two subunits – a small ribosomal subunit (40S) and a large ribosomal subunit (60S). Each subunit contains rRNA), which creates ribosome backbone and appropriate space for ribosomal protein annealing on

given rRNA. The large subunit consists of three rRNA (5S,28S, and 5,8S) and 46 RPs, whereas the small subunit contains only one rRNA (18S) and 33 RPs [12].

Ribosome biogenesis begins by transcription of 47S rRNA by DNA polymerase I. This transcript contains rRNA for both large and small ribosome subunits divided by internal transcribed spacers ITS1 and ITS2 and flanking regions EST1 and ETS2. During biogenesis, rRNA is folded around ribosomal proteins, cut (Fig. 2) and modified by many factors to assemble 90S pre-ribosome within the early biogenesis process. Cleavage of ITS1 between sequences of pre-18S and 5.8S rRNA leads to decay of 90S ribosome into two parts, pre-40S and the pre-60S ribosome.

At this stage, the 40S ribosome is almost completed. Just minor adjustments like 18S rRNA cleavage or beak formation are further required to achieve a full maturation state. However, the development of the 60S ribosome requires a wide range of further modifications before it matures. The most important is the connection of the pre-60S ribosome with the 5S ribonucleoprotein (5S RNP). Unlike other rRNAs, 5S rRNA is transcribed in the nucleolus by polymerase III. Subsequently, it is associated with RPL11 and RPL5 ribosomal proteins and forms 5SRNP. This complex functions as the main stress sensor, if not incorporated into the ribosome. After 5SRNP incorporation to pre-60S ribosome, mature 60S ribosome is translocated to the cytoplasm.

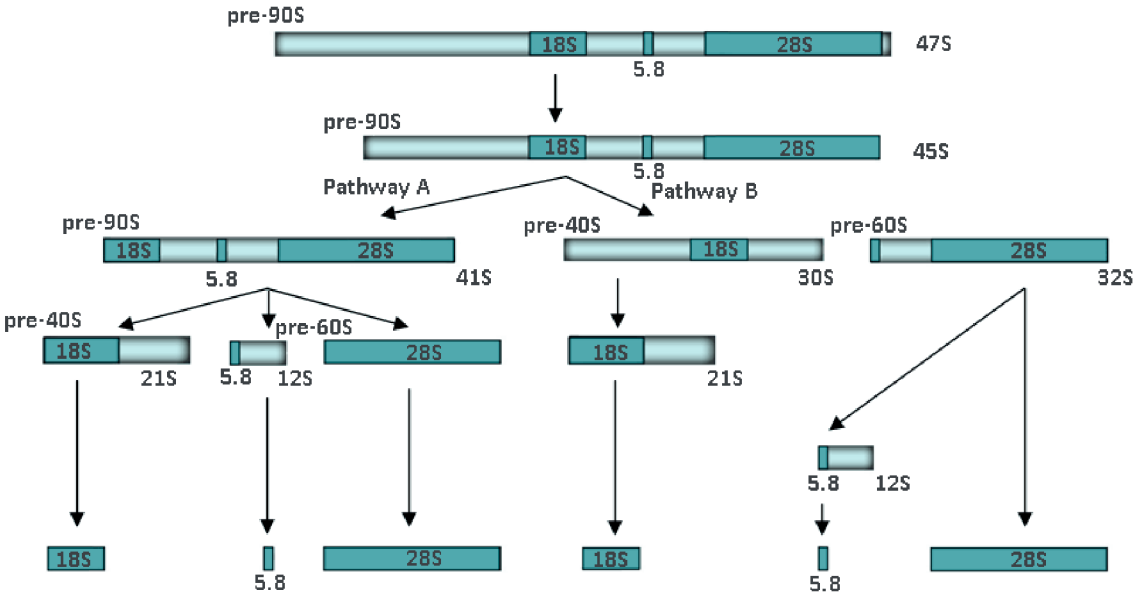

Figure. 2: Scheme of rRNA processing

1.1.2.2 The additional functions of the nucleolus

Ribosome production is an undeniable primary function of the nucleolus. Nevertheless, around 70% of proteins found in nucleolus do not participate in ribosome biogenesis [13]. Increasing evidence suggests nucleolus a key organell determining the cell fate. It was shown that the nucleolus regulates mitosis, cell cycle, or cellular metabolism. Although these roles of the nucleolus are important, they were not the main aim of this work, and comprehensive literature about extraribosomal functions of nucleoli can be found elsewhere [14-16]. The only function of the ribosome, which we have investigated more closely, was the nucleolus's role during cellular stress.

1.2 Ribosomal stress

Ribosomal biogenesis is essential for cell survival and proliferation. Not surprisingly, this process is energetically demanding and may consume substantial proportion of cellular energy reservoir. Correct ribosome assembly and function are strictly controlled, and any disruption in this orchestrated process can lead to so-called ribosomal and/or nucleolar stress.

1.2.1 Ribosomal stress induction

External or internal cellular conditions can induce ribosomal stress, which arises in fact from ribosome biogenesis impairment. This impairment can happen on several levels. More specifically, the ribosomal stress pathway is activated if aberration in the following processes occurs: rRNA transcription, rRNA maturation, and pre-ribosomal assembly. Furthermore, ribosomal stress can also be induced extrinsically by various nonspecific insults like UV light, hypoxia, heat shock, nucleotide depletion, and various chemotherapeutic agents [17]. Comprehensive reviews on this topic can be found elsewhere [3, 18, 19]. In this dissertation thesis, we will focus on impairment in pre-ribosomal assembly, usually caused by RP-rRNA imbalance. A typical example of such pathology is Diamon Blackfan anemia caused by an aberration, usually mutation, in RPs.

The degree of nucleolus damage can be naturally detected in nucleolar structure (Fig. 3). Depending on the stress inducer, we can distinguish two main types of nucleolar morphology aberration: nucleolar segregation vs nucleolar disruption.

Nucleolar segregation is usually characterized as the condensation and subsequent separation of the FC and Gc, together with the formation of nucleolar caps [20]. Nucleolar segregation is

caused by rDNA damage or impairment of rRNA transcription and can be caused by chemotherapy, typically actinomycin D, targeting rRNA transcription and/or early steps of RNA processing [21].

Nucleolar disruption can accompany nucleolar segregation, which means nucleolar proteins are released to the nucleoplasm. Nucleolar disruption results in homologous staining of the nucleus with nucleolar protein antibodies. Furthermore, different proteins behave differently during ribosomal stress. For example, fibrillarin forms nucleolar cups after actinomycin D treatment, while nucleophosmin is released to the nucleoplasm [22].

Interestingly, some insults can have only a minor impact on the nucleolar structure. Typically, the aberration of ribosomal protein leads to the accumulation of rRNA in the nucleolus and only a slight change in nucleolar morphology [23]. Nevertheless, any aberration in nucleolar structure impacts cellular well-being and the ability to generate fully-functional maturated ribosomes.

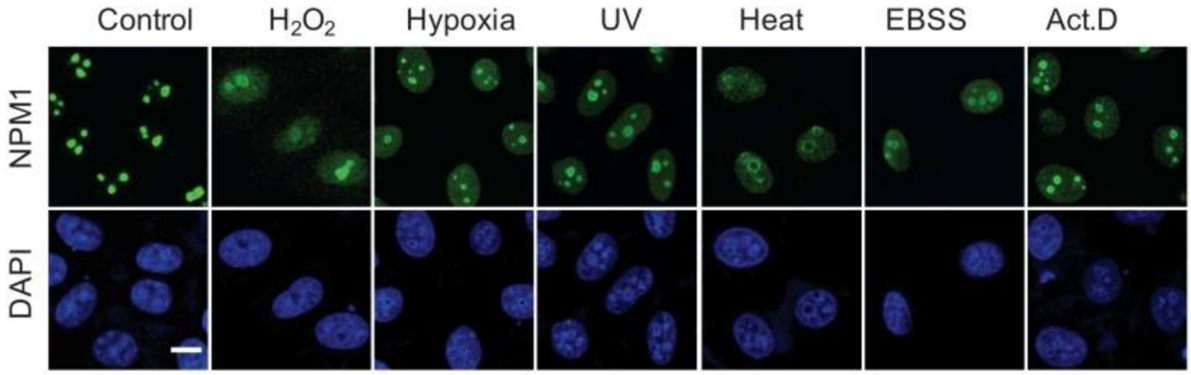

Figure. 3: Nucleoli structure: Malformation in nucleoli structure after various stimuli (adopted from [3])

1.2.2 p53 dependent ribosomal stress

The tumor suppressor p53 plays a key role in numerous stress signal pathways. Depending on stimuli, p53 activation determines cells to different fates – from cell cycle arrest to apoptosis. The key regulator of the p53 level is ubiquitin ligase MDM2. In the normal state, MDM2 binds to p53 and marks it for degradation by the proteasome. Various proteins can bind to MDM2 under stress conditions and modify its binding capacity to p53.

RPs are one class of MDM2 interacting proteins. The first MDM2 interacting RP reported was RPL5 [24], followed by many others. Over the years, an increasing amount of evidence

suggested that the main players in the ribosomal stress-dependent activation of p53 are RPL5 and RPL11 [25] (Fig. 4).

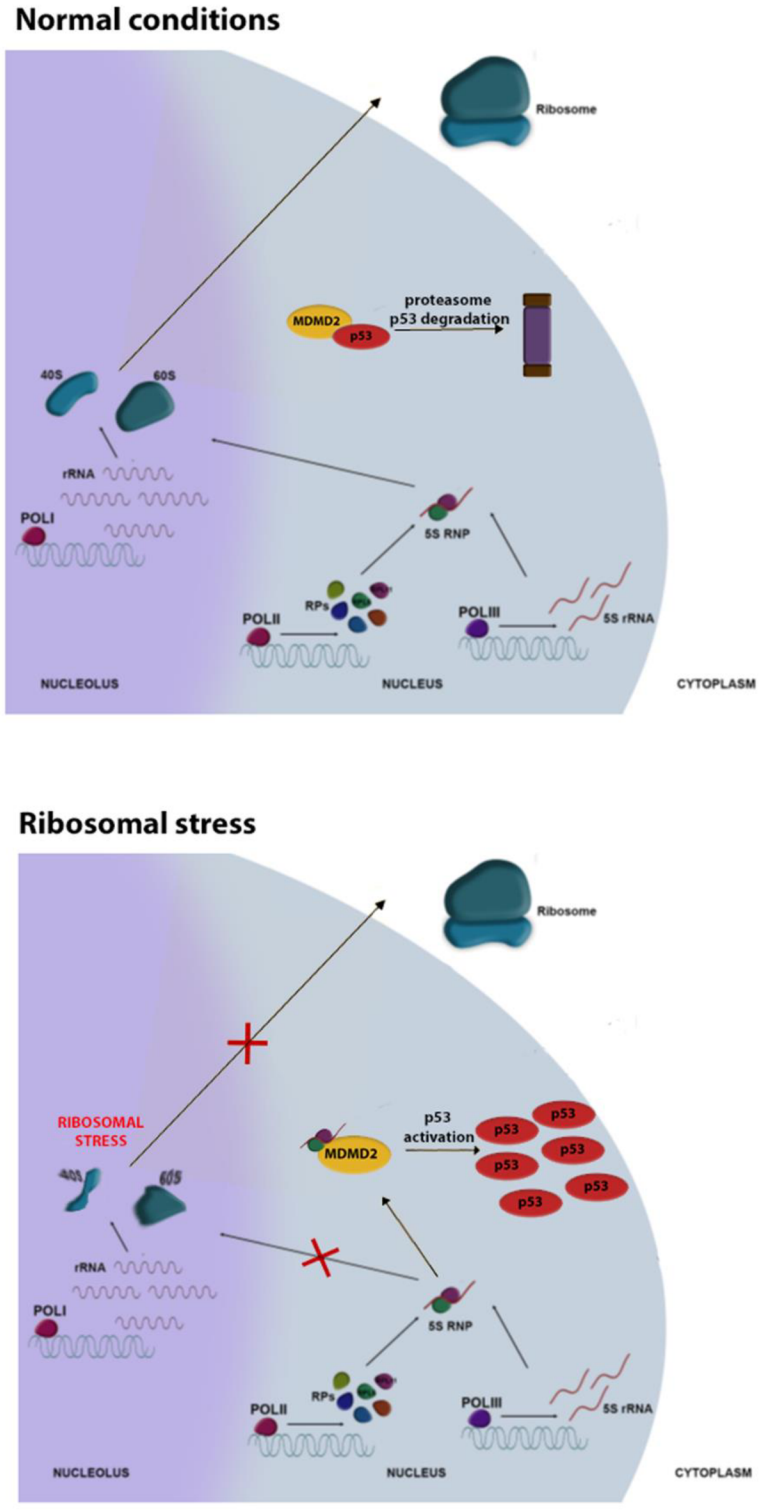

Figure. 4: Scheme of p53 activation during ribosomal stress.

The reason is obvious, the RPs are released from the nucleolus upon its disruption and can activate various stress response pathways. Fortunately, majority of free RPs are rapidly degraded via the ubiquitin-proteasome system and this mechanism is largely supressing their stress inducing capacity [26]. However, unlike other RPs, RPL5 and RPL11 form a stable complex with 5S rRNA – 5S ribonucleoprotein (5S RNP), which protects them from degradation and allows them to execute ribosomal stress sensor functions [25]. Moreover, 5S RNP binding to ribosome and MDM2 is mutually exclusive [27]. This highlights 5S RNP's role in ribosomal stress signalling. Extensive study by Nicolas et al. [23] showed that although numerous RPs bind to MDM2, only a small portion can activate p53. Furthermore, none of the p53 activating RPs can activate p53 upon simultaneous depletion of RPL5 or RPL11. This finding further supports the irreplaceable role of these two ribosomal proteins in p53 stabilization when translation machinery is altered.

Apart from p53-mediated ribosomal stress, nucleolus can respond to stress also by p53-independent pathways. Some of these mechanisms will be discussed later. More detailed description of p53-independent ribosomal stress induction can also be found elsewhere [28].

1.3 RP functions beyond building ribosomes

RPs are the main structural components of ribosomes and create a significant part of nucleolus content. Most RPs are rapidly degraded if not incorporated in the ribosome, but some have additional roles. Herein we summarise some of the most important roles of free RPs, except for p53 activation described above.

1.3.1 Oncogene regulation

Oncoprotein c-Myc is a crucial transcriptional factor promoting cell survival and proliferation [29]. c-Myc induces transcription of almost all components of translational machinery. It is involved in the translation of ribosomal proteins, proteins participating in rRNA synthesis, and some translational factors [30]. The Main RP regulators of c-Myc activity are RPL5, RPL11, and RPS14 [31, 32] (Fig. 5). All three interact with c-Myc mRNA and recruit the RISC complex, which is responsible for miRNA-mediated mRNA decay. Through this mechanism, free RPs prevent uncontrolled cell proliferation and cell cycle progression in a p53-independent manner. Moreover, RPL11 and RPS14 can inhibit c-Myc transcriptional activity

via direct interaction. Both proteins bind to c-Myc protein and block the motive essential for c-Myc coactivator TRRAP binding, which is necessary for c-Myc and DNA interaction [32]. All these findings were also validated in mouse models. RPL11 deficient mice lost p53-dependent responses to ribosomal stress and exhibited increased c-Myc protein expression, which promoted lymphomagenesis [33].

Apart from c-Myc, RPs are also involved in NF-kB signalling. RPS3 was identified as a component of the NF-kB complex required for its enhanced DNA binding [34]. Knockdown of RPS3 resulted in decreased NF-kB activity. RPS27 is another modulator of NF-kB activity. Its repression inhibited NF-kB function, suppressed cell migration and invasion and promoted apoptosis [35]. On the other hand, the knockdown of RPL22 stimulated NF-kB and accelerated transformation [36].

Transcriptional factor E2F can act both as an oncogene and tumor suppressor. Association with MDM2 stabilizes E2F. As mentioned above, during ribosomal stress free RPL11 binds to MDM2 and induces p53 activation. Apart from that, RPL11-MDM2 interaction competes with MDM2-E2F association and thus determines its kinetics of proteasomal degradation [37]. Decreased level of E2F results in G1 cell cycle arrest.

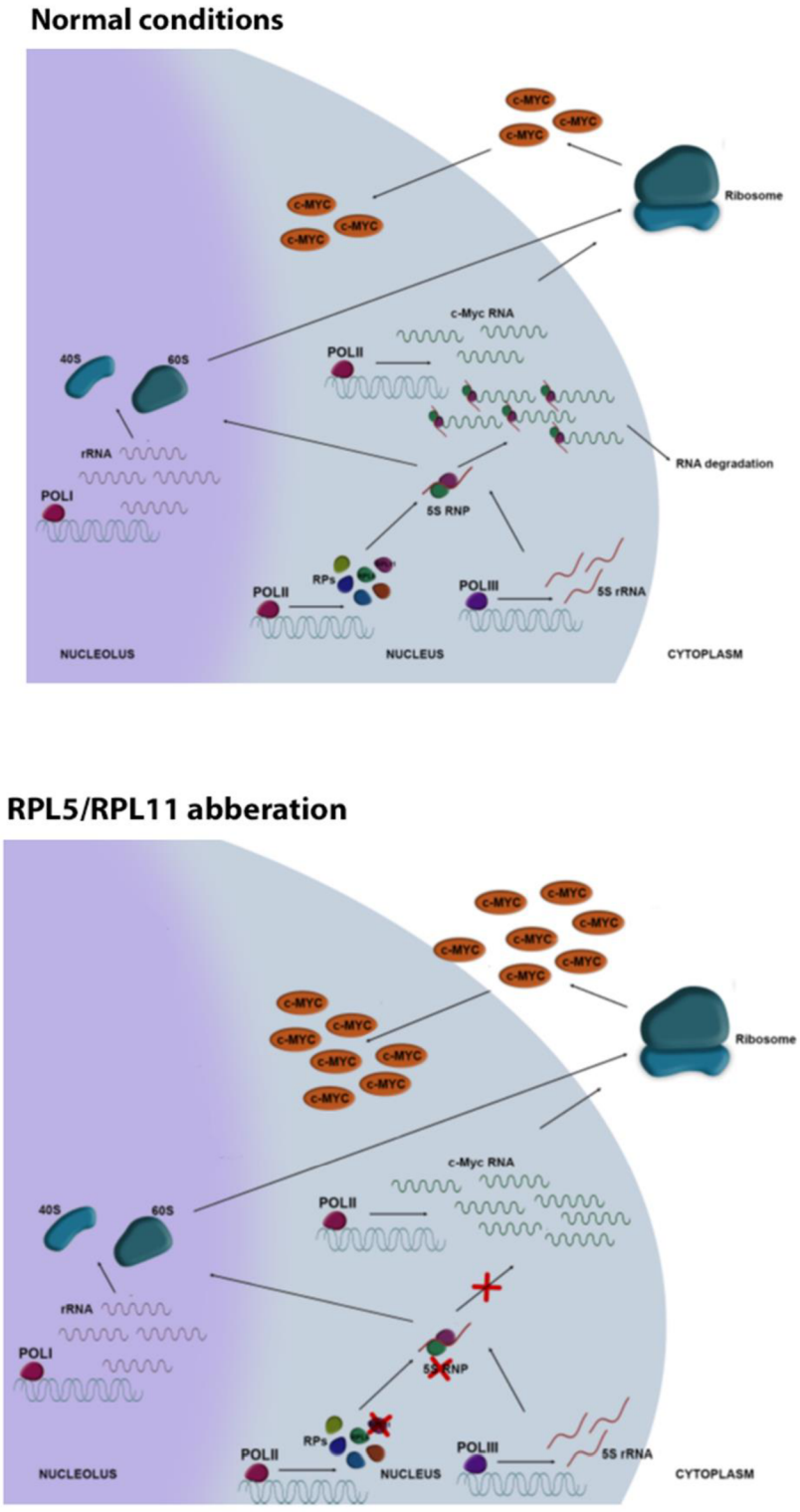

Figure 5: Activation of c-Myc upon RPL15/RPL11 aberration.

1.3.2 *Tumor suppressor regulation*

PIM1 is a constitutively active serotonin/threonine-protein kinase regulating survival, cell cycle, and proliferation, especially in hematopoietic cells. PIM1 is stabilized by interaction with RPS19 and binding to ribosomes [38]. Lack of available ribosomes results in decreased PIM1, consequently PIM1 dependent stabilization of CDK inhibitor p27, and G1 cell cycle arrest. Moreover, PIM1 also induces the increased activity of c-Myc by its phosphorylation. Decreased PIM1 reduce the activity of c-Myc and cellular proliferation [39].

p21 is a well-known p53-dependent cell cycle inhibitor. Apart from p53, the expression of p21 can be regulated by the RPL3-NMP-Sp1 complex [40]. RPL3 released from nucleolus or damaged ribosome initiates the formation of this complex and induces p53-independent expression of p21.

1.3.3 *RP in cancer*

RPs can act both as tumor suppressors and as oncogenes. RPs impairment is common in multiple types of cancer [41]. Common characteristics of cancers are rapid proliferation and relative resistance to cell-death mechanisms. Cancer cells need a tremendous amount of newly synthesized proteins for this purpose. This is consistent with the increased expression of many RPs in cancers. A complete overview of the upregulation of RP in cancers can be found elsewhere [42, 43].

Surprisingly, mutations and deletions of RPs have also been detected in several cancers. Notably, some deletions are identical to DBA patients [41]. Interestingly, cancer cells are willing to jeopardize effective translation to activate c-Myc signalling and deregulate 5SRNP dependent activation of p53 to escape several cancer checkpoints controls.

1.3.4 *RPs tissue-specific functions, specialized ribosomes*

Cells live in changing environments; therefore, they need to adapt rapid to internal and external conditions. Over the years, several mechanisms were described to regulate adaptation process - from DNA methylation through splicing and expression pattern changes to miRNA silencing. Recent studies suggest yet another mechanism involving the structure of ribosomes [44]. It seems that cells can create different types of ribosomes as a response to stress conditions.

Evidence has been given that specific RPs are responsible for translating a specific set of RNAs. For example, depletion of RPL38 results in skeletal development malformations [45]. Interestingly, RPL38 deficient mice did not manifest any other abnormalities apart from defects in the skeleton. The altered translation of Hox genes explained this defect. Similarly, deregulation of RPSA results in missing spleen in humans, but no other phenotype has been observed [46]. Furthermore, the absence of RPL22 and its homolog RPL22L is not lethal for cells or animals [47]. It was also shown that the depletion of these genes causes distinct phenotypes. Depletion of RPL22 results in T-cells development deficiency, while depletion of RPL22L leads to HSCs maturation impairment. Those results show that RPs homologs may have a distinct role in selecting translated mRNAs [47].

Surprisingly, yeast can create different ribosomes based on external conditions [48]. They showed that yeast in high-salt or high-pH environments creates ribosomes lacking RPS26 [48]. This type of ribosome preferably expresses mRNA with a mutation in their Kozak sequence, which usually encodes genes for stress response proteins. Unexpectedly, ribosomes lacking RPS26 are not the result of RPS26 down-regulation but RPS26 exclusion from mature ribosomes [48].

1.4 Ribosomal protein aberration in molecular pathology of diseases

Protein production is a fundamental process in cells. For this purpose, cells contain large and abundant quantity of ribosomes. Each ribosome consists of four rRNA and around 82 ribosomal proteins (RPs). Mature ribosomes require all components for proper function, and defects in rRNA or ribosomal protein(s) usually lead to instability and rapid ribosome degradation. Germinal defects in ribosome structure manifest as variety of phenotypes linked to individual ribosomopathy diseases. Interestingly, many congenital ribosomal protein aberrations are compatible with survival, one possible explanation is lethal mutations are eliminated in early embryonal development.

The most significant number of defective ribosomal proteins was associated with Diamond Blackfan anemia (DBA). DBA is usually diagnosed early after birth as severe macrocytic or normocytic anemia with reticulocytopenia, normal platelet and neutrophil counts, and deficiency of red blood cell precursors in bone marrow [49]. In approximately 35-50% of cases are, these symptoms accompanied by physical malformation, mainly of the craniofacial

region, upper limbs, and growth retardation [50]. Another clinical manifestation is the increased level of adenosine deaminase [51].

The first gene linked to DBA was RPS19 [52], and variants in RPS19 account for 25% of DBA cases [53]. Over the years, the number of RP genes associated with DBA has escalated, and to date, mutations in 16 RP genes of both large and small ribosomal subunits have been described [54]. Due to the rapid development of sequencing techniques, this number is expected to increase. But still, in up to 20-50% of cases, molecular disease pathology is unknown.

DBA phenotype is mainly attributed to RP haploinsufficiency, but several dominant-negative models of RP mutation have also been reported. RPS19 is the most extensively studied protein as a cause of DBA pathology. Interestingly, although none of the RPS19 mutated forms showed stability comparable with WT, there have been described two classes of point mutations in RPS19 – one induces protein instability and nucleus localization, and the other has a minor impact on stability and shows predominant nucleolus localization [55]. Notably, interactome analysis of R62W and R101H RPS19 mutants showed distinct binding capacities for numerous partner proteins. For example, both mutants but not WT have high binding capacity for BYSL [56]. The dominant-negative effect of several point mutations has been described on DBA animals' models. Introduction of mutated RPS19 mRNA to WT zebrafish background resulted in phenotype similar RPS19 depletion [57]. Furthermore, the introduction of mutated RPS19 mRNA to RPS19 depleted zebrafish background resulted in increased severity of phenotype [58]. Knock-in mice with RPS19 R62W also manifested developmental defects and harmed rRNA processing and erythropoiesis. All these studies indicate the dominant-negative effect of RPS19 mutants if located in selected domains of the protein [59].

Another interesting feature of DBA is incomplete penetrance and variable expressivity [60]. Commonly, family members sharing the same mutation manifest different severity of phenotype [61]. These observations point toward an important role of disease-modifying genes. However, until now, no such gene has been described.

To the same ribosome family, the biogenesis defect also belongs to the 5q- syndrome (5q-). 5q- originate in partial loss of the small arm of chromosome 5. The cause of the disease was traced to the depletion of RPS14 in the knock-down study [62]. Although 5q- is classified as a

separate disease, it shares a standard feature with DBA, reflecting a similar phenotype mechanism [63].

Another interesting example of RP imbalance disease is isolated congenital asplenia (ICA). Mutations in RPSA were recognized as a cause of ICA in genetic population studies [64]. Unlike DBA and 5q- MDS, the ICA does not present as anemia [63]. Patients diagnosed with ICA are born without a spleen, which puts them in danger of life threating infection, but they do not present any additional malformations.

Apart from RP disbalance, ribosomopathies can be also caused by other genetic alterations. A comprehensive review on this topic can be found elsewhere [63].

1.4.1 Possible causes of erythropoiesis failure in ribosomopathies

Since mutation in RPS19 has been pointed out as the cause of DBA, the link among ribosomal protein aberrations and anemia has been elusive. Our understanding of molecular mechanisms behind this phenomenon has been increasing over time, but the underlying mechanisms are still not fully understood. Here, we present possible mechanisms of how defective RPs may lead to specific blood phenotypes.

1.4.1.1 Uncoupling of transcription and translation

The common feature of ribosomopathies is decreased availability of ribosomes and, therefore, a decreased translational activity [65]. Diminished number of ribosomes can lead to an imbalance in between mRNA, which is supposed to be translated, and mRNA, which is being translated [66]. Indeed, it has been shown that the depletion of RPL11 or RPS19 causes a decrease in the translation of IRES-mediated transcripts compared to cap-dependent ones [66]. More specifically, the expression of several genes essential for erythropoiesis are driven by IRES. For example, Bag1 is crucial for red blood cell maturation. Bag1 knockdown mice die at E13.5 from absence of erythropoiesis [67]. Bag1 shows increased mRNA levels in RP deficient cells but decreased protein levels [66]. Furthermore, a similar trend was observed for the hemoglobin gene, its mRNA was 50-fold upregulated in RP depleted zebrafish, but protein level was significantly downregulated, while there was no change in mRNA to protein ratio in the neutrophil-specific gene [58].

On the other side, some transcripts are preferably translated. It seems that transcripts containing 5-terminal oligopyrimidine tract sequence in their 5’ UTR are more likely to enter

the ribosome successfully. The group of these mRNA, among others, accounts for ribosomal proteins and genes under transcriptional control of mTOR [66].

GATA1, the specific erythropoiesis master regulator, is affected in DBA [68]. GATA1 is expressed during the last steps of erythrocyte development. It triggers haemoglobin transcription, eliminates organelles during erythroid differentiation, and induces other erythropoiesis-related genes [69]. Its mRNA level is slightly increased or similar in RP-depleted cells or DBA patients compared to controls, but protein levels are downregulated [69]. The origin of this phenomenon is controlled by the 5' UTR region [69]. GATA1 protein level was restored when this region was substituted, and overall erythroid differentiation was improved [69].

It has been hypothesised that DBA anemia is due to GATA1 translation inhibition [68]. GATA1 is expressed when committed cells are in the CFU-E red blood cell development [70]. Downregulation of GATA1 protein, at this stage, leads to apoptosis [71] which is consistent with the DBA phenotype. Furthermore, if RBC precursors escape apoptosis at the CFU-E stage, GATA1 decreased signalling may lead to impaired cell responses in the following RBC developmental stages. Mutations in the GATA1 gene have been described in several DBA-like patients [72, 73]. However, in patients with impaired erythropoiesis similar to DBA, other typical features like physical malformations are missing [72, 73]. Furthermore, arsenic induced disruption of GATA1 also lead to DBA-like erythropoiesis disruption [74].

Nevertheless, recent findings suggest that erythropoiesis failure in DBA is more complicated than originally thought. More specifically, it seems that GATA1 impairment plays a key role in DBA phenotype, but only in RPS, not RPL-related disorders [75]. Furthermore, defects in small ribosomal subunits seem to significantly influence mRNA selected for translation more than those in large subunits [76]. Ribosome profiling combined with whole proteome and comprehensive transcriptome analysis can provide a deeper understanding of this phenomenon in future.

1.4.1.2 Metabolic changes

Erythrocytes differ from other cell types in many features. One, except for the early stages, is the absence of mitochondria and, therefore, the absence of aerobic respiration. Hence, erythrocyte energy metabolism relies mainly on glycolysis. Increased p53 and cellular stress

induce the expression of genes involved in aerobic respiration to increase available ATP. It suppresses the expression of genes involved in glycolysis [77]. This approach can be helpful in many types of cells, but in the case of erythrocytes, it results in further depletion of the ATP reservoir.

Reduced ATP cell content and elevated blood glucose levels have been also observed in DBA animal models [78]. This phenomenon is known from the initial state of diabetes II and suggests impaired insulin signalling in DBA. Moreover, insulin signalling is particularly important in erythrocyte development and its impairment reduces proliferation of red blood cell precursors [78].

Furthermore, autophagy is crucial in RBC development [79]. In erythrocyte differentiation, cells must discard almost all cellular structures from mitochondria to the nucleus. The nucleus is removed through the enucleation step, and the other organelles are removed mostly via autophagy [80]. Autophagy is mediated by GATA1 [81] and mTOR [82] induced of autophagy proteins transcription. Noteworthy, mTOR and/or autophagy aberrations lead to macrocytic anemia [83], consistent with the DBA phenotype [84].

mTOR kinase has a dual role in RBC development [85]. Its activity is necessary for proper BFU-E and CFU-E proliferation in the primary steps of RBC development. But in advance steps of erythropoiesis, it needs to be silenced for autophagy induction. The mTOR is frequently activated in DBA cells [86]. Activated mTOR in DBA probably facilitates the increased proliferation of BFU-E and CFU-E and translation status improvement via RPS6 phosphorylation [87].

Furthermore, L-leucine, an inductor of mTOR activation, is used as a DBA treatment [88, 89]. It can be assumed that induction of mTOR is beneficial for DBA cells, especially during RBC development until the CFU-E stage. On the other hand, high catalytic activity of mTOR during later steps of erythroid differentiation may lead to autophagy failure followed by aberrant terminal maturation to erythrocytes. We can speculate that this is the cause in DBA associated erythroid differentiation defect, because DBA derived erythroid progenitors treated with mTOR inhibitor rapamycin showed increase of late erythroid cells [90].

In DBA cells, autophagy is increased despite mTOR activation [86]. Autophagy in DBA cells seems to be induced by ROS [91], hypoxia [92], or some mTOR-independent pathways [93].

However, mTOR-independent autophagy may not be sufficient for proper RBC development [94]. Therefore, autophagy induction remains as a potential treatment for DBA [90].

1.4.1.3 Defective c-Myc signaling

Enucleation is a critical step in erythropoiesis; the cells lose the nucleus to generate reticulocytes. Inhibition of the process may explain reticulocytopenia in DBA patients [95]. Before enucleation, nucleolus must be condensed and histones deacetylated.

Transcriptional factor c-Myc is known to promote proliferation, and therefore one can speculate that genome-wide histone modification by c-Myc plays a role in several cell transduction pathways [96]. Interestingly, GATA1 silences c-Myc expression in RBC precursors [37], highlighting the importance of c-Myc during erythropoiesis. A slight increase in c-Myc levels may complicate enucleation and reticulocyte development by impairing histone deacetylases activity [96]. Activated c-Myc also induces proerythroblast apoptosis during RBC development [96].

c-Myc is deregulated in DBA in multiple ways. Downregulated GATA1 is probably the central axis of upregulation of c-Myc in all DBA erythroid cells. Some RPs affected in DBA regulate c-Myc independently; RPL11 and RPL5 are the best known examples. Both RPs actively induce ribosomal stress [25] and c-Myc regulation [31]; on both mRNA and protein levels [33]. The impairment of these RPs has been associated with the more severe DBA phenotype [97]. c-Myc driven lymphomagenesis was also observed in the DBA mice model [33]. Interestingly, similar or identical mutations of those RPs, reported in DBA are also detected in some cancers [98, 99], deactivating p53 and activating c-Myc signalling.

As was mentioned above, a high level of c-Myc is critical for the proliferation of bone marrow stem cells. Reduction of c-Myc expression by RPS19 deficiency can lead to decreased proliferation of erythroid stem cells. Furthermore, disruption of RPS19 leads to c-Myc downregulation through the PIM1 signalling pathway and upregulation of miR-34 known to regulate p53 levels.

The common feature of RP disbalance is decreased GATA1 translation. Apart from the primary function as transcriptional activator during erythropoiesis, GATA1 also acts as a transcriptional repressor. It was demonstrated that GATA1 binds directly to c-Myc promotor and blocks its transcription, thus decreasing c-Myc protein level and allowing condensation and enucleation

of the nucleolus. RP defect can therefore lead to aberrant negative c-Myc back-loop control and apoptosis of erythroblasts and markedly decreased count of reticulocytes, which is a typical DBA phenotype.

1.4.1.4 Iron metabolism

For a long time it has been hypothesized that the erythropoiesis phenotype can be in both DBA, and 5q- syndrome accounted for delayed globin synthesis and iron accumulation. Indeed, a recent study showed that early proerythroblast is particularly vulnerable because, at this stage, heme synthesis increases while globin expression is still low. Furthermore, defective erythropoiesis in DBA cells prolongs the window to heme and globin equilibrium. Thus, heme accumulates in RP deficient cells, which leads to increased ROS production. It has been shown that cells capable of reducing heme content in the cytoplasm are more likely to reach erythrocyte maturity.

There are to main pathways to decrease heme content in RB deficient cells. ALAS2 mediates the first step in heme synthesis. DBA cells expectedly display downregulation of ALAS2 mRNA expression, which helps to deal with heme overload. On the contrary, RP haploinsufficient cells upregulate the expression of heme exporter FLVCR1. Notably, due to aberrant splicing machinery, FLVCR1 mRNA undergoes alternative splicing resulting in a non-functional isoform. Thus, although cells are trying to export heme, their energy investment to FLVCR1 expression is frequently misplaced.

Hepcidin prevents cellular iron export and increases the iron content. Interestingly, increased hepcidin level is associated with transfusion dependency in DBA. All this finding highlights heme toxicity in DBA erythroid precursors.

Excess iron can also trigger apoptosis and a newly discovered type of cell death – ferroptosis. A detailed description of ferroptosis can be found elsewhere [100]. Briefly, ferroptosis is non-apoptotic iron-dependent cell death. Under normal circumstances, the SLC7A11 transporter mediates cysteine uptake and cellular glutamate efflux. Imported cysteine is a further process for glutathion (GSH). Glutathione peroxidase GPX4 uses GSH to repair ROS-induced lipid peroxidation. However, if ROS activation reaches a critical level, and the cell is incapable of appropriate repair due to insufficient cysteine influx or small-molecule inhibition of critical pathways and undergoes ferroptosis (Fig.6).

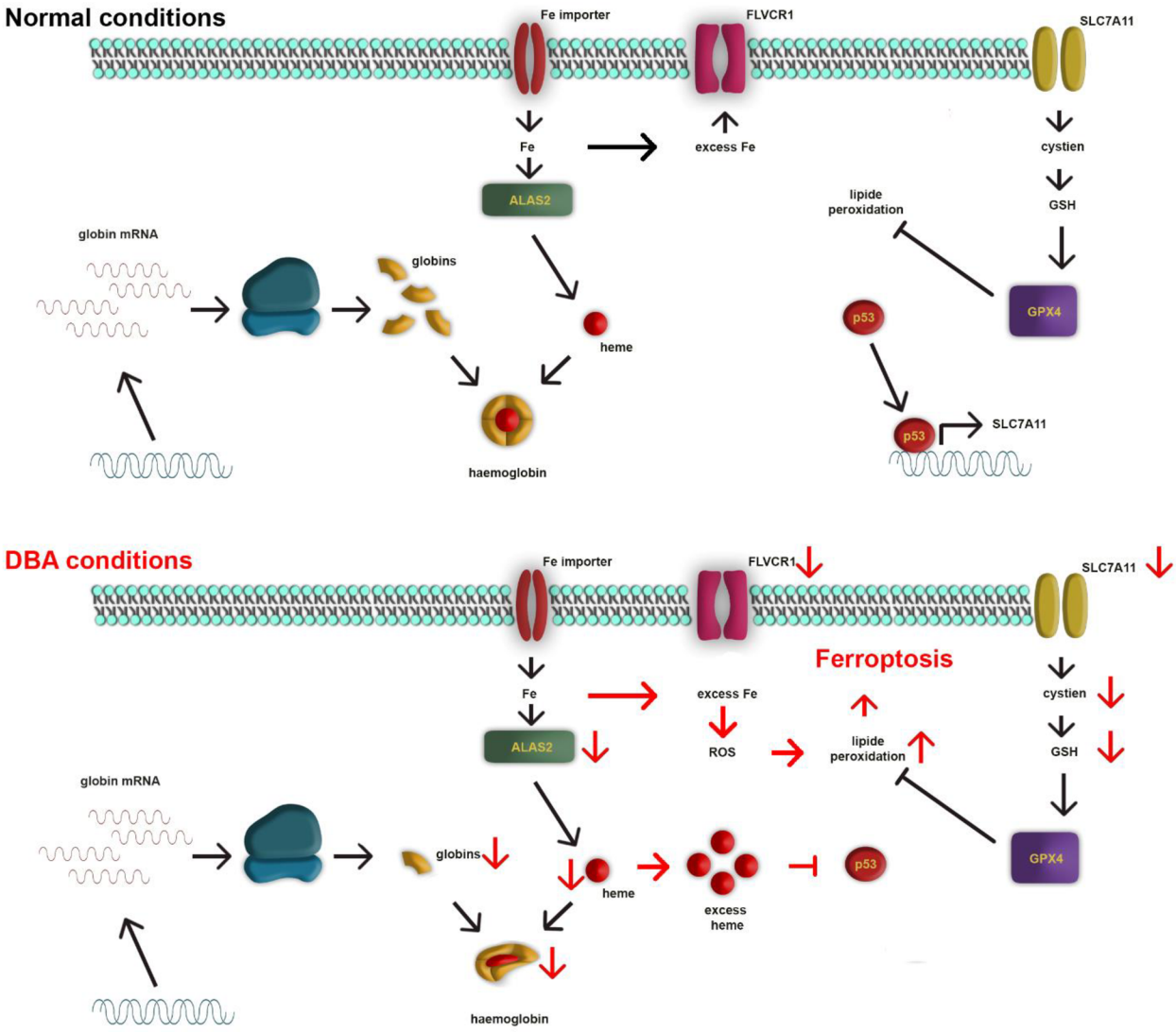

Figure.6: Scheme of ferroptosis activation in DBA cells.

Further evidence for crucial role of iron in cell homeostasis brought the discovery that heme iron binds directly to p53 and initiates its degradation without involvement of MDM2. Moreover, p53 is a transcriptional repressor of SLC7A11. Therefore, increased stress stimuli and in turn p53 activation sensitize cells to ferroptosis, which can be prevented by heme-mediated p53 degradation and increased expression of SLC7A11.

1.4.2 Glucocorticoid therapy in DBA treatment

Although DBA was discovered a long time ago, there is no curative treatment available. DBA phenotype is usually treated with glucocorticosteroids (GC). This type of treatment is nonspecific, leading to GC resistance and a high risk of severe GCs site effects.

1.4.2.1 Glucocorticosteroids

Glucocorticosteroids (GC) are stress hormones produced in the adrenal cortex. They regulate diverse cellular functions, including development, homeostasis, metabolism, cognition, and inflammation [101]. GCs are widely used as a treatment for many pathologies, from autoimmune syndromes to cancer [102]. GCs are also the first treatment option for DBA. Although GC has a wide range of applications, its use is limited by severe adverse effects, especially in long-term or high-dose therapies. These side effects include osteoporosis, skin atrophy, diabetes, abdominal obesity, glaucoma, cataracts, avascular necrosis and infection, growth retardation, and hypertension [103]. These adverse effects have a profound impact, especially on infants.

Most GC effects are mediated by the glucocorticoid receptor (GCR), encoded by the NR3C1 gene on chromosome 5. GCR is a ligand-activated transcription factor. In the inactive form, GCR is dominantly located in the cytoplasm in a complex with chaperone proteins and immunophilins [104]. Its conformation changes upon ligand binding. It gets disassociated from the complex and translocates to the nucleolus, where it binds to GCRe sequences and initiates the expression of target genes. Interestingly, GCR mediate expression is tissue-specific, and only a small portion of genes is activated in all tissues [105]. This is probably caused by tissue-specific DNA methylation [106]. Furthermore, activated GCR can also interact with other proteins except for expression initiation. For example, it can modulate the kinase activity of several kinases [107] or regulate GATA1 during erythropoiesis [108].

Moreover, GCR has several isoforms [109] and is highly polymorphic [110]. This impacts body mass index, bone density or coronary artery diseases, the probability of developing diabetes II, and GC treatment outcome [111, 112]. This also applies to DBA. Surprisingly, variability of GCR seems to have no or minor impact on GCs treatment outcome in DBA [113]. But, it seems to modulate the onset of disease [113]. It was shown that particular SNPs (rs6196 and rs860457) in GCR result in the early onset of DBA which can be caused by modified GCs response during ontology [113].

1.4.2.2 GCs and GATA1

The impaired GATA1 protein level seems to be the primary defect in DBA RBC precursor cell function [114]. Therefore, one could propose that GCs could restore GATA1 translation and related signalling pathways and consequently increase erythrocyte precursors counts. Nevertheless, GCs do not increase GATA1 but deplete it. GCs inhibit GATA1 by transcriptional repression and direct interaction of GR with GATA1 [25]. GCs also decrease protein synthesis in cells through mTOR and subsequent S6 phosphatase inhibition [115]. This reduction affects the levels of HSP70 [116], a chaperone that protects GATA1 from caspase-3 degradation during erythropoiesis [71]. Therefore, we can conclude that GCs do not improve GATA1 status but further deplete it.

GCs can promote erythropoiesis by two mechanisms to overcome GATA1 impairment. First, GCs can act before the CFU-E stage and increase the number of CFU-E precursors. Secondly, even though GCs do not rescue GATA1, they can regulate GATA1-related steps in erythropoiesis. In the following paragraphs, we will discuss these possibilities.

1.4.2.3 Role of GCs in CFU-E precursors

Stress erythropoiesis is caused by blood loss, oxygen deprivation, hemolytic anemia, or long-term stress [117] (Fig. 2). This type of erythropoiesis leads to the rapid proliferation of RBC precursors driven by Epo and GCs [21]. Because DBA fulfils several criteria, we can hypothesize that stress erythropoiesis plays a crucial role in RBC development in DBA patients.

When the body is under stress, cortisol, the body's GC, induces many physiological responses. One of them is erythropoietin produced in the kidney [118]. EPO stimulates CFU-E, and its primary target is GATA1 [119]. Due to GATA1 impairment, DBA is one of the few Epo-insensitive anemias [120]; therefore, we can speculate that Epo induction via stress erythropoiesis probably does not lead to DBA phenotype improvement.

GCs induce stress erythropoiesis directly by activating glucocorticosteroid receptors (GCR) and indirectly through Epo [121]. Activation of GR is conditional for stress erythropoiesis [121] and stimulates several transcription factors necessary for CFU-E precursor BFU-E proliferation, precisely, Myb, Kit, and Lmo2 [122]. Together with GATA1 inhibition, these transcription factors lead to the rapid proliferation of BFU-E. This induction is strictly specific to BFU-E cells and results in the expansion of CFU-E precursor up to 10-fold [123]. Increased BFU-E leads to

increased CFU-E, which, after Epo stimulation, results in rapid differentiation [117]. Thus, stress erythropoiesis leads to a significant increase in RBC number originating from one precursor cell.

Furthermore, it seems that stress erythropoiesis impairment mediated by ZFP36L2 plays a crucial role mainly in RPL-related DBA, and its external stimulation by corticosteroid treatment may result in the restoration of this pathway [75].

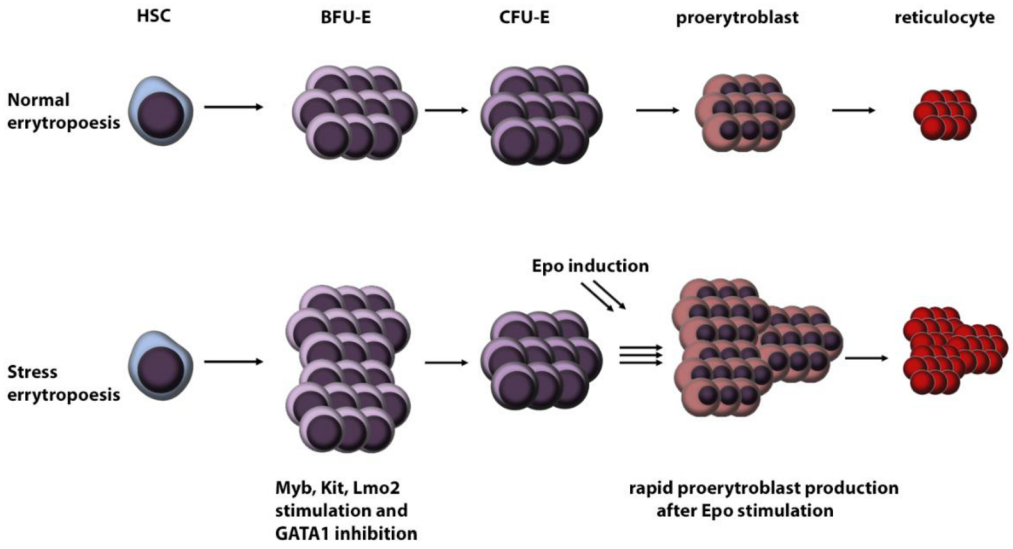

Figure7: Scheme of stress erythropoiesis.

1.4.2.4 Regulation of ribosomal stress and p53

It was believed that apoptosis in DBA RBC precursors is caused by p53 induction via ribosomal stress [124]. This hypothesis was partially refuted since the haploinsufficiency of most RP does not lead to p53 stimulation via ribosomal stress [23]. Even though ribosomal stress and p53 signalling are critical for normal erythropoiesis [125], the activation of p53 in DBA is most likely mediated by impaired metabolism and DNA damage [54, 126].

It is difficult to elucidate the interplay between p53 and GCs. On the one hand, GCs decrease p53 levels [127], and on the other hand, increased p53, common in DBA cells, limits proper GSs receptor activation [128]. Nevertheless, GCs don't need to regulate p53 directly but indirectly by reducing p53 activation signals. Furthermore, we can speculate that this may be the main course of action of GCs in p53 signalling.

As mentioned above, except for ribosomal stress, p53 could be activated by HEM-mediated ROS production [91, 129]. Although it was reported that GCs reduce ROS species [130-132], their overall influence on ROS production is ambiguous [133]. Short-term GC usage reduces ROS, while long-term exposure leads to ROS induction [133]. Furthermore, increased ROS level was detected in DBA patients regardless of treatment [91], so we can assume that GCs-mediated p53 regulation does not reflect ROS levels. The precise mechanism by which GCs modulate p53 levels in DBA is still elusive. Nevertheless, we can conclude that GCs treatment improves p53 status in DBA [134].

1.4.2.5 Regulation of enucleation through c-Myc

As mentioned above, c-Myc plays a crucial role in RBC development. Its silencing is important for the enucleation step. c-Myc levels are deregulated in DBA, which probably leads DBA associated reticulocytopenia.

GCs transcriptionally repress c-Myc expression [135], leading to cell cycle arrest but not apoptosis, necessary for proper RBCs differentiation [136]. In DBA, GCs may support enucleation during erythropoiesis and prevent reticulocytopenia by downregulating c-Myc.

1.4.2.6 mTOR and autophagy

Inhibition of mTOR by GCs is followed by autophagy, which was described in several cell types [137-139]. Therefore, a plausible hypothesis is that GCs may improve erythropoiesis by modulating mTOR and autophagy. The other important pathway is the inactivation of Akt signalling by GCs in DBA cells [86, 140]. Even though GCs mTOR inactivation may lead to a decreased proliferation of BFU-E and CFU-E [85], stress-induced erythropoiesis may overcome this obstacle [70].

1.4.2.7 GCs resistance

GCs resistance is common in almost all GCs-based therapies; DBA is no exception [141]. Multiple mechanisms may induce GCs resistance, and these mechanisms probably vary between patients [142]. GCR polymorphism, alternative splicing, or downregulation of GCR expression may also lead to GCR resistance [142]. GCs resistance in DBA is associated with p57 dysregulation [141]. The expression of p57 is directly induced by GCR responsive element promoter [143]. Therefore, more than one mechanism may play a role in the effect of GC resistance.

1.4.2.8 Other DBA treatment

Besides GCs, the treatment of DBA is limited. Another treatment option is supplementation of patients with the amino acid L-leucite [88]. When GCs or L-leucine fail, only treatment remains blood transfusion and chelation [49]. When also this treatment fails, a bone marrow transplant is the only option [49].

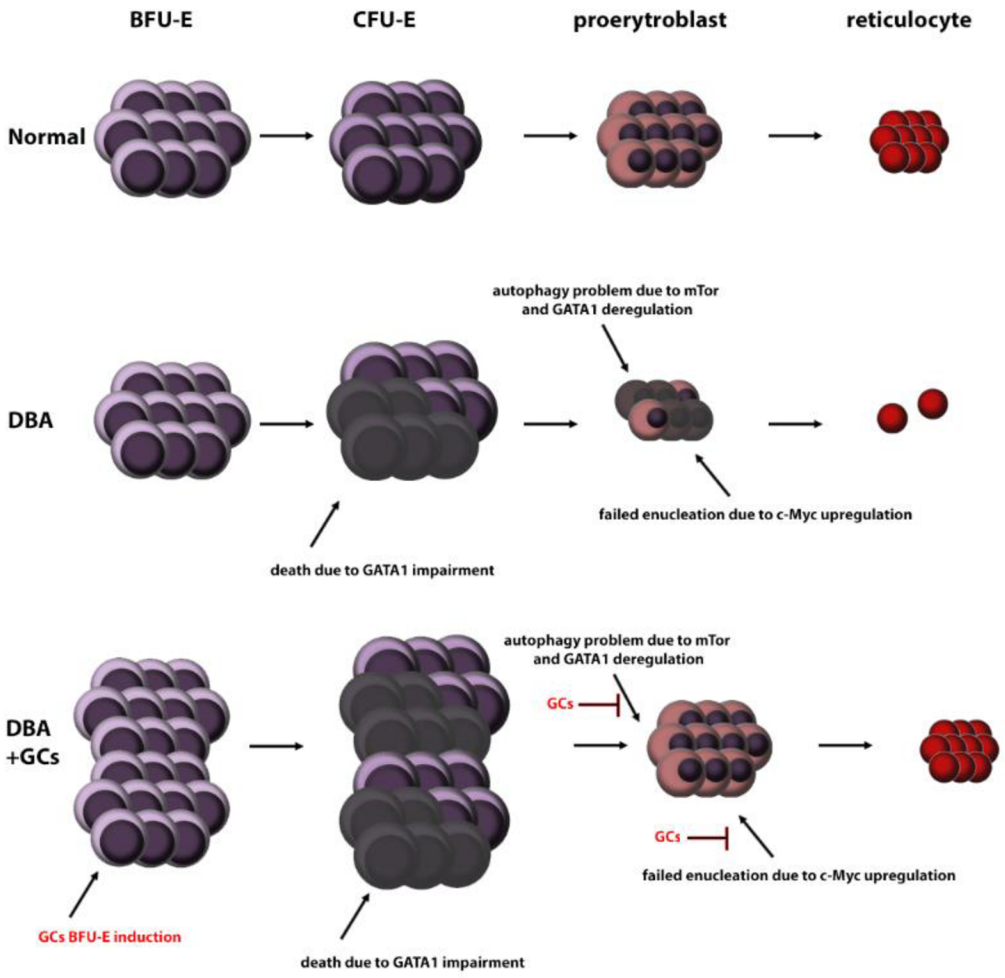

Figure. 7: Scheme of corticosteroids effect on erythropoiesis in DBA.

1.5 *Bystin*

Bystin (Bysl) is encoded by *BYSL* gene localized on the 6p21.1 chromosome and is conserved across many eukaryotes [144]. Bysl was first identified as cytoplasmic protein, forming a complex with tropin and tastin and enabling embryonal implantation [145]. Furthermore,

Bystin was subsequently identified as a structural protein of the nucleolus [144]. The gene is conserved across species, highlighting its significance in cells biology [146].

Recent data show that *Bysl* plays an irreplaceable role in small ribosomal subunit biogenesis [147]. It is responsible for the final steps of 18S rRNA maturation, and bystin downregulation leads to the accumulation of pre-18S rRNA [146]. Furthermore, BYSL seems to be critical nucleolar structure protein. Its knockdown leads to aberrant nucleoli restoration after mitosis [148]. Like other factors involved in ribosome biogenesis and protein translation, Bysl is a direct c-Myc target gene [149] and its role in nucleolar integrity was revealed by the siRNA screen [150].

Moreover, increased levels of *Bysl* have been observed in several cancers and cancer cell lines [148, 151-153]. Its role seems quite significant, especially in glioma cells [154-156], which can be due to bystin's ability to regulate mTOR and other signalling pathways [156, 157]. Based on existing literature we can hypothesize that up-regulated *Bysl* levels may lead to more rapid ribosome production and restoration of nucleolus after mitosis.

Altogether, we conclude that BYSL is a relatively poorly studied nucleolar protein and may play various roles waiting to be explored and described. Therefore, it become one of my research interests.

2 Aims

- Investigate impact of anticancer treatment by oxaliplatin on nucleolar structure.
- Determine impact of RPS7 V134F mutation on nucleolar structure and rRNA processing in clinical case of suspect DBA.
- Explain the role of *Bystin* in Diamond Blackfan anemia and glucocorticoid-based therapies.

3 Experimental part

3.1 Aberration of nucleoli structure caused by oxaliplatin

3.1.1 Introduction

Nucleolar structure reflects the cell state. Xenobiotics or congenital defects can lead to aberration in nucleolar structure and impairment in ribosomal production. Here, we have investigated an impact of oxaliplatin on nucleolus structure to confirm its ability to induce ribosomal stress indicated by proteomic analysis of oxaliplatin treated cells.

Oxaliplatin (L-OHP) belongs to the third generation of platinum-based chemotherapy. This drug is widely used to treat many types of cancer [158-160]. L-OHP is relatively nonspecific, and its interaction with nucleophiles, DNA, RNA, and proteins has been described [161]. To better elucidate the oxaliplatin mechanism of action, we performed a systematic proteomic analysis of the whole proteome of cells treated with L-OHP and discovered that a significant portion of deregulated protein after treatment belongs to the class of ribosomal proteins or proteins of the nucleolus (Appendix 1). To confirm the impact of L-OHP on nucleolar structure, we performed staining of nucleoli marker proteins and rRNA. Results indicate that oxaliplatin has a profound impact on nucleoli structure and therefore function.

3.1.2 Methods

3.1.2.1 Chemicals and antibodies, and lentiviral particles

Unless stated otherwise, chemicals were obtained from the Merck company. Used antibodies were anti-NCL (ab52631, Abcam), anti-FBL (ab5821, Abcam), anti-rabbit Alexa fluor 488 (A11017, Thermo Fisher Scientific), Origene (RPS7 (NM_001011), human ORF Clone Lentiviral Particles, RC209074L3V and Lentiviral Control Particles, PS100092V).

3.1.2.2 Cell lines

Cell lines were cultured in appropriate growth media supplemented with 10% fetal bovine serum and penicillin/streptomycin; and maintained at humidified, 5% CO2 atmosphere at 37°C. Cell line U2OS (ATCC) was cultured in McCoy medium (Lonza).

3.1.2.3 Immunodetection

The day before detection, cells were plated on cover glass or panels at an appropriate cell density. On the day of detection, cells were fixed with 4% formaldehyde for 15 minutes, washed with 1X PBST, and blocked for 45 minutes in a blocking buffer (5% FBS and 0,3%Triton X in 1XPBS). Cells were then rinsed in 1X PBST and incubated with the required primary antibody in blocking buffer overnight, washed in 1X PBST and incubated for one hour at RT with appropriate secondary antibody, washed in 1X PBST, and stained with Hoechst. Images were acquired using a Yokogawa CV7000 microscope (Yokogawa) and analyzed by Columbus Image Analysis System (PerkinElmer).

3.1.2.4 rRNA fluorescent in-situ hybridisation

Cells were seeded and fixed as described above and permeabilized by 70% ethanol at -20 °C overnight. Cells were washed twice in wash buffer (2 x SSC, 10% formamide), followed by hybridization at 37 °C for 4 hours in hybridization buffer (10% formamide, 2 x SSC, 0.5 mg/mL tRNA, 10% dextran sulphate, 250 µg/ml BSA, 10 mM ribonucleoside vanadyl complexes and 0.5 ng/µL 5`ITS1 probe: CCTCGCCCTCCGGGCTCCGTTAATGATC conjugated with cy5). Afterwards, samples were washed twice in preheated wash buffer at 37 °C and stained with Hoechst 33342 (62249, Thermo Scientific). The cells were examined using CV7000 Voyager Cell High throughput cellular imaging and discovery system (Yokogawa). Image quantification was calculated as a corrected spot intensity in the nucleolus by the Columbus software version

3.1.3 Results

3.1.3.1 Nucleoli structure at protein level

Cells treated with L-OHP show a markedly different distribution of nucleoli marker proteins compared to control cells. More specifically, FBL, which is generally concentrated in DFC and participates in rRNA transcription, is after L-OHP treatment concentrated in so-called nucleolar caps (Fig. 8). On the other hand, NCL, which is concentrated in the granular component of nucleoli, is after L-OHP treatment released into the nucleoplasm (Fig. 8).

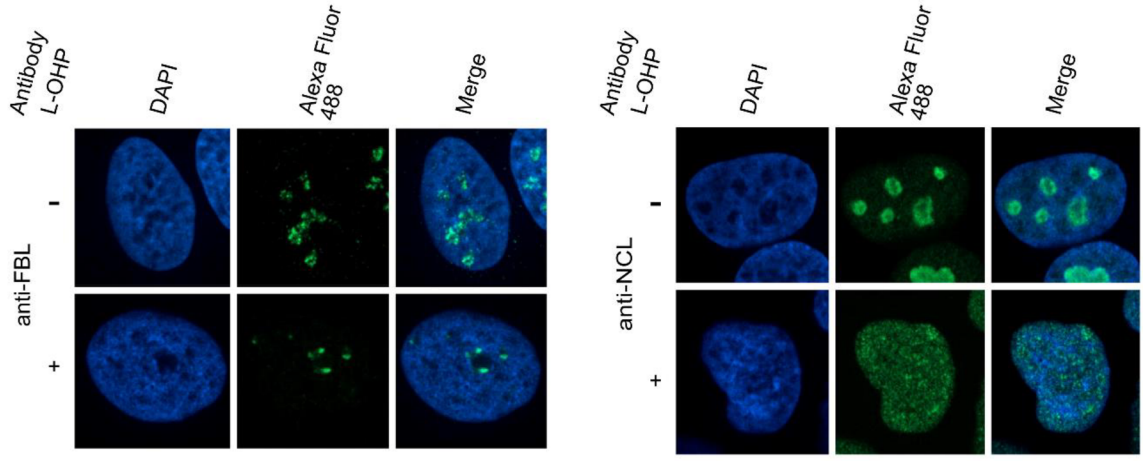

Figure 8: Impact of L-OHP on structural proteins of nucleoli.

3.1.3.1.1 rRNA aberration

rRNA in situ hybridization is a method that stains the amount of non-processed rRNA in the nucleolus. After L-OHP treatment, we detected a massive drop in rRNA amount in the nucleolus (Fig. 9), confirming a major insult to ribosome production.

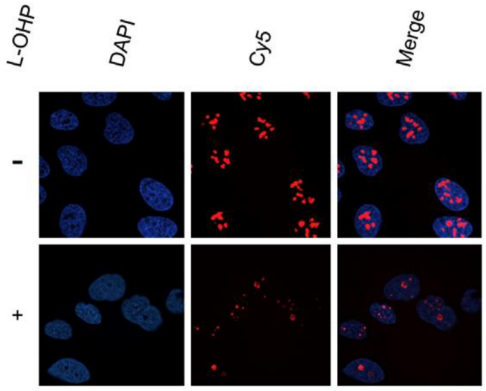

Figure 9: Impact of L-OHP on rRNA amount in the nucleolus.

3.1.4 Discussion

Ribosomal production is fundamental for the proliferation and survival of cells. Because a significant portion of this machinery is localized in the nucleolus, its structure and proper function are directly linked to ribosome biogenesis. Any internal or external insult may lead to the crippling of ribosome production machinery.

We show that the primary treatment by L-OHP impacts nucleolar structure and function. Not only that the proteomics study showed the deregulation of ribosome production machinery, but experiments on cells showed that L-OHP has a profound effect on the localization of nucleolar marker proteins, but we also show that L-OHP leads to inhibition of rRNA production. Furthermore, a recent report provides evidence that L-OHP causes cell death through a nucleolar stress response rather than through the DNA damage pathways long considered operative for cisplatin [162]. This finding leads to a growing picture that while both compounds form lesions on DNA and other biomolecules, oxaliplatin acts primarily through an impact on the nucleolus [163].

3.2 Impact of mutation V134F in RPS7 on nucleoli structure and rRNA processing

Diamond-Blackfan anemia (DBA) is a rare congenital red cell aplasia with causative mutations in genes encoding ribosomal proteins (RPs) [164]. Using NGS we detected RPS7 mutation in clinical DBA case (Apendix 2). This variant was discovered in one family suffering from DBA [164]. To better understand the pathophysiology of mutated RPS7 protein, we evaluated its impact on the CRISPR model of the given variant (Appendix 2). Part of this evaluation was also the investigation of nucleolar morphology by rRNA fluorescent in-situ hybridization.

3.2.1 Methods

All methods and materials were described in methodology 2, except for the northern blot method, which is described below.

3.2.1.1 Northern blotting

Pre-rRNA species were analyzed by northern blotting. 10 µg of total RNA were mixed with 1 volume of loading buffer (50% formamide, 0.06% formaldehyde, 10% glycerol, 0.05% bromophenol blue in 1x MOPS buffer) and separated on a 2% agarose gel in the presence of MOPS buffer (20mM MOPS, 5mM sodium acetate, 2mM EDTA, pH 7.0) containing 2% formaldehyde, and run in 1 x MOPS buffer at 23 V overnight at 4 °C. RNAs were then transferred to a nylon membrane (Amersham Hybond-N+, GE Healthcare, USA). After fixation by UV-crosslinking, the membranes were pre-hybridized for 1 h at 45 °C in DIG Easy Hyb (DIG Northern Starter Kit, Roche, Switzerland). The digoxigenin-labeled oligodeoxynucleotide

probe was then added and incubated overnight at 45 °C. The probes used in this study were: 5′ITS1 (5′-CCTCGCCCTCCGGGCTCCGTTAATGATC-3′), ITS2b (5′-CTGCGAGGGAACCCCCAGCCGCGCA-3′), ITS2d/e (5′-GCGCGACGGCGGACGACACCGCGGCGTC-3′) (Generi Biotech, Czech Republic) [23]. For detection of ITS2, probes ITS2b and ITS2d/e were mixed in equal amounts. After probes hybridization took place, the stringency washes followed. Firstly, two times for 5 min at room temperature in 2 x SSC (0.15 M NaCl, 15 mM sodium citrate, pH 7.0) containing 0.1% SDS and twice for 15 min in 0.25 x SSC with SDS 0.1%. Before the blocking step, the membranes were briefly washed in washing buffer (0.1 M Maleic acid, 0.15 M NaCl, 0.3% Tween 20, pH 7.5), then blocked in blocking solution for 30 min and incubated with the anti-digoxigenin-AP antibody (both DIG Northern Starter Kit, Roche, Switzerland) for 1 hour at room temperature. Unbound antibodies were removed by two washing steps for 15 min in a washing buffer. Before measurement of the chemiluminescence signal, membranes were equilibrated for 5 min at detection buffer (0.1 M Tris-HCl, 0.1 M NaCl, pH 9.5), then the CDP-Star substrate was added and the signals were acquired by the ChemiDoc MP Documentation system (Bio-Rad, USA).

3.2.2 Results

The V134F mutation in RPS7 leads to a significant accumulation of pre-rRNA in the nucleolus (Fig. 10a, b). This highlights the importance of WT RPS7 during rRNA processing. Next, we performed a northern blot to prove that aberration in RPS7 leads to defects in rRNA processing and accumulation of non-processed rRNA. Norther blot of pre-rRNA revealed that V134F RPS7 results in accumulation of 18S rRNA precursor, more specifically, 26S rRNA and c-18S rRNA, same as in patient and was reverted by transduction by RPS7 WT lentivirus (Fig. 10c, d).

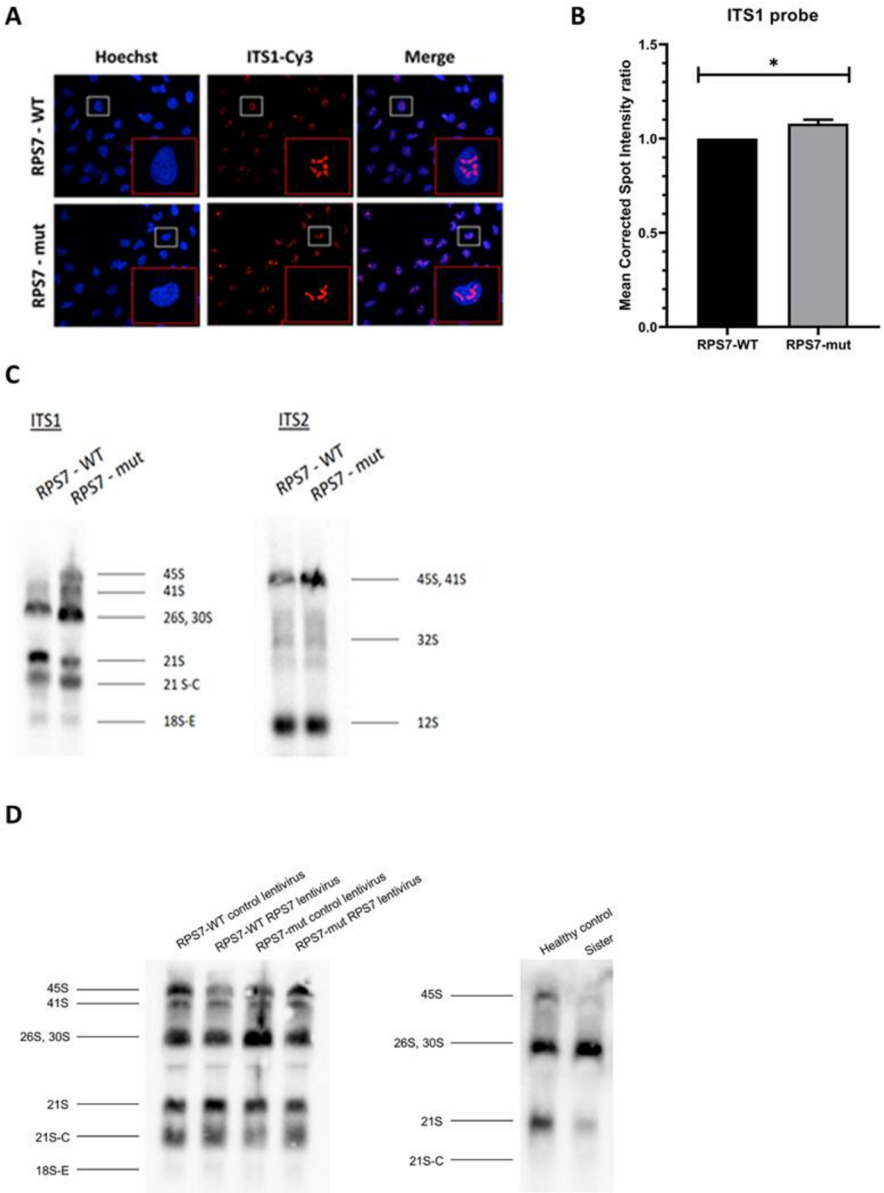

Figure 10: Detection of pre-ribosomal RNA by FISH and Northern blotting in the RPS7-WT and RPS7-mut cell lines. (A) From the left: cell nuclei stained with Hoechst 33342, localization of pre-rRNA using an ITS1 probe, merge. (B) Statistical analysis of pre-rRNA levels in nucleoli (mean corrected spot intensity per nucleolus). (C) Detection of pre-rRNA species in RPS7-WT and RPS7-mut cell lines by Northern blotting. (D) RPS7 p.V134F phenotype was reversed by transduction of RPS7-WT and RPS7-mut cell lines with control and RPS7 WT lentiviruses. And a comparison of rRNA maturation profiles (ITS1 probe) of the patient´s sister carrying identical.

3.2.3 Discussion

Here we show that congenital variant V134F in the RPS7 gene affects the processing of 18S rRNA precursors. Although the role of RPS7 in ribosome biogenesis is well established [23], we were wondering if the change only in one amino acid can lead to significant changes in nucleoli structure. Indeed, our results supports this hypothesis. Furthermore, *in situ* rRNA hybridization is cheap, quick, and carries fewer critical points than standardly used northern blots and could be easily used for diagnostics of ribosomal disorders. Here, we prove that the accumulation of non-processed rRNA in the nucleolus can serve as a validation parameter for the DBA phenotype.

3.3 Bysl drives Diamond Blackfan Anemia via c-Myc regulation

Although RPL11 is commonly mutated in DBA patients [165, 166], deletion of one whole allele of RPL11 should be incompatible with successful embryogenesis [33], yet we discovered one patient with single RPL11 allele deletion in our cohort with mild DBA phenotype. This clinical observation together with existing animal data on RPL11$^{-/+}$ mice suggested the presence of disease modifier gene(s) supressing otherwise lethal disease phenotype. Therefore we have preformed whole exome sequencing (WES) of the patient and discovered an interesting non-sense mutation in nucleoli structure protein BYSL [144]. Further study revealed that mutated BYSL normalizes RPL11 deregulated c-Myc activity.

As mentioned above, the treatment opportunities for DBA patients are limited. The most common approach is glucocorticosteroids therapy which has severe side effects, especially in infants. GCs have been used for DBA treatment since 50´, but their mechanism of action remains unclear [120]. Although many theories have been proposed, none seem fully explains pharmacological mechanism of action (for more details see appendix 3). More interestingly, GCs are also used as a treatment for many cancers, many of which are c-Myc driven [167]. Although some articles suggest that GCs can regulate mRNA c-Myc levels in leukaemias [135], we suggest in this work that GCs may also regulate c-Myc protein levels through BYSL GCs interaction.

In this study, we have explored BYSL as a potential new promising target for DBA and c-Myc-driven cancers using an extensive range of experimental techniques. Apart from identification c-Myc protein as direct BYSL partner, we also identified and experimentally confirmed binding of dexamethasone, the most frequent therapy for DBA to BYSL, thus preventing BYSL-c-Myc interaction and enabling c-Myc protein degradation via ubiquitin independent mechanisms. Herein, the *bystin* was for the first time identified as disease modifier gene for c-Myc dependent pathologies and a potential target for novel therapies avoiding GCs side effects.

3.3.1 Methods

3.3.1.1 Chemicals and antibodies

Unless stated otherwise, chemicals were obtained from the Merck company. Used antibodies were: anti-BYSL - N-terminal (ab194961, Abcam), anti-BYSL-middle (HPA031217, Merck), anti-BYSL-C-terminal (ab251811, Abcam), anti-c-Myc (ab32072, Abcam), anti-NMP1 (ab52631, Abcam), anti-actin (A2228, Abcam), anti-RPL11(18163S, CST), ani-p53 (ab154036, Abcam), anti-p21 (2947S, CST), anti-CD71 (11-0711-81, Thermo fisher scientific), anti-Ter116 (15-5921-81, Thermo fisher scientific), anti-OAZ2 (ab32072, Abcam), anti-GCR (18163S, Abcam), anti-mice HRP (A2304, Roche), anti-rabbit (A0545 Thermo fisher scientific), anti-rabbit Alexa fluor 568 (A11036, Thermo fisher scientific), anti-mice Alexa fluor 488 (A11017, Thermo fisher scientific).

3.3.1.2 Exome sequencing and analysis

DNA was isolated from blood samples using a Magcore isolation station (RBC bioscience). The sequencing library was prepared by Nextera Rapid Capture Exome and Expanded Exome Enrichment Kit (Illumina) according to the Nextera Rapid Capture Enrichment Guide (version November 2013, Illumina). Obtained data were aligned to hg19 by the BWA algorithm[168] and further processed by SAMtools [169]. The Mpileup algorithm of the SAMtools package was used for variant calling, followed by annotation by ANNOVAR [170]. From the resulting list, variants in gene-related to the nucleolus and ribosomal stress were extracted to select the final candidate gene.

3.3.1.3 Array GCH

Was performed by Josef Srovnal M.D., PhD. CNVs were tested using single nucleotide polymorphism (SNP) array for comparative genomic hybridization. A Cytoscan HD instrument

(Affymetrix) was used for SNP aCGH analysis according to the manufacturer's protocols. The CHAS v1.2.2 program (Affymetrix) was used to call CNVs.

3.3.1.4 cDNA generation and RT-PCR

RNA was isolated from blood samples or cell lines by the Trizol method. Following reverse transcription was performed using random primers (Thermo fisher scientific) and reverse transcriptase (Thermo fisher scientific). RT-PCR was performed using primers for *bystin* AGGAGAAGCGGAGGAAGAGTATG and GTCATTGTGGCAGCCTTCTCC or *c-myc* TAGTGGAAAACCAGCAGCCT and GGTGTGACCGCAACGTAGG and analyzed on a Light cycler 480 (Roche).

3.3.1.5 Sanger sequencing

Amplicon for sequencing was obtained from the family members' cDNA using specific primers ATCCTGGCCTTTCTTCAGTCC and AGTCACCAACGGGGGTCTTG for the seventh exon of the BYSL gene. The amplicon was sent to SEQme company (Czech Republic) for sequencing. The result was then analysed in Chromas software (Technelysium).

3.3.1.6 Plasmid generation

PCR products for plasmid generation were obtained from patient cDNA using specific primers AGGTCCCTGGGGAATACCAT and GCTTGGAGATCAAGGGAGGTG for BYSL transcripts. For the construction of the untagged BYSL plasmid, TOPOTA cloning kit (K490001, Thermo Fisher Scientific) was used. The inserted DNA was then analysed by sequencing, and BYSL WT and BYSL mutants were selected.

3.3.1.7 Cell lines and transfection

Cell lines were cultured in appropriate growth media supplemented with 10% foetal bovine serum and penicillin/streptomycin; and maintained at humidified, 5% CO2 atmosphere at 37°C. Cell line U2OS (ATCC) was cultured in McCoy medium (Lonza), and cell line K562 (ATCC) was cultured in Iscove's Modified Dulbecco's medium (Lonza).

Plasmid transfections into U2OS cells was performed using X-tremegene 9 (6365779001, Merck). For siRNA-mediated knockdown, appropriate siRNA (Origene) and jet prime (Polyplus transfection) were used. For both transfection and siRNA-mediated knockdown of K562, a

Neon electroporation system (Merck) was employed. Every transfection was performed according to the manufacturer's guidelines.

3.3.1.8 Immunoprecipitation

For immunoprecipitation, $5x10^6$ cells were lysed for 30 minutes in RIPA buffer (Thermo Fisher Scientific) supplemented with phosphatase and protease inhibitors (Roche), then centrifuged, and the supernatant was collected. Immunoprecipitation was performed by anti-c-Myc magnetic beads (Thermo Fisher Scientific) according to the manufacturer's protocol.

3.3.1.9 Western blot analysis

Samples were separated on SDS-page, transferred to PVDF membrane, blocked in blocking solution (37516, Thermo Fisher Scientific), incubated with required primary antibody overnight at 4°C, and washed in Tris buffered saline with 0.1% Tween (TBST) and incubated with appropriate secondary antibody in 5% BSA for 1 hour. Results were then visualized using Immobilon Forte Western HRP substrate (Merc) on the Odyssey FC instrument (Li-Cor). Band intensities were quantified using Li-cor software (Li-Cor).

3.3.1.10 Immunofluorescence analysis

The day before detection, cells were plated to 60-80% confluence on microscopic cover glass or plates and treated, eventually. 24 hours after incubation, cells were fixed with 4% formaldehyde for 15 minutes, washed with 1X Phosphate Buffered Saline with 0.1% tween 20 (PBST), and blocked for 45 minutes in a blocking buffer (5% FBS and 0,3%Triton X in 1XPBS). Cells were then rinsed in 1X PBST and incubated with the required primary antibody in blocking buffer overnight, washed in 1X PBST and incubated for one hour in RT with appropriate secondary antibody, washed in 1X PBST, and counterstained with Hoechst 33342. Photographs were taken by Yokogawa CV7000 confocal microscope (Yokogawa) and analysed by Columbus Image Analysis System (PerkinElmer).

3.3.1.11 Erythropoiesis differentiation analysis by flow cytometry

K562 cells were treated with 50 μM hemine and dexamethasone at in 10 μM concentration one day after transfection. Cells were processed after 3 days of incubation. For flow cytometry studies, cells were washed and fixed with Cellfix (BD) and labelled using CD71 (20438801, Thermo Fisher Scientific) and Ter119 (1953012, Thermo Fisher Scientific) antibodies in

Cellwash (BD Biosciences). After 30 min incubation with antibodies, cells were washed by PBS, stained with 10 nM Hoechst 33342 in PBS for 10 minutes, and then measured using a FACSAria II flow cytometer (BD Bioscences). First, the intact cells were gated from FCS/SSC dot-plot (not shown). Finally, the Ter119 positive cell population was brought to Hoechst histogram, and enucleated reticulocytes were quantified. At least $1x10^4$ cells have been acquired for each sample.

3.3.1.12 Benzidine staining

Differentiated, control and treated K562 cells were cytocentrifuged on glass slides using Cytotrack (Sakura), fixed for 5 minutes in ice-cold methanol, and dried. Vizualization of haemoglobin production was performed using benzidine staining (20 μg/ml) in water with 2% H_2O_2 for 2 hours in dark. This was followed by a wash in PBS and counterstaining with 1:20 Giemsa solution for 2 minutes in room temperature. After the final wash in PBS, cells were visualized by Zeiss LAB.A1 microscope (Zeiss) and images were processed in Zen software (Zeiss).

3.3.1.13 Isothermal Titration Calorimetry (ITC)

ITC was operated by my colleague Martina Medvedikova, M.Sc. ITC experiments were performed at 25 °C with a Nano ITC Low Volume (TA Instruments). During all measurements, injections of 2.5 μL of ligand (6 μM) were titrated into 250 μL protein (0.74 μM) with time intervals of 300 s, a stirring speed of 250 rpm. All ITC experiments were conducted with degassed buffered solutions 25 mM HEPES buffer, pH 7.4, in the presence of 1% DMSO.

The resulting thermograms were analysed using the independent model of the NanoAnalyze Software. ITC is a straightforward method for measuring not only the binding affinity constant (K) and binding stoichiometry (n), but also enthalpy of binding (ΔH) that occur throughout a reaction in solution, and the entropy changes (ΔS), was calculated from the equation $\Delta G = -R \cdot T \cdot \ln K_a = \Delta H - T\Delta S$.

3.3.1.14 In silico modelling

Thus part was performed by Olena Mokshyna, Ph.D. For all molecular docking studies, we employed the PLANTS [171] software both for blind docking and for docking into a particular binding site.

3.3.1.15 Statistics

All experiments were performed in triplicates, and the data were analysed by ANOVA or t-test method using Graphpad software (Prism).

3.3.2 Results

3.3.2.1 BYSL mutant compensates RPL11 depletion

In one patient from our DBA cohort, a small deletion in the 1p36.11-1p36.12 area (Fig. 1a) was detected by array GCH (comparative genome hybridization). This area includes the *RPL11* gene. Mutations in this gene are known to cause DBA, and deletion of this gene was previously reported [165, 166, 172]. Surprisingly, it was shown that deletion of single RPL11 allele is embryonically lethal in mice [33].

In subsequent WES analysis, we detected non-sense mutation R343X in the gene coding BYSL protein. We subjected the whole patient's family to Sanger sequencing, and have discovered that silent carriers of this mutation are the mother and the brother, but with no clinical symptomatology (Fig. 1b). Unexpectedly, when we performed protein analysis of family members, we detected the mutated short version of BYSL protein only in the patient but not in her mother or brother (Fig. 1c).

Additionally, we have studied the profile of selected proteins commonly deregulated in DBA and known to effect erythropoiesis to better understand the suppressive effect of mutant BYSL protein on DBA phenotype. Interestingly, the major difference observed after transfection of mutant *bysl* gene into U2OS cells was downregulation of c-Myc protein (Fig. 1d).

The major phenotype of DBA is a defect in erythropoiesis leading to reticulocytopenia [49], which means that during differentiation, pro-erythroblasts fail to exclude nucleolus. Reticulocytopenia is directly connected with c-Myc deregulation, inability of cells to supress c-Myc activity results in inefficient enucleation process [96]. To test whether mutated BYSL balances the RPL11 deficient DBA phenotype via regulation of c-Myc, we induced erythrocyte

differentiation in the K562 cell line by hemin [173] and analysed the impact of mutant BYSL on enucleation. As expected, the knockdown of RPL11 resulted in a drop in the number of cells with decreased DNA levels corresponding to enucleation failure. In contrast, mutant BYSL improves the number of RPL11 deficient (Fig. 11efg).

Our finding that mutant BYSL normalizes the c-Myc expression in RPL11 deficient cells may explain the mild erythropoietic phenotype in our patient and suggest *bystin* as a novel disease phenotype modifying gene in DBA. Based on our data we can also hypothesize BYSL may play broader and more important role in regulation of c-Myc dependent transcriptional activity in normal or cancer cells.

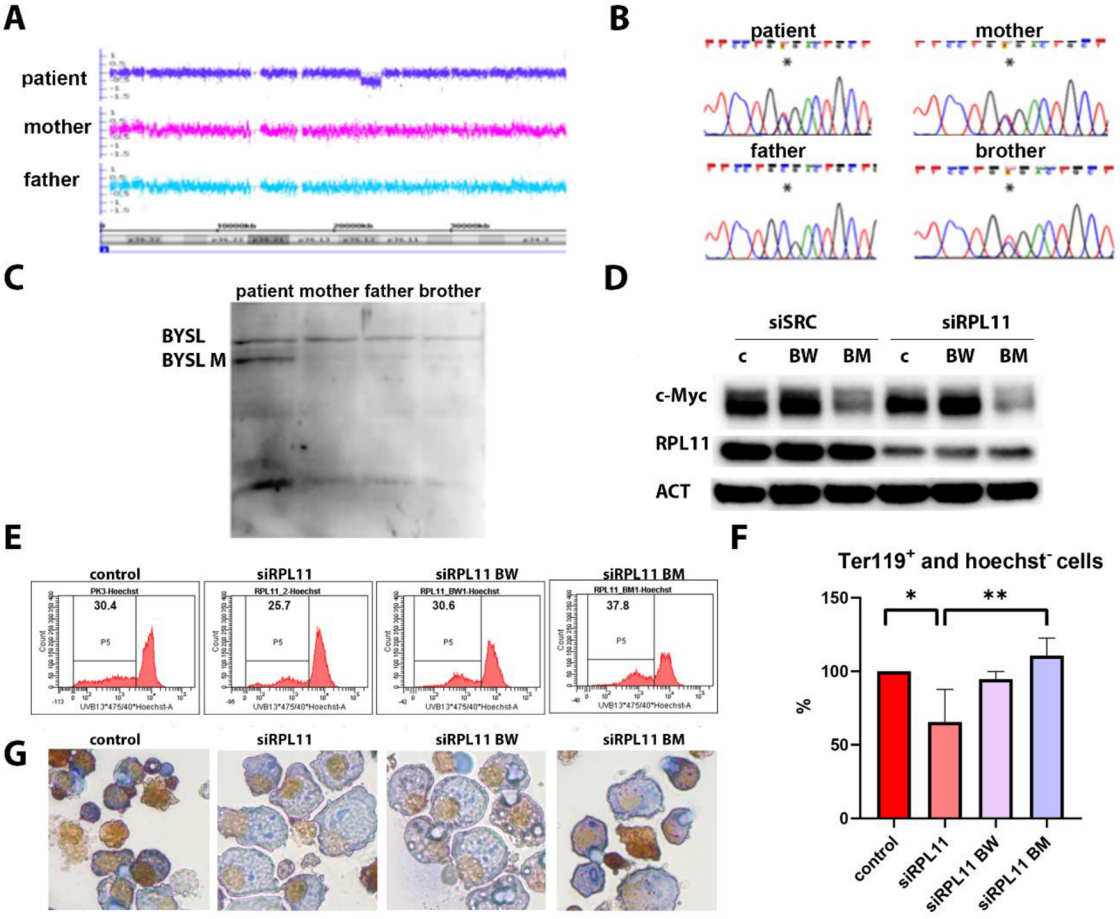

Figure 11: BYSL mutant protein compensates RPL11 depletion: A) Array CGH showed that our DBA patient was diagnosed with deletion on the first chromosome, including the RPL11 gene, B) Sanger sequencing of BYSL cDNA showed that patient,her mother and brother are carriers of mutant BYSL R343X, C) Western blot shows only the patient expresses mutant (truncated) BYSL protein, D) combination of mutant BYSL and RPL11 knockdown leads to normalization of c-Myc expression, E) combination of mutant BYSL and RPL11 knockdown leads to improvement of hemin induced erythroid differentiation of K562 cells, F) combination of mutant BYSL and RPL11

knockdown results in significantly increased number of Ter119^{+}, CD71$^{+,}$ and Hoechst^{-} cells compared to RPL11 knockdown alone, G) benzidine staining of hemoglobin producing differentiated cells showed combination of mutantBYSL and RPL11 knockdown leads to normalization of differentiation in hemin treated K562 cells.

3.3.2.2 BYSL regulates c-Myc through OAZ2 mediated proteasomal degradation

To better understand BYSL's role in c-Myc regulation, we used the BYSL knockdown model. This simple experiment revealed that siRNA knockdown of BYSL results in a decrease of c-Myc protein (Fig. 12a). Gene versus protein expression analysis of c-Myc in cells transfected with BYSL siRNA versus scrambled siRNA revealed both mRNA and protein levels are affected, however the decrease of protein levels was more significant (Fig. 12b).

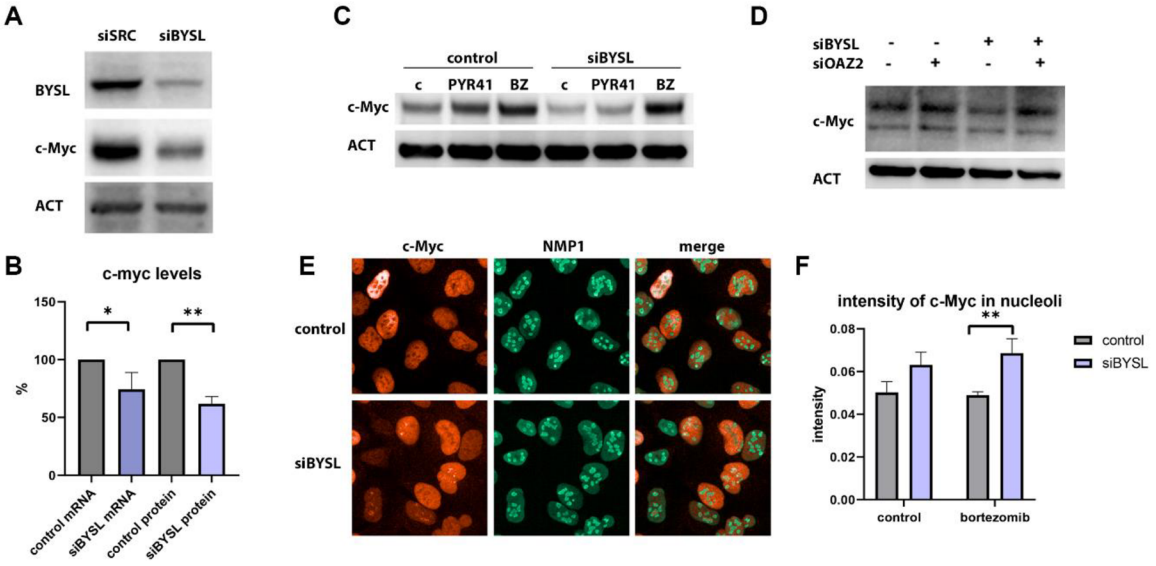

Fig. 12: BYSL regulates c-Myc predominantly on protein level: A) knock-down of BYSL leads to the distinct decrease of c-Myc protein level, B) knock-down of BYSL leads to more significant downregulation of c-Myc protein levels compared to mRNA levels, C) ubiquitination inhibitor PYR41 does not normalize protein c-Myc level upon BYSL knock-down compared to proteasome inhibitor bortezomib (BZ), D) knock-down of OAZ2 normalizes protein c-Myc levels in BYSL down-regulated U2OS cells, E) c-Myc translocate to the nucleolus (counterstained with anti-NMP1) of BYSL knock-down cells, F) translocation of c-Myc to the nucleolus is significantly increased in BYSL knock-down cells treated with bortezomib.

Because c-Myc is well known target of ubiquitin-dependent proteasome degradation, we inhibited proteasome by bortezomib and ubiquitination by PYR 41. Interestingly, results showed that although bortezomib increases c-Myc protein level in both control and BYSL

siRNA cells, PYR41 increases c-Myc protein level only in control cells (Fig. 12c). Furthermore, we noticed that upon BYSL siRNA, the c-Myc signal concentrates in the nucleolus compared to the control (Fig. 12e). C-Myc localization in the nucleolus was higher in BYSL siRNA cells, and the difference was significant when cells were treated with bortezomib (Fig. 12f). Those results cumulatively indicate BYSL mediated ubiquitin independent proteasome degradation of c-Myc in the nucleolus [174], which is a known space for c-Myc degradation. Recently, the novel ubiquitin-independent proteasome degradation mediator ornithine decarboxylase antizyme 2 (OAZ2) was described [175]. To test whether OAZ2 is involved in c-Myc degradation mediated via BYSL, we performed a double knockdown of BYSL and OAZ2. Results show that single OAZ2 knockdown of U2OS cells leads to slight increase in c-Myc level, but double knockdown results in high increase in c-Myc signal compared to BYSL knockdown alone (Fig. 12d). From all those observations, we conclude BYSL regulates c-Myc on protein levels via OAZ2 mediated proteasomal degradation.

3.3.2.3 BYSL is a target during glucocorticosteroid treatment in DBA

Because we assumed that BYSL improves DBA phenotype via c-Myc regulation, and since glucocorticosteroids (GCs) are a standard treatment available for DBA patients, however with an unknown mechanism of action [176], we tested effect of GCs on c-Myc and BYSL expression and function. In older publications, corticosteroids were reported to decrease c-Myc mRNA levels in leukemia cells [135]. We used dexamethasone as GCs representative on U2OS cells and did not observe any decrease in c-Myc mRNA level (Fig. 13b). Although corticosteroids did not reduce c-Myc mRNA level, on contrary it was increased 24 hours post treatment, we detected significant decrease in c-Myc protein level (Fig. 13a). One of the possibilities was that dexamethasone binds to the BYSL protein and mimicks (inhibits) its ability to bind and protect c-Myc from degradation. Indeed, hypothesis was independently confirmed by both ITC indicating specific binding of dexamethasone to recombinant BYSL protein (Fig. 13c) and molecular dynamic modelling on BYSL interaction with dexamethasone scaffold (Fig. 13de). Interestingly, the putative binding site of dexamethasone on BYSL was localized on C-terminal part of the protein, which is absent in BYSL mutant identified in our DBA patient, thus indirectly confirming the importance of BYSL C-terminus for c-Myc interaction.

Direct evidence that dexamethasone regulates c-Myc through BYSL came from immunoprecipitation experiments of cells (un)treated with dexamethasone. After 24 hours,

dexamethasone significantly decreased the amount of BYSL bound to c-Myc and subsequently increased its binding to OAZ2 (Fig. 13f-h). This observation together with isothermal calorimetry and molecular dynamic data indicate dexamethasone binds to BYSL in the c-Myc binding site and prevents interaction of both proteins, thus targeting c-Myc to OAZ2 dependent proteasomal degradation.

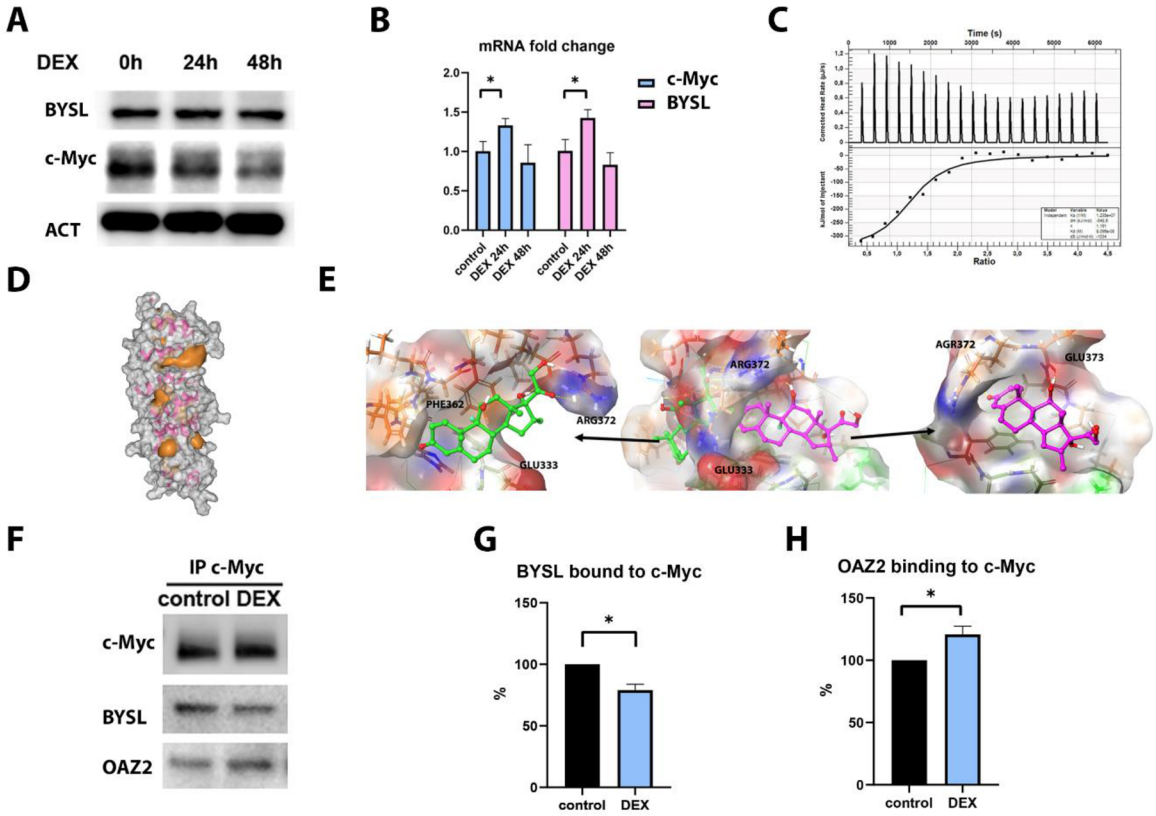

Fig.13: Corticosteroid dexamethasone directly interacts with BYSL, prevents BYSL-c-Myc interaction, thus targeting c-Myc to OAZ2 dependent degradation: A) DEX induced reduction of c-Myc protein levels is not due to decreased c-Myc gene transcription B) Dexamethasone (DEX) treatment of U2OS cells results in reduced c-Myc protein levels, C) ITC results indicate direct dexamethasone binding to BYSL, D) BYSL structure after replica exchange with binding sites detected by DeepSite, E) two stable binding poses of dexamethasone around ARG372, F), G), H) c-Myc immunoprecipitation experiments indicate reduced binding of BYSL to c-Myc and increased association with OAZ2 upon 24-hour treatment with DEX.

3.3.3 Discussion

Rare diseases are great models for basic molecular mechanisms studies[177]. DBA arises from RPs aberrations and helps us understand the roles of RPs beyond ribosome building blocks and to reveal the importance of RPs as stress detectors and regulators [31, 125, 178].

Furthermore, a novel expression regulation mechanism with great impact in cell biology was discovered exploiting DBA models – specialized ribosomes [45].

RPL11 alteration is known cause of DBA [165]. Moreover, RPL11 and RPL5 are superior to other RPs in ribosomal stress signalling capability [23]. It was shown that the loss of one allele of RPL11 led to failure in embryogenesis [33]. Interestingly, we diagnosed one patient with deletion of the whole RPL11 locus in our DBA registry. That led us to the hypothesis that some variants in other disease modifying genes may compensate for the RPL11 deficiency and lead to successful in-utero development of the patient and relatively mild form of DBA. We analysed WES data and found an interesting nonsense mutation in the BYSL gene, which results in expression of C-terminus truncated protein. Furthermore, although this variant was detected on mRNA in asymptomatic patient´s family members with normal RPL11 status, aberrated BYSL protein was expressed only in the DBA patient. Further experiments revealed that RPL11 depletion stabilizes BYSL mutated protein.

When we searched for the mechanism of DBA phenotype modification mediated by mutant BYSL, found C-terminus truncated BYSL compensated RPL11 mediated c-Myc upregulation. Furthermore, mutant BYSL significantly improved hemin induced erythroid differentiation K562 cells. The fact that mutated BYSL leads to c-Myc downregulation and erythropoiesis improvement suggests BYSL as the first DBA phenotype modifying gene.

In general, BYSL is a poorly understood structural protein of the nucleolus[144]. The nucleolus is known to play a key role in c-Myc turnover [174], and some nucleolar proteins regulate c-Myc to control ribosome production [174]. Moreover, nucleolus also controls c-Myc compartmentalization and degradation by proteasome [174]. As mutat BYSL controlled c-Myc protein levels in our model of RPL11 deficient cells, we further explored the relationship between c-Myc and BYSL. We discovered BYSL regulates c-Myc protein levels via ubiquitin-independent proteasomal mediated degradation in nucleolus mediated by OAZ2 [175]. Thus, our data also highlight BYSL as a novel modulator of c-Myc and putative target for novel therapies targeting c-Myc-dependent pathologies across several disorders, including cancer.

GCs are used to treat numerous disorders, including DBA [49] and cancers [120]. Because GCs regulate a broad range of cellular responses, their mechanism of action in individual pathologies remain poorly understood. Here we show that dexamethasone, one of the most

frequently used GCs in the clinic, binds to BYSL protein C- terminus, which is truncated in our RPL11 deficient DBA patient. Binding of DEX prevents protective interaction of BYSL and c-Myc, which is in turn subjected to OAZ2 mediated proteasomal degradation. We can assume that GCs may via binding to bystin regulate c-Myc level during the process of erythropoiesis and facilitate enucleation of DBA erythroid progenitors. Our research elucidates the mechanism of action of GCs in DBA and highlights BYSL as an interesting target for treatment of DBA patients and other c-Myc related disorders.

Altogether, we propose a new target to mitigate phenotypes connected with deregulated oncogene c-Myc. Importantly, c-Myc is a so-called undruggable target protein because of its structure [179]. Therefore, finding its targetable regulators may lead to discovery new therapeutic opportunities for other disorders. For example, GCs are used nowadays to treat a broad range of c-Myc-driven cancers [167]. The precise mechanism of action of GCs in these cancers is not fully understood [167], but our work suggests GCs may indirectly regulate c-Myc via inhibition of interaction with BYSL.

4 Conclusion

In this work, we focused on the role of the nucleolus in the cell. We explored its structure, nucleolar stress induction, and ribosomal disorders known to affect structure and function of the nucleolus. We have specifically focused on DBA, which is congenital rare anemia originating in ribosomal protein aberration, and the role of glucocorticosteroids in the disease management.

In the experimental part, we evaluated the impact of L-OHP and V134F RPS7 mutation on the structure of nucleoli. We revealed that both conditions impact structure, rRNA production or processing, and ribosome biogenesis.

Next, we identified *Bystin* as the first disease-modifying gene in DBA. Furthermore, we determined that BYSL modulates DBA pathology through direct interaction with c-Myc and regulation c-Myc protein stability. We also proved that BYSL is molecular target during dexamethasone treatment of DBA. We have employed various *in silico* modelling methods, physical and biochemical techniques to validate BYSL interaction with dexamethasone. Future studies should evaluate the role of BYSL in modulation of DBA pathologies other than caused by RPL11 deficiency and develop small molecular inhibitors of BYSL and c-Myc interaction

lacking corticosteroid side effects to improve erythroid differentiation and decrease cancer risk in DBA patients.

5 List of important abbreviations

5S RNP -5S ribonucleoprotein

BFU-E – burst forming unit-erythroid

CFU-E - colony-forming unit-erythroid

DBA – Diamond Blackfan anemia

DFC - dense fibrillary center

FC - fibrillar centers

GC – glucocrticosteroid

Gc – granular component

GCR – glucocrticosteroid receptor

ICA - isolated congenital asplenia

L-OHP - oxaliplatin

NOR - nucleolus organizer region

RBC – red blood cells

rDNA – ribosomal DNA

RP – ribosomal protein

RPL – ribosomal protein of large subunit

RPS - ribosomal protein of large subunit

rRNA – ribosomal RNA

ROS – reactive oxidative species

WT – wild type

6 References

1. Rudra, D. and J.R. Warner, *What better measure than ribosome synthesis?* Genes Dev, 2004. **18**(20): p. 2431-6.
2. Tiku, V. and A. Antebi, *Nucleolar Function in Lifespan Regulation.* Trends Cell Biol, 2018. **28**(8): p. 662-672.
3. Yang, K., J. Yang, and J. Yi, *Nucleolar Stress: hallmarks, sensing mechanism and diseases.* Cell Stress, 2018. **2**(6): p. 125-140.
4. Raska, I., P.J. Shaw, and D. Cmarko, *New insights into nucleolar architecture and activity.* Int Rev Cytol, 2006. **255**: p. 177-235.
5. McStay, B., *Nucleolar organizer regions: genomic 'dark matter' requiring illumination.* Genes Dev, 2016. **30**(14): p. 1598-610.
6. Henras, A.K., et al., *The post-transcriptional steps of eukaryotic ribosome biogenesis.* Cell Mol Life Sci, 2008. **65**(15): p. 2334-59.
7. Ciganda, M. and N. Williams, *Eukaryotic 5S rRNA biogenesis.* Wiley Interdiscip Rev RNA, 2011. **2**(4): p. 523-33.
8. Derenzini, M., et al., *Structural and functional organization of ribosomal genes within the mammalian cell nucleolus.* J Histochem Cytochem, 2006. **54**(2): p. 131-45.
9. Fatica, A., et al., *Fibrillarin binds directly and specifically to U16 box C/D snoRNA.* Rna, 2000. **6**(1): p. 88-95.
10. Zemp, I. and U. Kutay, *Nuclear export and cytoplasmic maturation of ribosomal subunits.* FEBS Lett, 2007. **581**(15): p. 2783-93.
11. Farley, K.I., et al., *Determinants of mammalian nucleolar architecture.* Chromosoma, 2015. **124**(3): p. 323-31.
12. Spahn, C.M., et al., *Structure of the 80S ribosome from Saccharomyces cerevisiae--tRNA-ribosome and subunit-subunit interactions.* Cell, 2001. **107**(3): p. 373-86.
13. Scherl, A., et al., *Functional proteomic analysis of human nucleolus.* Mol Biol Cell, 2002. **13**(11): p. 4100-9.
14. Lindström, M.S., et al., *Nucleolus as an emerging hub in maintenance of genome stability and cancer pathogenesis.* Oncogene, 2018. **37**(18): p. 2351-2366.
15. Popławski, P. and J. Bogusławska, *Nucleolar Proteins and Non-Coding RNAs: Roles in Renal Cancer.* 2021. **22**(23).
16. Mamontova, V., B. Trifault, and L. Boten, *Commuting to Work: Nucleolar Long Non-Coding RNA Control Ribosome Biogenesis from Near and Far.* 2021. **7**(3).
17. Rubbi, C.P. and J. Milner, *Disruption of the nucleolus mediates stabilization of p53 in response to DNA damage and other stresses.* Embo j, 2003. **22**(22): p. 6068-77.
18. James, A., et al., *Nucleolar stress with and without p53.* Nucleus, 2014. **5**(5): p. 402-26.
19. Turi, Z., et al., *Impaired ribosome biogenesis: mechanisms and relevance to cancer and aging.* Aging (Albany NY), 2019. **11**(8): p. 2512-2540.
20. Boulon, S., et al., *The nucleolus under stress.* Mol Cell, 2010. **40**(2): p. 216-27.
21. Hadjiolova, K.V., A.A. Hadjiolov, and J.P. Bachellerie, *Actinomycin D stimulates the transcription of rRNA minigenes transfected into mouse cells. Implications for the in vivo hypersensitivity of rRNA gene transcription.* Eur J Biochem, 1995. **228**(3): p. 605-15.
22. Burger, K., et al., *Chemotherapeutic drugs inhibit ribosome biogenesis at various levels.* J Biol Chem, 2010. **285**(16): p. 12416-25.

23. Nicolas, E., et al., *Involvement of human ribosomal proteins in nucleolar structure and p53-dependent nucleolar stress.* Nat Commun, 2016. **7**: p. 11390.
24. Marechal, V., et al., *The ribosomal L5 protein is associated with mdm-2 and mdm-2-p53 complexes.* Mol Cell Biol, 1994. **14**(11): p. 7414-20.
25. Sloan, K.E., M.T. Bohnsack, and N.J. Watkins, *The 5S RNP couples p53 homeostasis to ribosome biogenesis and nucleolar stress.* Cell Rep, 2013. **5**(1): p. 237-47.
26. Sung, M.K., et al., *Ribosomal proteins produced in excess are degraded by the ubiquitin-proteasome system.* Mol Biol Cell, 2016. **27**(17): p. 2642-52.
27. Zheng, J., et al., *Structure of human MDM2 complexed with RPL11 reveals the molecular basis of p53 activation.* Genes Dev, 2015. **29**(14): p. 1524-34.
28. Holmberg Olausson, K., M. Nistér, and M.S. Lindström, *p53 -Dependent and -Independent Nucleolar Stress Responses.* Cells, 2012. **1**(4): p. 774-98.
29. Duffy, M.J., et al., *MYC as a target for cancer treatment.* Cancer Treat Rev, 2021. **94**: p. 102154.
30. van Riggelen, J., A. Yetil, and D.W. Felsher, *MYC as a regulator of ribosome biogenesis and protein synthesis.* Nat Rev Cancer, 2010. **10**(4): p. 301-9.
31. Liao, J.M., et al., *Ribosomal proteins L5 and L11 co-operatively inactivate c-Myc via RNA-induced silencing complex.* Oncogene, 2014. **33**(41): p. 4916-23.
32. Zhou, X., et al., *Ribosomal protein S14 negatively regulates c-Myc activity.* J Biol Chem, 2013. **288**(30): p. 21793-801.
33. Morgado-Palacin, L., et al., *Partial Loss of Rpl11 in Adult Mice Recapitulates Diamond-Blackfan Anemia and Promotes Lymphomagenesis.* Cell Rep, 2015. **13**(4): p. 712-722.
34. Stanborough, T., et al., *Ribosomal protein S3 interacts with the NF-κB inhibitor IκBα.* FEBS Lett, 2014. **588**(5): p. 659-64.
35. Diao, M.Q., et al., *RPS27, a sORF-Encoded Polypeptide, Functions Antivirally by Activating the NF-κB Pathway and Interacting With Viral Envelope Proteins in Shrimp.* Front Immunol, 2019. **10**: p. 2763.
36. Rao, S., et al., *Ribosomal Protein Rpl22 Controls the Dissemination of T-cell Lymphoma.* Cancer Res, 2016. **76**(11): p. 3387-96.
37. Donati, G., et al., *Selective inhibition of rRNA transcription downregulates E2F-1: a new p53-independent mechanism linking cell growth to cell proliferation.* J Cell Sci, 2011. **124**(Pt 17): p. 3017-28.
38. Iadevaia, V., et al., *PIM1 kinase is destabilized by ribosomal stress causing inhibition of cell cycle progression.* Oncogene, 2010. **29**(40): p. 5490-9.
39. Morscio, J., D. Dierickx, and T. Tousseyn, *Molecular pathogenesis of B-cell posttransplant lymphoproliferative disorder: what do we know so far?* Clin Dev Immunol, 2013. **2013**: p. 150835.
40. Russo, A., et al., *Human rpL3 induces G_1/S arrest or apoptosis by modulating p21 (waf1/cip1) levels in a p53-independent manner.* Cell Cycle, 2013. **12**(1): p. 76-87.
41. Goudarzi, K.M. and M.S. Lindström, *Role of ribosomal protein mutations in tumor development (Review).* Int J Oncol, 2016. **48**(4): p. 1313-24.
42. Kang, J., et al., *Ribosomal proteins and human diseases: molecular mechanisms and targeted therapy.* Signal Transduct Target Ther, 2021. **6**(1): p. 323.
43. Bastide, A. and A. David, *The ribosome, (slow) beating heart of cancer (stem) cell.* Oncogenesis, 2018. **7**(4): p. 34.
44. Xue, S. and M. Barna, *Specialized ribosomes: a new frontier in gene regulation and organismal biology.* Nat Rev Mol Cell Biol, 2012. **13**(6): p. 355-69.

45. Kondrashov, N., et al., *Ribosome-mediated specificity in Hox mRNA translation and vertebrate tissue patterning.* Cell, 2011. **145**(3): p. 383-397.
46. Griffin, J.N., et al., *RPSA, a candidate gene for isolated congenital asplenia, is required for pre-rRNA processing and spleen formation in Xenopus.* 2018. **145**(20).
47. Zhang, Y., et al., *Control of hematopoietic stem cell emergence by antagonistic functions of ribosomal protein paralogs.* Dev Cell, 2013. **24**(4): p. 411-25.
48. Ferretti, M.B., et al., *Rps26 directs mRNA-specific translation by recognition of Kozak sequence elements.* 2017. **24**(9): p. 700-707.
49. Vlachos, A. and E. Muir, *How I treat Diamond-Blackfan anemia.* Blood, 2010. **116**(19): p. 3715-23.
50. Vlachos, A., et al., *Diagnosing and treating Diamond Blackfan anaemia: results of an international clinical consensus conference.* Br J Haematol, 2008. **142**(6): p. 859-76.
51. Glader, B.E. and K. Backer, *Elevated red cell adenosine deaminase activity: a marker of disordered erythropoiesis in Diamond-Blackfan anaemia and other haematologic diseases.* Br J Haematol, 1988. **68**(2): p. 165-8.
52. Draptchinskaia, N., et al., *The gene encoding ribosomal protein S19 is mutated in Diamond-Blackfan anaemia.* Nat Genet, 1999. **21**(2): p. 169-75.
53. Pospisilova, D., et al., *The Czech National Diamond-Blackfan Anemia Registry: clinical data and ribosomal protein mutations update.* Blood Cells Mol Dis, 2012. **48**(4): p. 209-18.
54. Danilova, N. and H.T. Gazda, *Ribosomopathies: how a common root can cause a tree of pathologies.* Dis Model Mech, 2015. **8**(9): p. 1013-26.
55. Angelini, M., et al., *Missense mutations associated with Diamond-Blackfan anemia affect the assembly of ribosomal protein S19 into the ribosome.* Hum Mol Genet, 2007. **16**(14): p. 1720-7.
56. Caterino, M., et al., *Analysis of the interactome of ribosomal protein S19 mutants.* Proteomics, 2014. **14**(20): p. 2286-96.
57. Uechi, T., et al., *Deficiency of ribosomal protein S19 during early embryogenesis leads to reduction of erythrocytes in a zebrafish model of Diamond-Blackfan anemia.* Hum Mol Genet, 2008. **17**(20): p. 3204-11.
58. Zhang, Y., et al., *Defects of protein production in erythroid cells revealed in a zebrafish Diamond-Blackfan anemia model for mutation in RPS19.* Cell Death Dis, 2014. **5**(7): p. e1352.
59. Devlin, E.E., et al., *A transgenic mouse model demonstrates a dominant negative effect of a point mutation in the RPS19 gene associated with Diamond-Blackfan anemia.* Blood, 2010. **116**(15): p. 2826-35.
60. Chae, H., et al., *Ribosomal protein mutations in Korean patients with Diamond-Blackfan anemia.* Exp Mol Med, 2014. **46**(3): p. e88.
61. Carlston, C.M., et al., *Variable expressivity and incomplete penetrance in a large family with non-classical Diamond-Blackfan anemia associated with ribosomal protein L11 splicing variant.* 2017. **173**(10): p. 2622-2627.
62. Ebert, B.L., et al., *Identification of RPS14 as a 5q- syndrome gene by RNA interference screen.* Nature, 2008. **451**(7176): p. 335-9.
63. Yelick, P.C. and P.A. Trainor, *Ribosomopathies: Global process, tissue specific defects.* Rare Dis, 2015. **3**(1): p. e1025185.
64. Bolze, A., et al., *Ribosomal protein SA haploinsufficiency in humans with isolated congenital asplenia.* Science, 2013. **340**(6135): p. 976-8.

65. Cmejlova, J., et al., *Translational efficiency in patients with Diamond-Blackfan anemia.* Haematologica, 2006. **91**(11): p. 1456-64.
66. Horos, R., et al., *Ribosomal deficiencies in Diamond-Blackfan anemia impair translation of transcripts essential for differentiation of murine and human erythroblasts.* Blood, 2012. **119**(1): p. 262-72.
67. Götz, R., et al., *Bag1 is essential for differentiation and survival of hematopoietic and neuronal cells.* Nat Neurosci, 2005. **8**(9): p. 1169-78.
68. Boultwood, J. and A. Pellagatti, *Reduced translation of GATA1 in Diamond-Blackfan anemia.* Nat Med, 2014. **20**(7): p. 703-4.
69. Gutiérrez, L., et al., *Regulation of GATA1 levels in erythropoiesis.* IUBMB Life, 2020. **72**(1): p. 89-105.
70. Akiyama, M., et al., *Successful treatment of Diamond-Blackfan anemia with metoclopramide.* Am J Hematol, 2005. **78**(4): p. 295-8.
71. Ribeil, J.A., et al., *Hsp70 regulates erythropoiesis by preventing caspase-3-mediated cleavage of GATA-1.* Nature, 2007. **445**(7123): p. 102-5.
72. Sankaran, V.G., et al., *Exome sequencing identifies GATA1 mutations resulting in Diamond-Blackfan anemia.* J Clin Invest, 2012. **122**(7): p. 2439-43.
73. Klar, J., et al., *Recurrent GATA1 mutations in Diamond-Blackfan anaemia.* Br J Haematol, 2014. **166**(6): p. 949-51.
74. Zhou, X., et al., *Inhibition of red blood cell development by arsenic-induced disruption of GATA-1.* Sci Rep, 2020. **10**(1): p. 19055.
75. Iskander, D. and G. Wang, *Single-cell profiling of human bone marrow progenitors reveals mechanisms of failing erythropoiesis in Diamond-Blackfan anemia.* 2021. **13**(610): p. eabf0113.
76. Cheng, Z., et al., *Small and Large Ribosomal Subunit Deficiencies Lead to Distinct Gene Expression Signatures that Reflect Cellular Growth Rate.* Mol Cell, 2019. **73**(1): p. 36-47.e10.
77. Matoba, S., et al., *p53 regulates mitochondrial respiration.* Science, 2006. **312**(5780): p. 1650-3.
78. Danilova, N., K.M. Sakamoto, and S. Lin, *Ribosomal protein L11 mutation in zebrafish leads to haematopoietic and metabolic defects.* Br J Haematol, 2011. **152**(2): p. 217-28.
79. Zhang, J., et al., *Autophagy as a regulatory component of erythropoiesis.* Int J Mol Sci, 2015. **16**(2): p. 4083-94.
80. Grosso, R., C.M. Fader, and M.I. Colombo, *Autophagy: A necessary event during erythropoiesis.* Blood Rev, 2017. **31**(5): p. 300-305.
81. Kang, Y.A., et al., *Autophagy driven by a master regulator of hematopoiesis.* Mol Cell Biol, 2012. **32**(1): p. 226-39.
82. Dunlop, E.A. and A.R. Tee, *mTOR and autophagy: a dynamic relationship governed by nutrients and energy.* Semin Cell Dev Biol, 2014. **36**: p. 121-9.
83. Knight, Z.A., et al., *A critical role for mTORC1 in erythropoiesis and anemia.* Elife, 2014. **3**: p. e01913.
84. Yang, Z., et al., *Delayed globin synthesis leads to excess heme and the macrocytic anemia of Diamond Blackfan anemia and del(5q) myelodysplastic syndrome.* Sci Transl Med, 2016. **8**(338): p. 338ra67.

85. Liu, Q., et al., *The opposing roles of the mTOR signaling pathway in different phases of human umbilical cord blood-derived CD34(+) cell erythropoiesis.* Stem Cells, 2020. **38**(11): p. 1492-1505.
86. Heijnen, H.F., et al., *Ribosomal protein mutations induce autophagy through S6 kinase inhibition of the insulin pathway.* PLoS Genet, 2014. **10**(5): p. e1004371.
87. Chauvin, C., et al., *Ribosomal protein S6 kinase activity controls the ribosome biogenesis transcriptional program.* Oncogene, 2014. **33**(4): p. 474-83.
88. Pospisilova, D., et al., *Successful treatment of a Diamond-Blackfan anemia patient with amino acid leucine.* Haematologica, 2007. **92**(5): p. e66-7.
89. Payne, E.M., et al., *L-Leucine improves the anemia and developmental defects associated with Diamond-Blackfan anemia and del(5q) MDS by activating the mTOR pathway.* Blood, 2012. **120**(11): p. 2214-24.
90. Doulatov, S., et al., *Drug discovery for Diamond-Blackfan anemia using reprogrammed hematopoietic progenitors.* Sci Transl Med, 2017. **9**(376).
91. Kapralova, K., et al., *Oxidative DNA Damage, Inflammatory Signature, and Altered Erythrocytes Properties in Diamond-Blackfan Anemia.* 2020. **21**(24).
92. Brumwell, A., et al., *Hypoxia influences polysome distribution of human ribosomal protein S12 and alternative splicing of ribosomal protein mRNAs.* Rna, 2020. **26**(3): p. 361-371.
93. Sarkar, S., *Regulation of autophagy by mTOR-dependent and mTOR-independent pathways: autophagy dysfunction in neurodegenerative diseases and therapeutic application of autophagy enhancers.* Biochem Soc Trans, 2013. **41**(5): p. 1103-30.
94. Malik, N., et al., *mTORC1 activity is essential for erythropoiesis and B cell lineage commitment.* Sci Rep, 2019. **9**(1): p. 16917.
95. Naithani, R., et al., *Diamond-Blackfan anemia: clinical features and treatment results in 4 cases.* Hematology, 2006. **11**(3): p. 193-5.
96. Jayapal, S.R., et al., *Down-regulation of Myc is essential for terminal erythroid maturation.* J Biol Chem, 2010. **285**(51): p. 40252-65.
97. Quarello, P., et al., *Diamond-Blackfan anemia: genotype-phenotype correlations in Italian patients with RPL5 and RPL11 mutations.* Haematologica, 2010. **95**(2): p. 206-13.
98. Oršolić, I., et al., *Cancer-associated mutations in the ribosomal protein L5 gene dysregulate the HDM2/p53-mediated ribosome biogenesis checkpoint.* 2020. **39**(17): p. 3443-3457.
99. Ajore, R., et al., *Deletion of ribosomal protein genes is a common vulnerability in human cancer, especially in concert with TP53 mutations.* 2017. **9**(4): p. 498-507.
100. Li, J., et al., *Ferroptosis: past, present and future.* Cell Death Dis, 2020. **11**(2): p. 88.
101. Ramamoorthy, S. and J.A. Cidlowski, *Corticosteroids: Mechanisms of Action in Health and Disease.* Rheum Dis Clin North Am, 2016. **42**(1): p. 15-31, vii.
102. Lossignol, D., *A little help from steroids in oncology.* J Transl Int Med, 2016. **4**(1): p. 52-54.
103. Schäcke, H., W.D. Döcke, and K. Asadullah, *Mechanisms involved in the side effects of glucocorticoids.* Pharmacol Ther, 2002. **96**(1): p. 23-43.
104. Grad, I. and D. Picard, *The glucocorticoid responses are shaped by molecular chaperones.* Mol Cell Endocrinol, 2007. **275**(1-2): p. 2-12.
105. Lamberts, S.W., et al., *Clinical aspects of glucocorticoid sensitivity.* Steroids, 1996. **61**(4): p. 157-60.

106. John, S., et al., *Chromatin accessibility pre-determines glucocorticoid receptor binding patterns.* Nat Genet, 2011. **43**(3): p. 264-8.
107. Samarasinghe, R.A., S.F. Witchell, and D.B. DeFranco, *Cooperativity and complementarity: synergies in non-classical and classical glucocorticoid signaling.* Cell Cycle, 2012. **11**(15): p. 2819-27.
108. Chang, T.J., et al., *Inhibition of mouse GATA-1 function by the glucocorticoid receptor: possible mechanism of steroid inhibition of erythroleukemia cell differentiation.* Mol Endocrinol, 1993. **7**(4): p. 528-42.
109. Lu, N.Z. and J.A. Cidlowski, *The origin and functions of multiple human glucocorticoid receptor isoforms.* Ann N Y Acad Sci, 2004. **1024**: p. 102-23.
110. Koper, J.W., E.F. van Rossum, and E.L. van den Akker, *Glucocorticoid receptor polymorphisms and haplotypes and their expression in health and disease.* Steroids, 2014. **92**: p. 62-73.
111. Jewell, C.M. and J.A. Cidlowski, *Molecular evidence for a link between the N363S glucocorticoid receptor polymorphism and altered gene expression.* J Clin Endocrinol Metab, 2007. **92**(8): p. 3268-77.
112. van Rossum, E.F. and S.W. Lamberts, *Polymorphisms in the glucocorticoid receptor gene and their associations with metabolic parameters and body composition.* Recent Prog Horm Res, 2004. **59**: p. 333-57.
113. Lonetti, A., et al., *The Glucocorticoid Receptor Polymorphism Landscape in Patients With Diamond Blackfan Anemia Reveals an Association Between Two Clinically Relevant Single Nucleotide Polymorphisms and Time to Diagnosis.* Front Physiol, 2021. **12**: p. 745032.
114. Ludwig, L.S., et al., *Altered translation of GATA1 in Diamond-Blackfan anemia.* Nat Med, 2014. **20**(7): p. 748-53.
115. Long, W., L. Wei, and E.J. Barrett, *Dexamethasone inhibits the stimulation of muscle protein synthesis and PHAS-I and p70 S6-kinase phosphorylation.* Am J Physiol Endocrinol Metab, 2001. **280**(4): p. E570-5.
116. Yu, J., et al., *The Effects of Venlafaxine and Dexamethasone on the Expression of HSP70 in Rat C6 Glioma Cells.* Psychiatry Investig, 2010. **7**(1): p. 43-8.
117. Paulson, R.F., S. Hariharan, and J.A. Little, *Stress erythropoiesis: definitions and models for its study.* Exp Hematol, 2020. **89**: p. 43-54.e2.
118. Malgor, L.A., et al., *Effects of dexamethasone on bone marrow erythropoiesis.* Horm Res, 1974. **5**(5): p. 269-77.
119. Zhao, W., et al., *Erythropoietin stimulates phosphorylation and activation of GATA-1 via the PI3-kinase/AKT signaling pathway.* Blood, 2006. **107**(3): p. 907-15.
120. Sjögren, S.E. and J. Flygare, *Progress towards mechanism-based treatment for Diamond-Blackfan anemia.* ScientificWorldJournal, 2012. **2012**: p. 184362.
121. Bauer, A., et al., *The glucocorticoid receptor is required for stress erythropoiesis.* Genes Dev, 1999. **13**(22): p. 2996-3002.
122. Hattangadi, S.M., et al., *From stem cell to red cell: regulation of erythropoiesis at multiple levels by multiple proteins, RNAs, and chromatin modifications.* Blood, 2011. **118**(24): p. 6258-68.
123. Flygare, J., et al., *HIF1alpha synergizes with glucocorticoids to promote BFU-E progenitor self-renewal.* Blood, 2011. **117**(12): p. 3435-44.
124. Russo, A. and G. Russo, *Ribosomal Proteins Control or Bypass p53 during Nucleolar Stress.* Int J Mol Sci, 2017. **18**(1).

125. Le Goff, S., et al., *p53 activation during ribosome biogenesis regulates normal erythroid differentiation.* Blood, 2021. **137**(1): p. 89-102.
126. Danilova, N., et al., *The role of the DNA damage response in zebrafish and cellular models of Diamond Blackfan anemia.* Dis Model Mech, 2014. **7**(7): p. 895-905.
127. Li, H., et al., *Glucocorticoid receptor and sequential P53 activation by dexamethasone mediates apoptosis and cell cycle arrest of osteoblastic MC3T3-E1 cells.* PLoS One, 2012. **7**(6): p. e37030.
128. Sengupta, S., et al., *Negative cross-talk between p53 and the glucocorticoid receptor and its role in neuroblastoma cells.* Embo j, 2000. **19**(22): p. 6051-64.
129. Rio, S., et al., *Regulation of globin-heme balance in Diamond-Blackfan anemia by HSP70/GATA1.* Blood, 2019. **133**(12): p. 1358-1370.
130. Sanner, B.M., et al., *Effects of glucocorticoids on generation of reactive oxygen species in platelets.* Steroids, 2002. **67**(8): p. 715-9.
131. Gerö, D. and C. Szabo, *Glucocorticoids Suppress Mitochondrial Oxidant Production via Upregulation of Uncoupling Protein 2 in Hyperglycemic Endothelial Cells.* PLoS One, 2016. **11**(4): p. e0154813.
132. Dandona, P., et al., *Effect of dexamethasone on reactive oxygen species generation by leukocytes and plasma interleukin-10 concentrations: a pharmacodynamic study.* Clin Pharmacol Ther, 1999. **66**(1): p. 58-65.
133. Chen, L., et al., *Proanthocyanidins-Mediated Nrf2 Activation Ameliorates Glucocorticoid-Induced Oxidative Stress and Mitochondrial Dysfunction in Osteoblasts.* Oxid Med Cell Longev, 2020. **2020**: p. 9102012.
134. Sjögren, S.E., et al., *Glucocorticoids improve erythroid progenitor maintenance and dampen Trp53 response in a mouse model of Diamond-Blackfan anaemia.* Br J Haematol, 2015. **171**(4): p. 517-29.
135. Zhou, F., R.D. Medh, and E.B. Thompson, *Glucocorticoid mediated transcriptional repression of c-myc in apoptotic human leukemic CEM cells.* J Steroid Biochem Mol Biol, 2000. **73**(5): p. 195-202.
136. Ausserlechner, M.J., et al., *Cyclin D3 and c-MYC control glucocorticoid-induced cell cycle arrest but not apoptosis in lymphoblastic leukemia cells.* Cell Death Differ, 2004. **11**(2): p. 165-74.
137. Shimizu, N., et al., *Crosstalk between glucocorticoid receptor and nutritional sensor mTOR in skeletal muscle.* Cell Metab, 2011. **13**(2): p. 170-82.
138. Fu, L., et al., *Glucocorticoids Enhanced Osteoclast Autophagy Through the PI3K/Akt/mTOR Signaling Pathway.* Calcif Tissue Int, 2020. **107**(1): p. 60-71.
139. Polman, J.A., et al., *Glucocorticoids modulate the mTOR pathway in the hippocampus: differential effects depending on stress history.* Endocrinology, 2012. **153**(9): p. 4317-27.
140. Pan, J.M., et al., *Dexamethasone suppresses osteogenesis of osteoblast via the PI3K/Akt signaling pathway in vitro and in vivo.* J Recept Signal Transduct Res, 2019. **39**(1): p. 80-86.
141. Ashley, R.J., et al., *Steroid resistance in Diamond Blackfan anemia associates with p57Kip2 dysregulation in erythroid progenitors.* J Clin Invest, 2020. **130**(4): p. 2097-2110.
142. Adcock, I.M. and P.J. Barnes, *Molecular mechanisms of corticosteroid resistance.* Chest, 2008. **134**(2): p. 394-401.

143. Samuelsson, M.K., et al., *p57Kip2, a glucocorticoid-induced inhibitor of cell cycle progression in HeLa cells.* Mol Endocrinol, 1999. **13**(11): p. 1811-22.
144. Adachi, K., et al., *Crucial role of Bysl in mammalian preimplantation development as an integral factor for 40S ribosome biogenesis.* Mol Cell Biol, 2007. **27**(6): p. 2202-14.
145. Suzuki, N., et al., *A cytoplasmic protein, bystin, interacts with trophinin, tastin, and cytokeratin and may be involved in trophinin-mediated cell adhesion between trophoblast and endometrial epithelial cells.* Proc Natl Acad Sci U S A, 1998. **95**(9): p. 5027-32.
146. Carron, C., et al., *Analysis of two human pre-ribosomal factors, bystin and hTsr1, highlights differences in evolution of ribosome biogenesis between yeast and mammals.* Nucleic Acids Res, 2011. **39**(1): p. 280-91.
147. Ishikawa, H., et al., *Poly(A)-specific ribonuclease regulates the processing of small-subunit rRNAs in human cells.* Nucleic Acids Res, 2017. **45**(6): p. 3437-3447.
148. Wang, H., et al., *Bystin-like protein is upregulated in hepatocellular carcinoma and required for nucleologenesis in cancer cell proliferation.* Cell Res, 2009. **19**(10): p. 1150-64.
149. Basso, K., et al., *Reverse engineering of regulatory networks in human B cells.* Nat Genet, 2005. **37**(4): p. 382-90.
150. Moudry, P. and K. Chroma, *RNA-interference screen for p53 regulators unveils a role of WDR75 in ribosome biogenesis.* 2021.
151. Miyoshi, M., et al., *Bystin in human cancer cells: intracellular localization and function in ribosome biogenesis.* Biochem J, 2007. **404**(3): p. 373-81.
152. Ochnik, A.M., et al., *Amplified in Breast Cancer Regulates Transcription and Translation in Breast Cancer Cells.* Neoplasia, 2016. **18**(2): p. 100-10.
153. Godoy, H., et al., *Developmentally restricted differentiation antigens are targets for immunotherapy in epithelial ovarian carcinoma.* Int J Gynecol Pathol, 2013. **32**(6): p. 536-40.
154. Quan, X., et al., *DDX10 and BYSL as the potential targets of chondrosarcoma and glioma.* Medicine (Baltimore), 2021. **100**(46): p. e27669.
155. Bhushan, A., R. Kumari, and T. Srivastava, *Scouting for common genes in the heterogenous hypoxic tumor microenvironment and their validation in glioblastoma.* 2021. **11**(10): p. 451.
156. Sha, Z., et al., *BYSL Promotes Glioblastoma Cell Migration, Invasion, and Mesenchymal Transition Through the GSK-3β/β-Catenin Signaling Pathway.* Front Oncol, 2020. **10**: p. 565225.
157. Gao, S., et al., *BYSL contributes to tumor growth by cooperating with the mTORC2 complex in gliomas.* 2021. **18**(1): p. 88-104.
158. Dilruba, S. and G.V. Kalayda, *Platinum-based drugs: past, present and future.* Cancer Chemother Pharmacol, 2016. **77**(6): p. 1103-24.
159. Mounier, N., et al., *Rituximab plus gemcitabine and oxaliplatin in patients with refractory/relapsed diffuse large B-cell lymphoma who are not candidates for high-dose therapy. A phase II Lymphoma Study Association trial.* Haematologica, 2013. **98**(11): p. 1726-31.
160. Garrido-Laguna, I. and M. Hidalgo, *Pancreatic cancer: from state-of-the-art treatments to promising novel therapies.* Nat Rev Clin Oncol, 2015. **12**(6): p. 319-34.
161. Li, L., et al., *Study on the interactions between anti-cancer drug oxaliplatin and DNA by atomic force microscopy.* Micron, 2015. **76**: p. 46-51.

162. Bruno, P.M., et al., *A subset of platinum-containing chemotherapeutic agents kills cells by inducing ribosome biogenesis stress.* Nat Med, 2017. **23**(4): p. 461-471.
163. Sutton, E.C. and V.J. DeRose, *Early nucleolar responses differentiate mechanisms of cell death induced by oxaliplatin and cisplatin.* J Biol Chem, 2021. **296**: p. 100633.
164. Volejnikova, J., et al., *Czech and Slovak Diamond-Blackfan Anemia (DBA) Registry update: Clinical data and novel causative genetic lesions.* Blood Cells Mol Dis, 2020. **81**: p. 102380.
165. Gazda, H.T., et al., *Ribosomal protein L5 and L11 mutations are associated with cleft palate and abnormal thumbs in Diamond-Blackfan anemia patients.* Am J Hum Genet, 2008. **83**(6): p. 769-80.
166. Quarello, P., et al., *High frequency of ribosomal protein gene deletions in Italian Diamond-Blackfan anemia patients detected by multiplex ligation-dependent probe amplification assay.* Haematologica, 2012. **97**(12): p. 1813-7.
167. Pufall, M.A., *Glucocorticoids and Cancer.* Adv Exp Med Biol, 2015. **872**: p. 315-33.
168. Li, H. and R. Durbin, *Fast and accurate short read alignment with Burrows-Wheeler transform.* Bioinformatics, 2009. **25**(14): p. 1754-60.
169. Li, H., et al., *The Sequence Alignment/Map format and SAMtools.* Bioinformatics, 2009. **25**(16): p. 2078-9.
170. Wang, K., M. Li, and H. Hakonarson, *ANNOVAR: functional annotation of genetic variants from high-throughput sequencing data.* Nucleic Acids Res, 2010. **38**(16): p. e164.
171. Korb, O., T. Stutzle, and T.E. Exner, *Empirical scoring functions for advanced protein-ligand docking with PLANTS.* J Chem Inf Model, 2009. **49**(1): p. 84-96.
172. Flores Ballester, E., et al., *Adult-onset Diamond-Blackfan anemia with a novel mutation in the exon 5 of RPL11: too late and too rare.* Clin Case Rep, 2015. **3**(6): p. 392-5.
173. Huo, X.F., et al., *Differential expression changes in K562 cells during the hemin-induced erythroid differentiation and the phorbol myristate acetate (PMA)-induced megakaryocytic differentiation.* Mol Cell Biochem, 2006. **292**(1-2): p. 155-67.
174. Li, Z. and S.R. Hann, *Nucleophosmin is essential for c-Myc nucleolar localization and c-Myc-mediated rDNA transcription.* Oncogene, 2013. **32**(15): p. 1988-94.
175. Murai, N., et al., *Novel ubiquitin-independent nucleolar c-Myc degradation pathway mediated by antizyme 2.* Sci Rep, 2018. **8**(1): p. 3005.
176. Engidaye, G., M. Melku, and B. Enawgaw, *Diamond Blackfan Anemia: Genetics, Pathogenesis, Diagnosis and Treatment.* Ejifcc, 2019. **30**(1): p. 67-81.
177. Hmeljak, J. and M.J. Justice, *From gene to treatment: supporting rare disease translational research through model systems.* Dis Model Mech, 2019. **12**(2).
178. Cui, D., et al., *The ribosomal protein S26 regulates p53 activity in response to DNA damage.* Oncogene, 2014. **33**(17): p. 2225-35.
179. Wang, C., et al., *Targeting "undruggable" c-Myc protein by synthetic lethality.* Front Med, 2021.

7 Bibliography

7.1 Original articles and reviews in peer-reviewed journals

Ozdian, T., Holub, D., **Maceckova, Z.**, Varanasi, L., Rylova, G., Rehulka, J., Vaclavkova, J., Slavik, H., Moudry, P., Znojek, P., Stankova, J., de Sanctis, J. B., Hajduch, M. and Dzubak, P. **Proteomic profiling reveals DNA damage, nucleolar and ribosomal stress are the main responses to oxaliplatin treatment in cancer cells.** J Proteomics, 2017. **162**: p. 73-85.

Nardone, G., Oliver-De La Cruz, J., Vrbsky, J., Martini, C., Pribyl, J., Skládal, P., Pešl, M., Caluori, G., Pagliari, S., Martino, F., **Maceckova, Z**., Hajduch, M., Sanz-Garcia, A., Pugno, N. M., Stokin, G. B. and Forte, G. **YAP regulates cell mechanics by controlling focal adhesion assembly.** Nat Commun. 2017 May 15;8:15321.

Zuzana Macečková , Agáta Kubíčková, Juan Bautista De Sanctis, Marian Hajdúch . **Effect of Glucocorticosteroids in Diamond-Blackfan Anaemia: Maybe Not as Elusive as It Seems.** Int J Mol Sci 2022 Feb 8;23(3):1886.

Agata Kubickova* , **Zuzana Maceckova***, Petr Vojta, Martin Ondra, Jana Volejnikova, Pavla Koralkova, Alexandra Jungova, Ondřej Jahoda, Renata Mojzikova, Ivana Hadacova, Jaroslav Cermak , Monika Horvathova, Dagmar Pospisilova, Marian Hajduch. **Missense mutation in RPS7 causes Diamond-Blackfan anemia via alteration of erythrocyte metabolism, protein translation and induction of ribosomal stress.** Blood Cells Mol Dis, 2022 Nov;97:102690.

7.2 Conference oral or poster presentation

Maceckova Z, Koralkova P, Volejnikova J et al. Two Novel Mutations in Ribosomal Proteins in the Czech National Diamond-Blackfan Anemia Registry. ASH conference, San Diego, 2.12.2016.

Maceckova Z et al. Bysl as DBA modifier. IMTM reactor, Pastviny, 14-16. 7. 2017.

Maceckova Z, Znojek P, Ozdian T, Dzubak P, Hajduch M. Fluorescent dye labeling nucleolus through covalent interaction with BYSL. IMTM reactor, Pastviny, 18-21. 9. 2018.

Maceckova Z, Kubickova A, Ondra M, Vojta P, Hajduch M. Bysl drives Diamond Blackfan pathology through c-Myc regulation. IMTM reactor, Skalský drvůr, 16-18. 9. 2019.

Maceckova Z, Mokshyna E, Kubickova A, Ondra M, Vojta P, Hajduch M. *Bystin* regulates c-Myc on protein level. DDPEO, Olomouc, 25-27. 11. 2019.

Maceckova Z, Mokshyna E, Kubickova A, Ondra M, Vojta P, Hajduch M. *Bystin* regulates c-Myc on protein level. IMTM reactor, Skalský drvůr, 7-9. 9. 2020.

Maceckova Z, Frydrych I, Ozdian T, Hajduch M. *Bystin* regulates AURORA A during mitosis. IMTM reactor, Skalský drvůr, 6-8. 9. 2021.

8 Appendix

Full text of publications related to the thesis.

Appendix 1

Ozdian, T., Holub, D., **Maceckova, Z.**, Varanasi, L., Rylova, G., Rehulka, J., Vaclavkova, J., Slavik, H., Moudry, P., Znojek, P., Stankova, J., de Sanctis, J. B., Hajduch, M. and Dzubak, P. **Proteomic profiling reveals DNA damage, nucleolar and ribosomal stress are the main responses to oxaliplatin treatment in cancer cells.** J Proteomics, 2017. **162**: p. 73-85.

Appendix 2

Agata Kubickova* , **Zuzana Maceckova***, Petr Vojta, Martin Ondra, Jana Volejnikova, Pavla Koralkova, Alexandra Jungova, Ondřej Jahoda, Renata Mojzikova, Ivana Hadacova, Jaroslav Cermak , Monika Horvathova, Dagmar Pospisilova, Marian Hajduch. **Missense mutation in RPS7 causes Diamond-Blackfan anemia via alteration of erythrocyte metabolism, protein translation and induction of ribosomal stress.** Blood Cells Mol Dis, 2022 Nov;97:102690.

Appendix 3

Zuzana Macečková , Agáta Kubíčková, Juan Bautista De Sanctis, Marian Hajdúch . **Effect of Glucocorticosteroids in Diamond-Blackfan Anaemia: Maybe Not as Elusive as It Seems.** Int J Mol Sci 2022 Feb 8;23(3):1886.

Appendix 1

Journal of Proteomics 162 (2017) 73–85

Contents lists available at ScienceDirect

Journal of Proteomics

journal homepage: www.elsevier.com/locate/jprot

Proteomic profiling reveals DNA damage, nucleolar and ribosomal stress are the main responses to oxaliplatin treatment in cancer cells

Tomas Ozdian [a], Dusan Holub [a], Zuzana Maceckova [a], Lakshman Varanasi [a], Gabriela Rylova [a], Jiri Rehulka [a], Jana Vaclavkova [a], Hanus Slavik [a], Pavel Moudry [b], Pawel Znojek [a], Jarmila Stankova [a], Juan Bautista de Sanctis [c], Marian Hajduch [a], Petr Dzubak [a,*]

[a] Laboratory of Experimental Medicine, Institute of Molecular and Translational Medicine, Faculty of Medicine and Dentistry, Palacky University and University Hospital in Olomouc, Olomouc, Czech Republic
[b] Laboratory of Genome Integrity, Institute of Molecular and Translational Medicine, Faculty of Medicine and Dentistry, Palacky University, Olomouc, Czech Republic
[c] Institute of Immunology, National Center of Clinical Immunology and FOCIS Center of Excellence, Faculty of Medicine, Universidad Central de Venezuela, Caracas, Venezuela

ARTICLE INFO

Article history:
Received 18 September 2016
Received in revised form 26 April 2017
Accepted 2 May 2017
Available online 3 May 2017

Keywords:
Oxaliplatin
Proteomics
LC-MS
Nucleolar stress
Ribosomal stress

ABSTRACT

Oxaliplatin is widely used to treat colorectal cancer in both palliative and adjuvant settings. It is also being tested for use in treating hematological, esophageal, biliary tract, pancreatic, gastric, and hepatocellular cancers. Despite its routine clinical use, little is known about the responses it induces in cancer cells. Therefore the whole-cell proteomics study was conducted to characterize the cellular response induced by oxaliplatin. Chemosensitive CCRF-CEM cells were treated with oxaliplatin at 29.3 μM ($5 \times IC_{50}$) for 240 min (half-time to caspase activation). The proteomes of un−/treated cells were then compared by high-resolution mass spectrometry, revealing 4049 proteins expressed over 3 biological replicates. Among these proteins, 76 were significantly downregulated and 31 significantly upregulated in at least two replicates. In agreement with the DNA-damaging effects of platinum drugs, proteins involved in DNA damage responses were present in both the upregulated and downregulated groups. The downregulated proteins were divided into three subgroups; i) centrosomal proteins, ii) RNA processing and iii) ribosomal proteins, which indicates nucleolar and ribosomal stress. In conclusion, our data supported by further validation experiments indicate the initial cellular response to oxaliplatin is the activation of DNA damage response, which in turn or in parallel triggers nucleolar and ribosomal stress.

Biological significance: We have performed a whole-cell proteomic study of cellular response to oxaliplatin treatment, which is the drug predominantly used in the treatment of colorectal cancer. Compared to its predecessors, cisplatin and carboplatin, there is only a small fraction of studies dedicated to oxaliplatin. From those studies, most of them are focused on modification of treatment regimens or study of oxaliplatin in new cancer diagnoses. Cellular response hasn't been studied deeply and to our best knowledge, this is the first whole-cell proteomics study focused exclusively to this important topic, which can help to understand molecular mechanisms of action.

1. Introduction

Oxaliplatin ([(1R,2R)-cyclohexane-1,2-diamine](ethanedioato-O,O′)platinum(II); L-OHP) is a member of the platinum drug family. Members of this family are derived from cisplatin, which can be regarded as the first generation platinum drug. Cisplatin has some serious side effects that limit its clinical utility, particularly nephrotoxicity [1]. The second generation platinum agents (of which carboplatin is the most well-known) were introduced to avoid these drawbacks. While these drugs have fewer side-effects than cisplatin, they suffer from cross-resistance with the first generation agent [2]. To overcome this issue, the newer and safer platinum drug L-OHP was synthesized in 1980 and approved by the FDA in 2005 [3]. L-OHP differs from cisplatin in that the amine groups of the latter are replaced with a diaminocyclohexane moiety. In plasma, L-OHP rapidly undergoes non-enzymatic transformations to form various reactive species. Most of these are pharmacologically inactive, but some are dichloro platinum complexes that can enter cells and exert cytotoxic effects.

L-OHP is widely used to treat colorectal, but also gastric and pancreatic metastatic cancer [4,5], and is being evaluated for the treatment of hematological, ovarian, breast, biliary tract, hepatocellular and non-small cell lung cancers [6,7]. It is generally applied in combination with other therapeutic agents. For example, in the FOLFOX regimen it is combined with 5-fluorouracil and folinic acid; when applied as a first-line therapy, this combination yields response rates of up to 50% in colorectal cancer, compared to 15% for 5-fluorouracil

* Corresponding author at: Institute of Molecular and Translational Medicine, Faculty of Medicine and Dentistry, Palacky University Olomouc, Hnevotinska 1333/5, Olomouc 775 15, Czech Republic.
E-mail address: petr.dzubak@upol.cz (P. Dzubak).

http://dx.doi.org/10.1016/j.jprot.2017.05.005
1874-3919/

alone [8]. Similarly, in the GEMOX regimen it is applied in combination with gemcitabine to treat pancreatic cancer and non-Hodgkin lymphomas [7,8]. It can also be combined with a range of other agents, including targeted biologics such as bevacizumab [9] or rituximab [7]. The use of targeted therapy and monoclonal antibody drugs with conventional drugs like L-OHP should be based on rational and scientific combinations. It is therefore valuable to study and understand molecular mechanisms of conventional chemotherapeutic agents which can help to design new synergistic combinations for clinical trials and avoid rapid development of drug resistant disease.

The most serious side-effect of L-OHP treatment is peripheral neuropathy, and most of the research on its use has focused on this side-effect [10] and the development of existing and novel treatment combinations. Only a few studies have investigated L-OHP resistance [11] or DNA damage induced by L-OHP treatment [12] and the potential resulting ionic [13] and/or oxidative stress [14]. L-OHP binds to nucleophiles, DNA, RNA and proteins, and forms intra-strand adducts between guanine and/or adenine residues, thus disrupting replication and transcription. Nucleotide excision repair pathway is believed to be main DNA damage repair system induced by L-OHP treatment. However, it has also been reported to induce epigenetic changes, detoxification pathways, cell death, and changes in NF-kB signaling [15].

Cellular response to L-OHP can be elucidated by very powerful tools, such as systematic proteomic analysis. Previously, we have conducted complex proteomic studies based on 2D electrophoresis profiling to characterize the responses of cancer cells to anthracyclines (doxorubicin, daunorubicin and mitoxantrone), revealing that exposure to these drugs changes the expression and activity of proteins involved in metabolic processes, transport proteins, and immune system proteins, among others [16]. A similar workflow based on 2D electrophoresis has also been used by us to elucidate the mechanisms responsible for resistance to the kinase inhibitor bohemine [17]. This proteomic approach is thus a valuable tool for elucidation of cellular response to single drugs. Proteomic profilling of single drugs cellular response can be valuable tool in comparison of drug effects in vitro.

In recent years there have been several important advances in the methods and technologies available for use in proteomic analysis; as a result, we have replaced our electrophoresis-based approach with a more straightforward alternative based on high resolution mass spectrometry (Orbitrap) that offers increased sensitivity and a greater ability to detect and quantify changes in the expression of less abundant proteins. Here, we describe this new approach and its application in an analysis of the cellular effects of L-OHP treatment. Our aim in conducting this work was both to obtain new knowledge concerning the response to the drug and (perhaps more importantly) to establish a generally applicable set of conditions for mechanism of action testing and -omics profiling of cytotoxic drugs. Our method involves treating a cancer cell line (in this work, the highly chemosensitive CCRF-CEM line was used as a model of L-OHP use in hematological cancers) with the agent of interest at 5 times its IC_{50} and for half the time required for caspase activation. The time to caspase activation is a measure of the time elapsed from exposure of cells to cytotoxic drug to induction of cell death; the aim of stopping the experiment at half the time to caspase activation is to minimize the risk of identifying late and non-specific changes in protein expression and processing induced by apoptotic machinery and the proteome more generally.

2. Material and methods

2.1. Chemicals and reagents

Oxaliplatin (Eloxatin) was obtained as a 5 mg/ml stock solution from Sanofi. If not mentioned otherwise, all chemicals were obtained from Sigma. Fetal calf serum (FCS) was purchased from Pan Biotech (Germany). The MagicRed Caspase detection kit for caspases 3 and 7 was purchased from Immunochemistry Technologies, USA. RPMI media lacking arginine and lysine was obtained from Biowest, USA. HPLC/MS grade water was produced using a Merck Millipore Milli-Q Direct-8 purifier with an LC-PAK polisher (Merck), and HPLC/MS grade acetonitrile was purchased from J. T. Baker, USA. Proteomic grade trypsin was purchased from Promega. Benzonase and Luminata Forte were obtained from Merck. Pierce 660 nm Protein Assay kits for protein concentration measurements with Ionic Detergent Compatibility Reagent were purchased from ThermoFisher Scientific, USA. Pertex rapid drying medium was used for slide mounting (Histolab, Sweden). The following antibodies were used: Anti-UTP11 (AbCam), Anti-WDR46 (Sigma), Anti-TRF1 (Santa Cruz), Anti-RPS19 (Santa Cruz), Anti-p53 (Cell Signaling), Anti-Fibrilarin (Sigma) and Anti-β-actin (Sigma), horseradish peroxidase conjugated anti-rabbit (Sigma), horseradish peroxidase conjugated anti-mouse (Sigma), Alexa-488 anti-goat (Life technologies) and Alexa 488 anti-rabbit (Invitrogen). ELISA kits were purchased from Thermo Fisher (Ferritin) and RnD Systems (Apolipoprotein A1).

2.2. Cell culture, analysis of IC50 and time to apoptosis

The T-lymphoblastic leukemia-derived cell line CCRF-CEM was purchased from the American Tissue Culture Collection (ATCC) and cultivated according to the recommended procedure in RPMI media supplemented with 20% FCS, 100 IU/ml penicillin and 10 μg/ml streptomycin. Inhibition of tumor growth/survival, measured in terms of the 50% inhibition constant (IC_{50}), was determined by the MTT assay as described previously [18]. Time to apoptosis was determined using the Magic Red assay (Immunochemistry Technologies). For proteomic analyses, CCRF-CEM cells (10^6/ml) were treated with a 5 × IC 50 concentration of L-OHP, which approximately corresponds to the IC 50 value when compared to cell count used in cytotoxic MTT assay [18]. Assay was performed according to the manufacturer's instructions, with fluorescence analysis based on excitation at 590 nm and emission at 630 nm.

2.3. SILAC labeling and treatment with drugs

Three biological replicates of the proteomic analysis were performed. CCRF-CEM cells were grown in complete RPMI media lacking arginine and lysine or media containing either $^{12}C_6$ (light) or $^{13}C_6$ (heavy) labeled arginine and lysine. In all cases, the cells were cultured for five passages to ensure that the "light" or "heavy" amino acids were completely incorporated. The completeness of the labeling was verified by mass spectrometry (data not shown). Light cell lines were diluted to a concentration of 10^6 cells per ml and treated with a 5 × IC_{50} concentration of L-OHP for half the time required to induce apoptosis ($TA_{1/2}$). After treatment, light and heavy cells were mixed in a 1:1 ratio, and the mixed cell suspension was washed twice in ice-cold PBS with protease inhibitors and once with ice-cold PBS. The washed cells were lysed in lysis buffer containing 20 mM Tris-HCl, 7 M Urea, 10 mM DTT, 1% Triton X-100 and 0.5% SDS, and 2 U benzonase, and transferred to 1.5 ml microfuge tubes. The lysate was then incubated on ice for 5 min, after which two extra units of benzonase were added and the resulting mixture was incubated for an additional 5 min. Lysates were cleared at 16,000 g at 4 °C for 10 min and the supernatants were transferred into 1.5 ml Eppendorf tubes and stored at −80 °C.

2.4. Sample preparation for LC-MS/MS

The 100 μl of whole cell lysates was resolved by preparative SDS-PAGE (MiniPrep Cell, BioRad), and the resulting gels were cut into 20 slices corresponding to protein fractions separated by molecular weight. The gel slices were then dehydrated with acetonitrile, after which the proteins were reduced with 50 mM Tris(2-carboxyethyl)phosphine at

90 °C for 10 min and then alkylated with 50 mM iodoacetamide for 1 h in the dark. The alkylated samples were washed three times with water and acetonitrile successively, and finally washed with 50% acetonitrile. After washing, the samples were solubilized and trypsinized in trypsin buffer (6.25 ng/μl trypsin, 50 mM 4-ethylmorpholine, 10% v/v acetonitrile, pH 8.3) overnight at 37 °C. The resulting supernatant was transferred into a new Eppendorf tube and peptides were extracted from the gel pieces, first with 80% acetonitrile containing 0.1% TFA, then with 0.1% TFA in water, and finally with 50% acetonitrile. The extracts were then pooled and dried in a SpeedVac (Eppendorf). Dried samples were reconstituted in 5 μl of 80% ACN with 0.1% TFA, diluted with 145 μl of 0.1% TFA, and purified using a C-18 MacroTrap column (Michrom Bioresources, USA). The purified samples were then re-dried in the SpeedVac and resuspended in 20 μl of 5% acetonitrile with 0.1% formic acid for LC-MS/MS analysis.

2.5. LC/MS

Mass spectrometric analysis was performed on an Orbitrap Elite (Thermo) instrument fitted with a Proxeon Easy-Spray ionization source, coupled to an Ultimate 3000 RSLCnano chromatograph. One microliter of sample was loaded on a PepMap 100 (75 μm × 2 cm, 3 μm, 100 Å pore size) desalting column (Thermo) "in-line" with a PepMap RSLC (75 μm × 15 cm, 3 μm, 100 Å pore size) analytical column (Thermo) heated to 35 °C. The peptides were subsequently separated on the analytical column by ramping the organic phase from 5% to 35% over a total run time of 150 min. The aqueous and organic mobile phases were, respectively, 0.1% formic acid in water and acetonitrile containing 0.1% formic acid. The FTMS resolution was set to 120,000 and precursor ions were scanned across an m/z range of 300.0–1950.0. The twenty most intense ions were selected in the linear ion-trap for fragmentation by collision (CID) in the Orbitrap. A collision energy of 35 eV was applied throughout.

2.6. Data analysis

Peak picking and peptide searching were performed with MaxQuant v.1.3.0.5 [19] using the SwissProt human database (downloaded 4/4/2013). All fractions of a single sample were searched together. Carbamidomethylation of cysteines was selected as a fixed modification, with oxidation of methionines and protein N-terminal acetylation as variable modifications. The minimal peptide and razor peptide count was set to 1 and the peptide length to 6. The mass tolerance was set to 20 ppm for parent ions and 0.5 Da for fragments. The FDR rate for peptides and proteins was set to 1%. Arginine and lysine were specified as special amino acids to filter for labeled amino acids. Razor peptides were used for quantification, with unmodified counterpart peptides being discarded; re-quantification and iBAQ were permitted. Search results were processed in Perseus 1.4.0.6, which was used to remove decoy search results and contaminant items. Significance was evaluated using the significance B test, using normalized ratios of replicates and their respective intensities to capture the effect of abundance on significance. Proteins that had significance B scores below 0.05 in at least two replicates were selected for further study.

Venn diagrams were created in Perseus and Venn Diagram Plotter 1.5 (http://omics.pnl.gov). Pearson coefficients were calculated in Microsoft Excel by plotting the $\log_2$ of each replicate's L/H ratio against the $\log_2$ of the average L/H ratio for proteins that were quantified in all replicates.

Bioinformatics analyses of the B significant protein list were performed with the Database for Annotation, Visualization and Integrated Discovery (DAVID, v6.7, http://david.abcc.ncifcrf.gov/, downloaded 13/1/2016) [20]. Results were visualized using DAVID's Functional Annotation Clustering method. Protein-protein interactions of B significantly changed proteins were analysed using the STRING database (http://string-db.org, downloaded 13/1/2016) [21]. The graphical output of STRING was divided into clusters, with a cluster being defined as a close group of at least 7 proteins that are closer to one-another than to proteins outside the cluster.

2.7. Validation of proteomic data

2.7.1. Immunoblotting

CCRF-CEM cells were-treated with L-OHP as before. Cells were harvested and centrifuged at 90g for 5 min at 4 °C and then washed twice in PBS with 5 mM sodium pyrophosphate, 1 mM sodium orthovanadate, 5 mM sodium fluoride and 1 mM PMSF. After washing, the cells were lysed with SDS lysis buffer (62.5 mM Tris-HCl, pH 6.8, 10% glycerol, 2% SDS, 1% mercaptoethanol, 0.5% bromophenol blue), heated for 10 min at 95 °C, and incubated with 2 units of benzonase for one hour at room temperature to prepare a whole cell lysate. Protein content was measured using the Pierce 660 nm Protein Assay containing the Ionic Detergent Compatibility Reagent. Samples were loaded to SDS-PAGE with uniform loading 10 μg of total protein and were resolved by 12% T gels. The separated proteins were then blotted onto a nitrocellulose membrane (0.2 μm pore size, Bio-Rad) using the TransBlot Turbo semi-dry system (Bio-Rad), after which the membrane was blocked for 1 h with 5% non-fat dry milk in TBS/T (Tris-buffered saliva with 0.1% Tween-20) and incubated with appropriate antibodies in 5% v/v BSA in TBS/T overnight, at 4 °C, with agitation. After incubation, the membranes were washed with TBS/T, incubated with a peroxidase-labeled secondary antibody, and visualized using the Luminata Forte peroxidase substrate. Chemiluminiscence was recorded using a HCD camera (Li-Cor Odyssey FC). Band intensities were normalized against those of the corresponding actin band, and averages of three biological replicates were processed into bar graphs. The significance of observed changes in protein abundance was evaluated using the t-test, with a p-value threshold of 0.05.

2.8. ELISA assay

Cell lysates were prepared in the same way as for immunoblotting. Proteins from approximately 10 million cells were precipitated with ethanol and centrifuged for 10 min at 2000g, after which the supernatant was removed and the pellet was reconstituted in water. The total protein content was then measured using the bicinchoninic acid assay. Additionally, ELISA assays for ferritin and apolipoprotein A1 were performed using the kits specified above, according to the manufacturer's instructions.

2.9. Immunoprecipitation

For preparation of lysates for immunoprecipitation, cells were washed three times in PBS and lysed in TNE buffer (150 mM NaCl, 50 mM Tris-HCl pH 8.0, 1 mM EDTA, 0.5% NP-40) supplemented with cOmplete and PhosSTOP tablets (Roche). After 30 min incubation on ice, lysates were cleared by centrifugation. Appropriate antibodies were pre-conjugated to Dynabeads M-280 Sheep anti Rabbit IgG (Novex) for 1 h at 4 °C and cleared lysates incubated with beads and antibodies for 2 h at 4 °C. Immunoglobulin-antigen complexes were washed extensively before elution in 20 μl 2× Laemmli sample buffer before SDS-PAGE. Protein interaction was detected by immunoblot as described above.

2.10. Reverse transcription PCR

The washed cell pellets were resuspended in 1 ml of TRI Reagent (Molecular Research Centre, Cincinnati, OH, USA) and stored at −20 °C until RNA purification. Total RNA was extracted according to manufacturer's instructions. RNA concentration and purity were assessed by a Nanodrop ND 1000 (ThermoScientific, Wilmington, DE, USA). For reverse transcription, we pre-incubated 3 μg of total RNA with 0.3 μg of Random Primers

(Promega, Madison, WI, USA) at 70 °C for 5 min, and immediately placed the mixture on ice. Then 6 μl of RevertAid 5× RT buffer (Fermentas, Vilnius, Lithuania), 3 μl of 10 mM deoxyribonucletotide triphosphates (dNTPs), 0.75 μl of 40 U/μl RNAsin ribonuclease inhibitor (Promega, Madison, WI, USA), and DEPC treated water (Ambion, Austin, TX, USA) up to a final volume of 30 μl were added, and the mixture was incubated for 5 min at room temperature. During the final step, 150 U of RevertAid Moloney Murine Leukemia Virus reverse transcriptase (Fermentas, Vilnius, Lithuania) were added to each tube and the samples were incubated at room temperature for 10 min. Finally, samples were incubated at 42 °C for 60 min and then 70 °C for 10 min. Prepared cDNA were stored at −20 °C until qPCR.

TaqMan technology was used for gene expression analyses for each sample and marker (CCNB1, UTP11L, WDR46, DDX56, RPS19, TP53, APOA1, FTH1, CDKN1A and ACTB). Reaction mixtures were prepared using 1 μl 20× TaqMan Gene Expression Assay (ThermoScientific, Wilmington, DE, USA), 10 μl 2× LightCycler 480 Probes Master (Roche, Basil, Switzerland), 8 μl DEPC treated water (Ambion, Austin, TX, USA) and 1 μl cDNA. Reactions were performed on LightCycler 480 II/96 (Roche, Basil, Switzerland) in two replicates according to manufacturer's instructions.

Relative quantification was used for data evaluation. ACTB was used for endogenous normalization of Ct values for each marker. Fold differences were calculated from ΔΔCt values as treated samples versus controls. Results are average values from three biological replicates with standard deviations.

2.11. Nucleolar staining

The CCRF-CEM cell line was treated in the same way as for proteomic analysis. After treatment, the cells were spun onto microscopy slides using a Cytospin centrifuge (Sakura, Japan) at 500 rpm for 5 min. Spun cells were allowed to dry, fixed with 4% paraformaldehyde in PBS, and stained with toluidine blue as described by Smetana [22]. After staining, the slides were mounted with Pertex (Histolab, Sweden). Three replicates were observed using a Zeiss Axio microscope with a Zeiss AxioCamERc 5 s digital camera at 400× magnification. In each sample, 100 nucleoli were counted and classified visually as either (a) compact nucleoli, (b) ring nucleoli, or (c) micronucleoli as described by Smetana et al. [22].

2.12. Immunofluorescence

Cells were spun using a Cytospin centrifuge as described above, fixed with 4% paraformaldehyde in PBS for 15 min at room temperature, and permeabilized with 0.5% TritonX-100 in PBS for 15 min. The cells were then washed three times in PBS with 0.1% Tween 20 and incubated overnight at 4 °C with primary rabbit or goat antibodies against fibrillarin, DDX56, WDR46, RPS9 and UT11L in 5% FCS. The samples were then washed three times in PBS with 0.1% Tween 20 and incubated with the corresponding anti-rabbit/goat secondary antibodies conjugated to Alexa Fluor 488 in 5% FCS for 1 h at room temperature. Coverslips were stained with DAPI for nuclei counterstaining and mounted in mounting medium. The localization of the proteins of interest was examined using confocal spinning disc fluorescent microscopy (Carl-Zeiss Observer Z1) at 1000× magnification. Image quantification was calculated as number of spots per nuclei in Columbus software version 2.71 (Perkin-Elmer). The number of nuclei entered into the analysis ranged from 900 to 30,000 per sample. Obtained data were analysed with General Linear Model (GLM) and significance was calculated with post hoc Tukey's HSD test in Statistica 12 (StatSoft).

Data analysed with General Linear Model (GLM) and significance was calculated with post hoc Tukey HSD test.

2.13. Fluorescent in-situ hybridization of 47S pre-rRNA

Fluorescent in-situ hybridization of 47S pre-rRNA has been performed according to [23]. Briefly, cells were treated, transferred to microscope glass and fixed as in immunofluorescence experiment. After being rinsed in PBS, cells were permeabilized for 18 h in 70% ethanol at 4 °C. After two washes in 2 × SSC containing 10% formamide, hybridization was performed in the dark at 37 °C for 5 h in a buffer containing 10% formamide, 2 × SSC, 0.5 mg/ml tRNA, 10% dextran sulfate, 250 μg/ml BSA, 10 mM ribonucleoside vanadyl complexes and 0.5 ng/μl of ETS1-1399 probe (5′-cgctagagaaggcttttctc-3′) conjugated to Cy5 (which hybridizes to the 47S pre-rRNA between 01/A′ and A0 cleavage sites). After two washes at 37 °C with 2 × SSC containing 10% formamide, the cover slips were rinsed in PBS and DNA was counterstained with DAPI, mounted and examined as in immunofluorescence.

2.14. Flow cytometry

Flow cytometry analysis was performed using standard protocol described in Borková et al. [24]. Briefly, CCRF-CEM cell line at concentration 2.5. 10^5 cells/ml were seeded in 6-well plates, incubated for 24 h and treated with L-OHP concentrations 1 × IC_{50} and 5 × IC_{50} in time intervals 1, 2, 4, 8, 12, 24 and 36 h in three replicates. Non-treated control for each analysis and time point was done in one replicate, except analysis of proteosynthesis, where negative control was performed together with positive control, 5 μM puromycin, for 24 h.

After treatment, samples for cell cycle analysis were washed with cold PBS and fixed with 70% ethanol and stored overnight at −20 °C. For cell cycle analysis, fixed cells were split into two halves. First half was washed in hypotonic citrate buffer, treated with RNAse (50 μg/mL) and stained with propidium iodide. Second half was used for $pH3^{Ser10}$ antibody (Sigma) labeling and subsequent flow cytometry analysis of mitotic cells.

Samples for DNA synthesis analysis were processed as following. Before harvesting, 10 μM 5-bromo-2-deoxyuridine (BrDU), was added to the cells for pulse-labeling for 30 min. Cells were fixed with ice-cold 70% ethanol and stored overnight. Before the analysis, cells were washed with PBS, and resuspended in 2 M HCl for 30 min at room temperature to denature their DNA. Following neutralization with 0.1 M $Na_2B_4O_7$ (Borax), cells were washed with PBS containing 0.5% Tween-20 and 1% BSA. Staining with primary anti-BrDU antibody for 30 min at room temperature in the dark followed. Cells were than washed with PBS and stained with secondary FITC antibody. Cells were then washed with PBS again and incubated with propidium iodide (0.1 mg/ml) and RNAse A (0.5 mg/ml) for 1 h at room temperature in the dark.

For analysis of RNA synthesis, pulse-labeling with 1 mM 5-bromo uridine (BrU) for 30 min followed the time of treatment. The cells were then fixed in 1% buffered paraformaldehyde with 0.05% of NP-40 in room temperature for 15 min, and then stored at 4 °C overnight. Cells were then washed in PBS with 1% glycine, washed in PBS again, and stained by primary anti-BrDU antibody cross-reacting to BrU for 30 min at room temperature in the dark. After another washing step in PBS cells were stained by secondary FITC antibody. Following the staining, cells were washed with PBS and fixed with 1% PBS-buffered paraformaldehyde with 0.05% of NP-40 for 1 h. Cells were then treated as in DNA analysis, washed with PBS, incubated with propidium iodide and RNAse A for 1 h at room temperature in the dark.

Analysis of protein synthesis was performed using commercial Thermo Click-It kit [25]. Samples were after incubation washed in PBS, transferred into methionine-free RMPI 1640 medium for 1 h to deplete intracellular deposits of methionine. Then, L-azidohomoalanine was added for another 1 h. Samples were then washed with PBS, fixed with 4% paraformaldehyde, permeabilized with 0.25% Triton-X100 in PBS and washed in 3% BSA in PBS. Detection was performed using Click-It Cell reaction buffer kit.

(Promega, Madison, WI, USA) at 70 °C for 5 min, and immediately placed the mixture on ice. Then 6 μl of RevertAid 5× RT buffer (Fermentas, Vilnius, Lithuania), 3 μl of 10 mM deoxyribonucletotide triphosphates (dNTPs), 0.75 μl of 40 U/μl RNAsin ribonuclease inhibitor (Promega, Madison, WI, USA), and DEPC treated water (Ambion, Austin, TX, USA) up to a final volume of 30 μl were added, and the mixture was incubated for 5 min at room temperature. During the final step, 150 U of RevertAid Moloney Murine Leukemia Virus reverse transcriptase (Fermentas, Vilnius, Lithuania) were added to each tube and the samples were incubated at room temperature for 10 min. Finally, samples were incubated at 42 °C for 60 min and then 70 °C for 10 min. Prepared cDNA were stored at −20 °C until qPCR.

TaqMan technology was used for gene expression analyses for each sample and marker (CCNB1, UTP11L, WDR46, DDX56, RPS19, TP53, APOA1, FTH1, CDKN1A and ACTB). Reaction mixtures were prepared using 1 μl 20× TaqMan Gene Expression Assay (ThermoScientific, Wilmington, DE, USA), 10 μl 2× LightCycler 480 Probes Master (Roche, Basil, Switzerland), 8 μl DEPC treated water (Ambion, Austin, TX, USA) and 1 μl cDNA. Reactions were performed on LightCycler 480 II/96 (Roche, Basil, Switzerland) in two replicates according to manufacturer's instructions.

Relative quantification was used for data evaluation. ACTB was used for endogenous normalization of Ct values for each marker. Fold differences were calculated from ΔΔCt values as treated samples versus controls. Results are average values from three biological replicates with standard deviations.

2.11. Nucleolar staining

The CCRF-CEM cell line was treated in the same way as for proteomic analysis. After treatment, the cells were spun onto microscopy slides using a Cytospin centrifuge (Sakura, Japan) at 500 rpm for 5 min. Spun cells were allowed to dry, fixed with 4% paraformaldehyde in PBS, and stained with toluidine blue as described by Smetana [22]. After staining, the slides were mounted with Pertex (Histolab, Sweden). Three replicates were observed using a Zeiss Axio microscope with a Zeiss AxioCamERc 5 s digital camera at 400× magnification. In each sample, 100 nucleoli were counted and classified visually as either (a) compact nucleoli, (b) ring nucleoli, or (c) micronucleoli as described by Smetana et al. [22].

2.12. Immunofluorescence

Cells were spun using a Cytospin centrifuge as described above, fixed with 4% paraformaldehyde in PBS for 15 min at room temperature, and permeabilized with 0.5% TritonX-100 in PBS for 15 min. The cells were then washed three times in PBS with 0.1% Tween 20 and incubated overnight at 4 °C with primary rabbit or goat antibodies against fibrillarin, DDX56, WDR46, RPS9 and UT11L in 5% FCS. The samples were then washed three times in PBS with 0.1% Tween 20 and incubated with the corresponding anti-rabbit/goat secondary antibodies conjugated to Alexa Fluor 488 in 5% FCS for 1 h at room temperature. Coverslips were stained with DAPI for nuclei counterstaining and mounted in mounting medium. The localization of the proteins of interest was examined using confocal spinning disc fluorescent microscopy (Carl-Zeiss Observer Z1) at 1000× magnification. Image quantification was calculated as number of spots per nuclei in Columbus software version 2.71 (Perkin-Elmer). The number of nuclei entered into the analysis ranged from 900 to 30,000 per sample. Obtained data were analysed with General Linear Model (GLM) and significance was calculated with post hoc Tukey's HSD test in Statistica 12 (StatSoft).

Data analysed with General Linear Model (GLM) and significance was calculated with post hoc Tukey HSD test.

2.13. Fluorescent in-situ hybridization of 47S pre-rRNA

Fluorescent in-situ hybridization of 47S pre-rRNA has been performed according to [23]. Briefly, cells were treated, transferred to microscope glass and fixed as in immunofluorescence experiment. After being rinsed in PBS, cells were permeabilized for 18 h in 70% ethanol at 4 °C. After two washes in 2 × SSC containing 10% formamide, hybridization was performed in the dark at 37 °C for 5 h in a buffer containing 10% formamide, 2 × SSC, 0.5 mg/ml tRNA, 10% dextran sulfate, 250 μg/ml BSA, 10 mM ribonucleoside vanadyl complexes and 0.5 ng/μl of ETS1-1399 probe (5′-cgctagagaaggcttttctc-3′) conjugated to Cy5 (which hybridizes to the 47S pre-rRNA between 01/A′ and A0 cleavage sites). After two washes at 37 °C with 2 × SSC containing 10% formamide, the cover slips were rinsed in PBS and DNA was counterstained with DAPI, mounted and examined as in immunofluorescence.

2.14. Flow cytometry

Flow cytometry analysis was performed using standard protocol described in Borková et al. [24]. Briefly, CCRF-CEM cell line at concentration 2.5. 10^5 cells/ml were seeded in 6-well plates, incubated for 24 h and treated with L-OHP concentrations 1 × IC_{50} and 5 × IC_{50} in time intervals 1, 2, 4, 8, 12, 24 and 36 h in three replicates. Non-treated control for each analysis and time point was done in one replicate, except analysis of proteosynthesis, where negative control was performed together with positive control, 5 μM puromycin, for 24 h.

After treatment, samples for cell cycle analysis were washed with cold PBS and fixed with 70% ethanol and stored overnight at −20 °C. For cell cycle analysis, fixed cells were split into two halves. First half was washed in hypotonic citrate buffer, treated with RNAse (50 μg/mL) and stained with propidium iodide. Second half was used for $pH3^{Ser10}$ antibody (Sigma) labeling and subsequent flow cytometry analysis of mitotic cells.

Samples for DNA synthesis analysis were processed as following. Before harvesting, 10 μM 5-bromo-2-deoxyuridine (BrDU), was added to the cells for pulse-labeling for 30 min. Cells were fixed with ice-cold 70% ethanol and stored overnight. Before the analysis, cells were washed with PBS, and resuspended in 2 M HCl for 30 min at room temperature to denature their DNA. Following neutralization with 0.1 M $Na_2B_4O_7$ (Borax), cells were washed with PBS containing 0.5% Tween-20 and 1% BSA. Staining with primary anti-BrDU antibody for 30 min at room temperature in the dark followed. Cells were than washed with PBS and stained with secondary FITC antibody. Cells were then washed with PBS again and incubated with propidium iodide (0.1 mg/ml) and RNAse A (0.5 mg/ml) for 1 h at room temperature in the dark.

For analysis of RNA synthesis, pulse-labeling with 1 mM 5-bromo uridine (BrU) for 30 min followed the time of treatment. The cells were then fixed in 1% buffered paraformaldehyde with 0.05% of NP-40 in room temperature for 15 min, and then stored at 4 °C overnight. Cells were then washed in PBS with 1% glycine, washed in PBS again, and stained by primary anti-BrDU antibody cross-reacting to BrU for 30 min at room temperature in the dark. After another washing step in PBS cells were stained by secondary FITC antibody. Following the staining, cells were washed with PBS and fixed with 1% PBS-buffered paraformaldehyde with 0.05% of NP-40 for 1 h. Cells were then treated as in DNA analysis, washed with PBS, incubated with propidium iodide and RNAse A for 1 h at room temperature in the dark.

Analysis of protein synthesis was performed using commercial Thermo Click-It kit [25]. Samples were after incubation washed in PBS, transferred into methionine-free RMPI 1640 medium for 1 h to deplete intracellular deposits of methionine. Then, L-azidohomoalanine was added for another 1 h. Samples were then washed with PBS, fixed with 4% paraformaldehyde, permeabilized with 0.25% Triton-X100 in PBS and washed in 3% BSA in PBS. Detection was performed using Click-It Cell reaction buffer kit.

All flow cytometry analyses were analysed on FACS Calibur (Becton Dickinson) flow cytometer equipped with 488 nm single beam laser.

3. Results

The IC_{50} value of L-OHP was determined to be 5.9 μM by the 3-day MTT cytotoxicity assay. In all subsequent experiments, the CCRF-CEM cells were treated with a concentration of L-OHP equal to 5 times the calculated IC_{50}, i.e. 29.3 μM. To determine appropriate timings for sample preparation and to ensure that only early events leading later to apoptosis were included in the analysis, we analysed caspase 3 activity in L-OHP-treated samples using the Magic Red assay kit. In these assays, the time to onset of apoptosis (TA) was defined as the time required for the fluorescence signal of treated cells to become 10% greater than that for untreated control cells. On the basis of these assays, the TA (i.e. the time to caspase activation) was determined to be approximately 480 min, so in all subsequent experiments the CCRF-CEM cells were treated with $5 \times IC_{50}$ L-OHP and then lysed 240 min later, at TA_{50}.

MS analysis of SILAC-labeled whole cell lysates resulted in the identification of 4164, 4087 and 3896 proteins across three replicates, with 3171, 3369 and 3069 of these proteins being quantified, respectively. The three replicates had 3260 identified and 2356 quantified proteins in common. The Pearson coefficients for the three replicates, which reflect the quality of the quantification, were 0.94, 0.88 and 0.84 (Fig. 1). A complete list of the identified and quantified proteins is presented in Supplementary Table 1 and the corresponding raw data have been deposited with the ProteomeXchange Consortium (http://proteomecentral.proteomexchange.org) via the PRIDE partner repository [26], using the dataset identifier PXD003543.

We defined a protein as having been significantly up or downregulated if it had a significance B p-value below 0.05 in at least two replicates (Supplementary Table 2). Bioinformatic analyses of these proteins were performed using the functional annotation clustering method implemented in DAVID. This method assigned high scores to ribosomal and nucleolar clusters (Table 1). A second, complementary, analysis based on protein-protein interactions was performed using STRING. This revealed four distinct clusters (Fig. 2) corresponding to proteins related to the centromere and G2/M checkpoint (Fig. 2A), secreted proteins (Fig. 2B), ribosomal (Fig. 2C) and nucleolar proteins (Fig. 2D). Proteins from clusters A, C and D are also involved in responses to cellular damage and stress [27].

For a next step, we have selected proteins, which were the most significantly changed in each cluster. Change in abundance of each of selected proteins, CCNB1, UTP11L, WDR46, DDX56, RPS19, TP53 was determined using immunoblotting. For determination of change in abundance of the remaining two proteins, APOA1 and FTH1, commercially available ELISA kit was used. The change in abundance of all those proteins was confirmed - the immunoblot and ELISA results shared the same trend of change, although the numbers weren't exactly the same (Fig. 3). As another orthogonal method, we have used RT-PCR for those proteins. However, the only protein which mRNA changed in expression was CCNB1 with L-OHP/control ratio 0.69 ± 0.14, other tested proteins (UTP11L, WDR46, DDX56, RPS19, TP53, APOA1 and FTH1) haven't changed in mRNA expression.

The first cluster from STRING analysis is cluster of proteins involved in G2/M stop or in centromere assembly. The representing protein of this group, CCNB1 showed decrease in abundance in both protein and mRNA level. To evaluate possible stop in G2/M, or more generally changes in cell cycle after L-OHP treatment, a flow cytometry analysis was performed with multiple time points - 1, 2, 4, 8, 12, 24 and 36 h and with two concentrations – $1 \times IC_{50}$ and $5 \times IC_{50}$ (Fig. 4). The reason for two concentrations is simple - standardised flow cytometry protocol uses lower concentration of cells - 1 million cells in 4 ml, thus $1 \times IC_{50}$ represents cell adjusted concentration and $5 \times IC_{50}$ volume adjusted concentration of L-OHP. The changes of cell cycle after treatment are following: In $1 \times IC_{50}$ is coming about decrease in G0/G1 and increase in S. The G2/M phase remains more less constant; however, phosphorylation of histone H3 at serine 10, a marker of mitosis, is decreasing

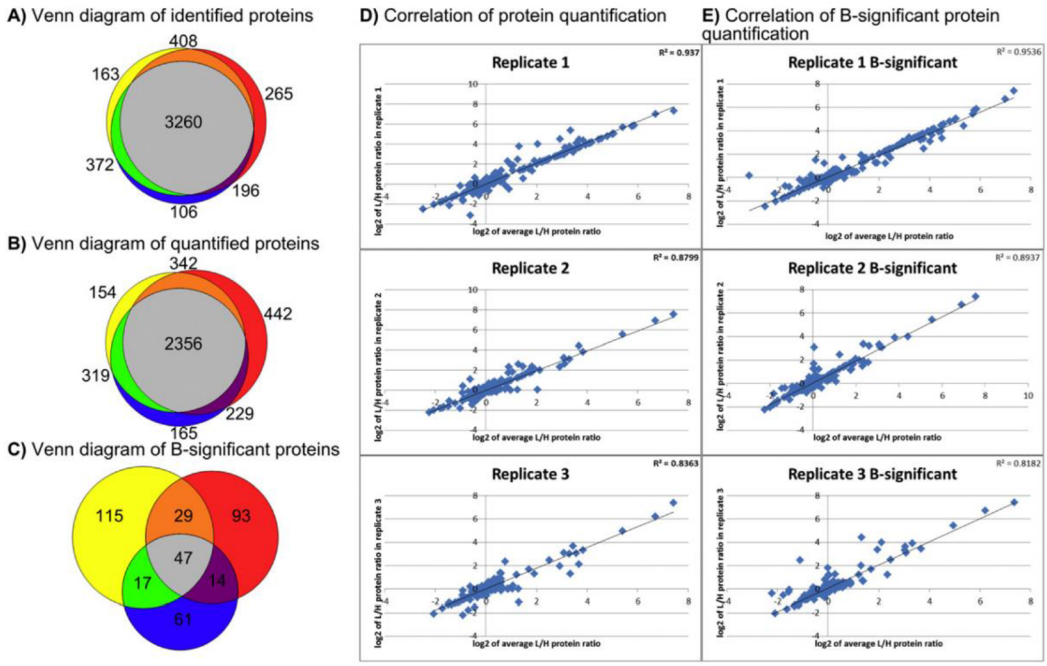

Fig. 1. Characterization of the proteomic dataset. Venn diagram of all identified proteins (A) and quantified proteins (B). Results shown in yellow, red, and blue correspond to replicates 1, 2, and 3, respectively. Correlation of protein quantifications in individual replicates relative to the average (C) and correlations of B-significant protein quantifications relative to the average (D).

Table 1
DAVID annotation analysis of B-significant proteins. For simplicity, only annotation clusters with enrichment scores above 10 are shown, along with the six most highly scored processes for each cluster. Annotation cluster 1 includes ribosomal proteins, cluster 2 includes proteins involved in ribosome biogenesis and rRNA processing, and cluster 3 includes nucleolar proteins.

Category	Term	Count	%	P value
Annotation cluster 1	*Enrichment score: 42.00*			
KEGG_PATHWAY	hsa03010:Ribosome	38	36.89	6.54E-58
GOTERM_BP_FAT	GO:0006414 ~ translational elongation	38	36.89	1.26E-57
GOTERM_MF_FAT	GO:0003735 ~ structural constituent of ribosome	41	39.81	7.40E-56
SP_PIR_KEYWORDS	Ribosomal protein	41	39.81	1.10E-54
SP_PIR_KEYWORDS	Ribonucleoprotein	43	41.75	9.59E-51
SP_PIR_KEYWORDS	Ribosome	31	30.10	1.14E-50
Annotation Cluster 2	*Enrichment score: 12.26*			
GOTERM_BP_FAT	GO:0042254 ~ ribosome biogenesis	19	18.45	7.37E-20
GOTERM_BP_FAT	GO:0022613 ~ ribonucleoprotein complex biogenesis	19	18.45	9.22E-17
GOTERM_BP_FAT	GO:0006364 ~ rRNA processing	15	14.56	7.94E-16
GOTERM_BP_FAT	GO:0016072 ~ rRNA metabolic process	15	14.56	1.48E-15
GOTERM_BP_FAT	GO:0034470 ~ ncRNA processing	15	14.56	1.76E-11
GOTERM_BP_FAT	GO:0034660 ~ ncRNA metabolic process	16	15.53	2.27E-11
Annotation Cluster 3	*Enrichment score: 11.78*			
GOTERM_CC_FAT	GO:0005730 ~ nucleolus	33	32.04	1.32E-17
GOTERM_CC_FAT	GO:0031981 ~ nuclear lumen	40	38.83	1.03E-13
GOTERM_CC_FAT	GO:0070013 ~ intracellular organelle lumen	44	42.72	1.21E-13
GOTERM_CC_FAT	GO:0043233 ~ organelle lumen	44	42.72	2.70E-13
GOTERM_CC_FAT	GO:0031974 ~ membrane-enclosed lumen	44	42.72	5.36E-13
SP_PIR_KEYWORDS	Nucleus	38	36.89	8.83E-04

over the time. Thus more cells are blocked in G2 and not enter to mitosis. In 5 × IC_{50} is distribution of cell cycle stages similar to control. The most visible changes are slight increase of G0/G1, slight decrease of S and G2/M and, mainly, increase in sub G1 fraction, which is fraction of apoptotic cells (Fig. 4).

Other clusters were validated in the following way: Cluster of secreted proteins has been validated using ELISA kit only. Influence of L-OHP to ribosomes has been validated using immunofluorescence microscopy (IFM) for RPS19 showing its translocation from nucleus to the whole cell and disappearing of positive foci (Fig. 5; with L-OHP/control ratio of spot numbers 0.09, p-value < 0.0001). Further validation of ribosomal stress has been performed by 47S pre-rRNA FISH, where the pure nucleolar concentration of 47 s pre-rRNA changed after L-OHP treatment to whole cellular localization (Fig. 6; ratio of spot numbers 0.05, p-value < 0.0001). Cluster of nucleolar proteins has been validated using IFM for regulated proteins UTP11L with L-OHP/control ratio of spot number 155.32 (p-value < 0.0001) showing disintegration of nucleoli (Fig. 5) and DDX56 (ratio 0.01, p-value < 0.0001) as well as for known nucleolar markers FBL (ratio 0.09, p-value < 0.0001) and NCL (ratio 1.76 showing nucleolar decomposition, p-value < 0.0001; Fig. 5). In all cases, there is a visible trend of nucleolar disintegration. Nucleolar morphology was further examined using light microscopy with toluidine blue staining with a shift towards metabolically inactive micronucleoli (12% to 69%, p-value < 0.0001 Fig. 6).

The most often discussed effect of L-OHP, the DNA damage, is not included in any of bioinformatic result for this study. However, according to literature mining of proteins changed in abundance, there are several proteins involved in DNA damage response (Table 2). The DNA damage caused by L-OHP was observed using IFM of H2AX with increase of protein phosphorylation at serine 139 (Supplementary Fig. 1) without change in total protein expression (Supplementary Table 1).

The common downstream result of all three stress pathways, DNA damage, nucleolar and ribosomal stress, is activation of p53. In the proteomic result, there were significant upregulation of TP53 with ratio 1.73 in only one of three replicates and this protein was not quantified in remaining two (Supplementary Table 1). Western blot verification showed upregulation of this protein with lower ratio 1.21. However, immunoprecipitation experiment using enrichment of the HDM2 and RPL5, the known activators of p53 in those stresses, haven't show any increase in this pathway (Supplementary Fig. 2).

The next step was confirmation of obtained results in other cell lines. For this purpose, we have selected osteosarcoma cell line U2OS and colorectal cancer cell line HCT116. Those cell lines were treated with 5× of their specific IC_{50} (34.5 μM for U2OS and 53.5 μM for HCT116) for uniform time 4 h corresponding to $TA_{1/2}$ of CCRF-CEM. Those cells were examined for levels of UTP11L, WDR46 and DDX56 proteins, for nucleolar stress by monitoring FBL and NCL and 47S pre-rRNA FISH for ribosomal stress. Whereas U2OS showed similar trend in behaviour with CCRF-CEM based on IFM or FISH, the trend in HCT116 was just opposite to CCRF-CEM based on FISH or immunoblot DDX56 (Fig. 7).

4. Discussion

The IC_{50} concentration of L-OHP was determined to 5.9 μM. We have used concentration 5 × IC_{50} of L-OHP, which is similar concentration of drug as in reported blood concentration of L-OHP, which is 4.15 μM [28]. Last but not least, advance in proteomic methods allowed us to use lower concentration than in previous study [16], where concentration 10 × IC_{50} was necessary to observe visible results, whereas 5 × IC_{50} haven't caused any changes observable at 2D electrophoresis (Tylečková, unpublished results). The advance in instrumentation and implementation of Orbitrap-based proteomics led to increase of significantly changed proteins. In this study we have identified 107 differently regulated proteins compared to Tylečková with an average of 31 differently regulated protein spots [16]. Such an increase allowed us to utilize modern bioinformatic tools such as DAVID or STRING. Mainly STRING analysis (Fig. 2) showed totally four clusters of interacting proteins.

Some of the proteins remained unclustered in the STRING analysis (FAM207A, ACTR10, HSPA1A, FTH1, MARS2, MRPL43 and LPCAT1). The relevant information in the literature is available only for proteins HSPA1A, FTH1 and LPCAT1. HSPA1A functions as a protein chaperone, but it is also involved in anti-inflammatory and anti-oxidant processes [29] and DNA damage responses [30]. FTH1 is involved in innate immune reactions and is overexpressed upon lipopolysaccharide stimulation [31], anoxia or oxidative stress [32], among other things. FTH1 (ferritin) has been considered as a vehicle for platinum drugs; it is possible that such drugs may form ferritin conjugates and thus induce its overexpression. LPCAT1 is reported to have anti-inflammatory properties [33]. The change in the levels of FTH1 was verified by ELISA (Fig. 3).

The first cluster from STRING analysis, cluster A (Fig. 2) contained proteins related to the centromere and G2/M cell cycle phase. L-OHP has been reported to arrest mitosis at the G2/M checkpoint [34]. This is consistent with our observation that L-OHP treatment caused the downregulation of cyclin B1 (CCNB1) and PLK1 [36], as well as proteins interacting both with centromeres and microtubules such as NUSAP1 [37], MAD1L1 [38], HOOK3 [39], CEP41 [40] and CENPF [41] (Table 2). The downregulation of CCNB1 following L-OHP treatment has been observed previously [42] and was verified by immunoblotting (Fig. 3) and mRNA expression. Arrest in G2/M was confirmed by flow cytometric analysis of cellular cycle and decrease phosphorylation of serine 10 of histone H3 in both analysed concentrations.

Protein cluster B (Fig. 2B) consisted of proteins secreted extracellularly, all of which were upregulated and many of them seems to associate with histogenetic origin of CCRF-CEM cells (T lymphocytes/lymphoblasts). LYZ is involved in innate immunity and ameliorates oxidative stress [43], and has previously been reported to be elevated after cisplatin treatment [44]. SPN is a one of the major glycoproteins in T-

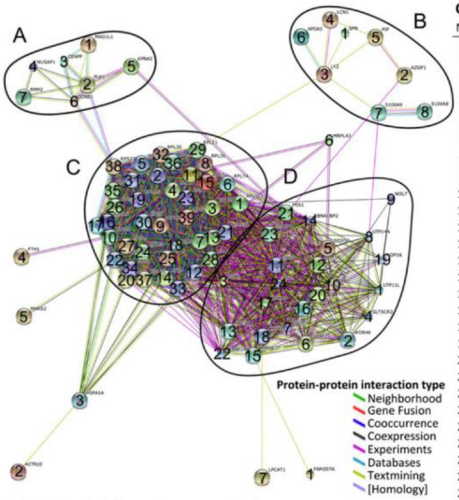

A Proteins related to centromere or mitosis

Nr.	Protein names	Gene	Ratio L/H
1	Mitotic spindle assembly checkpoint protein MAD1	MAD1L1	0.58
2	Serine/threonine-protein kinase PLK1	PLK1	0.74
3	Centromere protein F	CENPF	0.82
4	Nucleolar and spindle-associated protein 1	NUSAP1	0.85
5	Importin subunit alpha	KPNA2	0.86
6	G2/mitotic-specific cyclin-B1	CCNB1	0.87
7	Ribonucleoside-diphosphate reductase subunit M2	RRM2	1.11

B Secretory proteins

Nr.	Protein names	Gene	Ratio L/H
1	Leukosialin	SPN	3.27
2	Zinc-alpha-2-glycoprotein	AZGP1	3.97
3	Lysozyme C	LYZ	5.49
4	Lipocalin-1	LCN1	5.70
5	Prolactin-inducible protein	PIP	8.46
6	Apolipoprotein A-I	APOA1	9.30
7	Protein S100-A9	S100A9	10.45
8	Protein S100-A8	S100A8	12.61

Unclustered proteins

Nr.	Protein names	Gene	Ratio L/H
1	Protein FAM207A	FAM207A	0.68
2	Actin-related protein 10	ACTR10	0.74
3	Heat shock 70 kDa protein 1A/1B	HSPA1A	1.13
4	Ferritin	FTH1	1.22
5	Methionine--tRNA ligase, mitochondrial	MARS2	3.79
6	39S ribosomal protein L43, mitochondrial	MRPL43	4.38
7	Lysophosphatidylcholine acyltransferase 1	LPCAT1	10.96

C Ribosomal proteins

Nr.	Protein names	Gene	Ratio L/H
1	60S ribosomal protein L7-like 1	RPL7L1	0.43
2	60S ribosomal protein L35a	RPL35A	0.86
3	60S ribosomal protein L15	RPL15	0.86
4	60S ribosomal protein L13	RPL13	0.86
5	60S ribosomal protein L34	RPL34	0.86
6	60S ribosomal protein L7a	RPL7A	0.86
7	60S ribosomal protein L27a	RPL27A	0.87
8	60S ribosomal protein L36	RPL36	0.87
9	60S ribosomal protein L6	RPL6	0.87
10	60S ribosomal protein L19	RPL19	0.87
11	60S ribosomal protein L18a	RPL18A	0.88
12	40S ribosomal protein S8	RPS8	0.88
13	60S ribosomal protein L7	RPL7	0.88
14	60S ribosomal protein L4	RPL4	0.88
15	40S ribosomal protein S5	RPS5	0.88
16	40S ribosomal protein S16	RPS16	0.88
17	40S ribosomal protein S4, X isoform	RPS4X	0.88
18	60S ribosomal protein L10a	RPL10A	0.89
19	60S ribosomal protein L18	RPL18	0.89
20	40S ribosomal protein S23	RPS23	0.89
21	60S ribosomal protein L23a	RPL23A	0.89
22	60S ribosomal protein L13a	RPL13A	0.89
23	40S ribosomal protein S24	RPS24	0.89
24	Ribosomal protein L14 variant	RPL14	0.90
25	60S ribosomal protein L8	RPL8	0.90
26	40S ribosomal protein S3a	RPS3A	0.90
27	40S ribosomal protein S11	RPS11	0.90
28	60S ribosomal protein L3	RPL3	0.90
29	60S ribosomal protein L21	RPL21	0.90
30	40S ribosomal protein S6	RPS6	0.90
31	60S ribosomal protein L32	RPL32	0.90
32	60S ribosomal protein L35	RPL35	0.90
33	40S ribosomal protein S13	RPS13	0.90
34	40S ribosomal protein S3	RPS3	0.91
35	60S ribosomal protein L10	RPL10	0.91
36	60S ribosomal protein L12	RPL12	0.92
37	60S ribosomal protein L26	RPL26	0.96
38	Ubiquitin-40S ribosomal protein S27a	RPS27A	1.13
39	60S ribosomal protein L27	RPL27	1.20

D Nucleolar proteins

Nr.	Protein names	Gene	Ratio L/H
1	Probable U3 small nucleolar RNA-associated protein 11	UTP11L	0.24
2	WD repeat-containing protein 46	WDR46	0.28
3	Ribosome biogenesis protein NSA2 homolog	NSA2	0.31
4	Glioma tumor suppressor candidate region gene 2 protein	GLTSCR2	0.36
5	Probable ATP-dependent RNA helicase DDX56	DDX56	0.53
6	DDB1- and CUL4-associated factor 13	DCAF13	0.54
7	Ribosomal L1 domain-containing protein 1	RSL1D1	0.58
8	U3 small nucleolar RNA-associated protein 14 homolog A	UTP14A	0.63
9	Nucleolar protein 7	NOL7	0.66
10	U3 small nucleolar RNA-associated protein 6 homolog	UTP6	0.69
11	Guanine nucleotide-binding protein-like 3	GNL3	0.73
12	ATP-dependent RNA helicase DDX54	DDX54	0.76
13	Protein RRP5 homolog	PDCD11	0.76
14	Probable rRNA-processing protein EBP2	EBNA1BP2	0.76
15	RRP12-like protein	RRP12	0.78
16	Probable ATP-dependent RNA helicase DDX27	DDX27	0.80
17	Ribosome biogenesis protein BRX1 homolog	BRIX1	0.80
18	Pumilio domain-containing protein KIAA0020	KIAA0020	0.81
19	Nucleolar protein 16	NOP16	0.82
20	RNA-binding protein 28	RBM28	0.83
21	Pescadillo homolog	PES1	0.87
22	Myb-binding protein 1A	MYBBP1A	0.87
23	Nucleolar GTP-binding protein 1	GTPBP4	0.90
24	Ribosome production factor 2 homolog	RPF2	1.10

Fig. 2. STRING analysis of B-significant proteins. The yellow cluster (A) includes centromere proteins and proteins involved in G2/M arrest. The purple cluster (B) includes common secretory proteins. The blue cluster (C) includes ribosomal proteins. The red cluster (D) includes nucleolar proteins. The proteins in the clusters are listed in the corresponding tables.

cells; it is involved in cellular adhesion and its upregulation activates the p53 protein, which can lead to cell cycle arrest [45]. In addition, p53 plays a central role in DNA damage responses, as discussed below. Lipocalin 1 (LCN1) is a transporter of small hydrophobic molecules [46], and the increase in its expression is probably linked to L-OHP detoxification. According to a previous report [47], LCN1 is a potential biomarker of cisplatin-induced nephrotoxicity. AZGP1 is involved in lipid metabolism and has been identified as a promising biomarker of different types of carcinomas. It effects the cell cycle by downregulating the cyclin dependent kinase cdc2 and slows the G2/M transition [48]. PIP, which was also upregulated in our experiments, is a potential cancer biomarker whose abundance increases in breast and prostate cancers and which binds to AZGP1 [49]. Variation of APOA1 level can be linked to poor prognosis in cancer, both without [50] and with cisplatin treatment [51]. APOA1 reportedly has anti-inflammatory, anti-apoptotic, and (of particular relevance during L-OHP treatment), antioxidant activity. As such, it is reasonable to suppose that the increase in APOA1 expression following L-OHP treatment is due to the high oxidative stress induced by the drug, so an increase in APOA1 expression can be regarded as a biomarker for effective L-OHP therapy [52]. The interaction between APOA1 and its cellular receptor, ABCA1, triggers several signaling events. These include the activation of the Cdc42 protein (which leads to cytoskeletal reorganization) and changes in the ability of other oncoproteins, including Ras and EGFR, to induce cellular transformation. In addition, binding partners of APOA1 such as APOL1 are involved in autophagy. Identifying the mechanisms that modulate APOA1 gene expression could lead to a deeper understanding of L-OHP's mechanism of action,

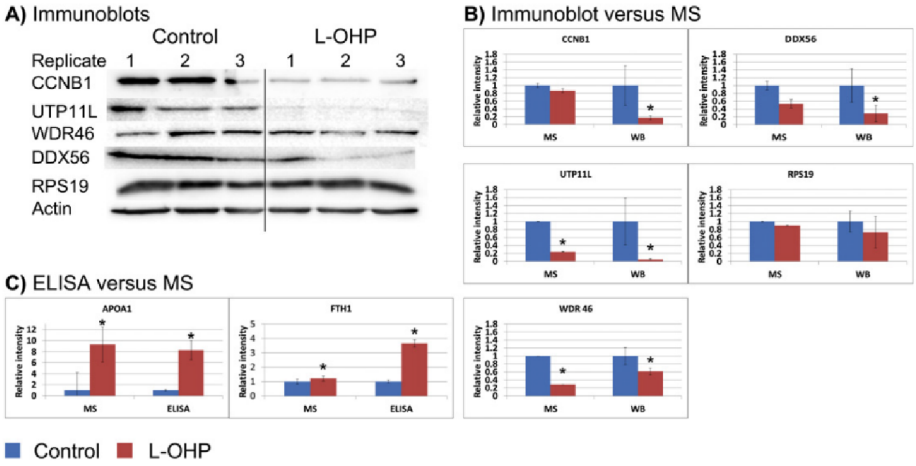

Fig. 3. Verification of the up/down-regulation of the proteins TERF1, UTP11L, WDR46, DDX56, RPS1, APOA1 and FTH1. The results of triplicate Western blot analyses for L-OHP-treated and control cells are shown in A, with the corresponding normalized base intensities in B. The results for the proteins APOA1 and FTH1 were further verified by ELISA. The relative intensities for these proteins in the treated and untreated cells are compared to the relative MS intensities in C.

and APOA1 expression could be monitored as a biomarker for treatment response. Two other proteins that were identified as being significantly upregulated, S100A8 and S100A9, are known to be involved in acute inflammatory responses and the induction of apoptosis via the release of nitric oxide and reactive oxygen species [53]. The differential overexpression of APOA1 following L-OHP treatment was verified using ELISA (Fig. 3).

We observed statistically significant downregulation of several ribosomal proteins in cluster C (Fig. 2C). This is a sign of ribosomal stress, which causes the shutdown of ribosome biosynthesis [27]. However, ribosomal proteins were not regulated uniformly: some ribosomal proteins were downregulated non-significantly (e.g. RPS19, whose downregulation was verified by immunoblotting and microscopy - Figs. 3 and 5) and others exhibited no detectable change in expression (e.g. RPL5, RPL11; Supplementary Table 1). These differences in ribosomal protein expression may be connected to the roles of the ribosomal proteins in nucleolar stability, rRNA synthesis or p53 activation [54]. Decrease in ribosome content was further confirmed by decrease of 47S pre-rRNA level and its translocation from nucleoli to nucleoplasm and cytoplasm. Contrary to decrease of ribosome synthesis, the proteosynthesis decreased very slowly indicating full functionality of remaining ribosomes (Fig. 4). The L-OHP treatment is reported to affect ribosomes [55], and the ribosomal pathway is involved in the development of L-OHP resistance [56].

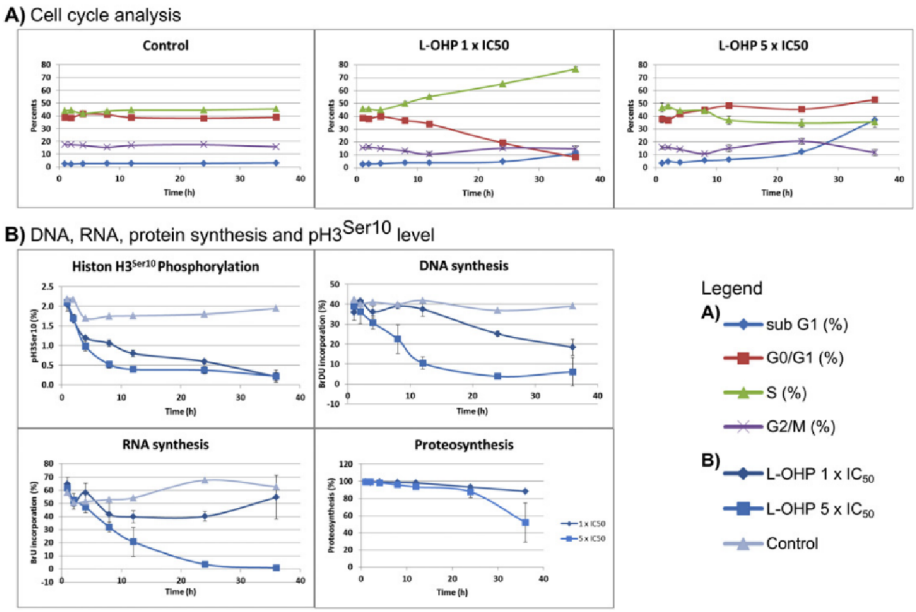

Fig. 4. Flow cytometric analysis of cellular response to L-OHP. This analysis is split into cell cycle analysis (A) showing cell cycle to be influenced mainly at lower L-OHP concentration and analysis of mitosis rate by phosphorylation of histone H3 at Ser10, DNA, RNA and proteosynthesis (B).

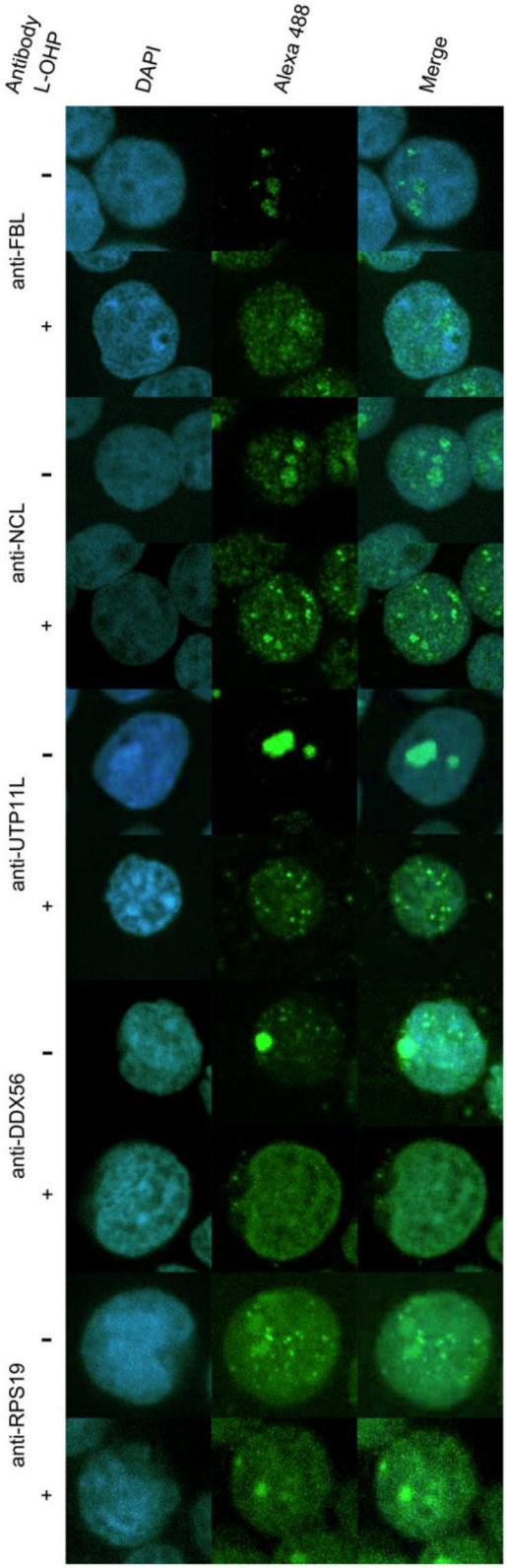

Correspondingly to down-regulation or ribosome biosynthesis, the concentration and distribution of proteins localized in nucleolus shown in Fig. 2D may indicate nucleolar stress, which reportedly causes the shrinkage or disruption of nucleoli under stress conditions [57] and has been reported to occur after L-OHP treatment [58,59]. We were able to reproduce these results during the early stages of the L-OHP response (Fig. 6) and observed a clear shift towards metabolically inactive micronucleoli (12% to 69%, Fig. 6D). This phenomenon is reflected in our proteomic data, which show the downregulation of proteins involved in the small (UTP11L, UTP6, UTP14A, DCAF13, PNO1 and WDR46 [60,61]) and large (NSA2, PES1, DDX27, EBNA1BP2 (EBP2), RBM28, RPF2 and EFTUD1 [62–66]) ribosomal subunit processomes, RNA processing proteins (NOP16, DDX proteins [67,68]), nucleolar stress sensors (MYBBP1 [69]), and PES1 interactors (BRIX1, RRP12 [62]). We selected three proteins from this set - UTP11L, WDR46 and DDX56 - for immunoblot verification because of their high fold changes (Fig. 2); in all three cases, immunoblotting confirmed their downregulation (Fig. 3) and change of nucleolar localization was confirmed by IFM (Fig. 5). Nucleolar desintegration was also observed using FBL and NCL as nucleolar markers and observed on FISH monitoring of 47S pre-rRNA, where decrease of rRNA followed the same trend as was observed in toluidine blue staining (Fig. 6).

In addition to the proteins assigned to the clusters shown in Fig. 2, we found that several of the proteins identified in the proteomic analysis have previously been reported to be involved in DNA damage responses (Table 2). DNA damage is known to trigger nucleolar and ribosomal stress [27] and the formation of DNA-platinum crosslinks is well established as the main effect of platinum drugs [6]. In our experiments with L-OHP treatment, we observed the upregulation of the DNA damage response proteins TERF2 [70] and RRM2 [71], as well as the downregulation of other DNA damage response proteins such as NHEJ1 [72], NUSAP1 [73], GLTSCR2 [74], and KIAA0020 [75]. The DNA damage was confirmed by the increase of H2AX phosphorylation at Ser139 (Supplementary Fig. 1).

Ribosomal and nucleolar stress are closely linked because nucleolus is the place of ribosome biogenesis and this biogenesis is thus dependent on nucleoli in good condition. Nucleolar stress is triggered after DNA damage by inhibition of RNA polymerase I [27]. Our experiments revealed no changes in the expression of RNA polymerase I upon L-OHP treatment (Supplementary Table 1). However, nucleolar stress responses can also be activated via TOPBP1 [76]. While our analysis identified TOPBP1, we were not able to quantify this protein (Supplementary Table 1). The actual pathway of DNA-damage-activated nucleolar stress caused by L-OHP is not elucidated yet.

All three stress responses (ribosomal, nucleolar and DNA damage) are known to activate the p53 pathway. The activation of this pathway by DNA damage responses is well described and reviewed elsewhere, and the main pathway of DNA damage-dependent p53 activation is through nucleolar disruption and activation of p53 as a consequence of the binding of MDM 2 to the free ribosomal subunits RPL5 and RPL11 [27]. Based on results from immunoprecipitation experiment, this pathway is not activated in CCRF-CEM after L-OHP treatment (Supplementary Fig. 2). Protein p53 is thus not participating in L-OHP induced nucleolar and ribosomal stress in CCRF-CEM cell line. However, there are other mechanisms of apoptosis activation driven by nucleolar stress occurring in cancer or organisms lacking a p53 protein homolog are reviewed by James et al. [77]. Cancer cells generally have unusually large nucleoli [78], and one of the proteins involved in the p53-independent nucleolar stress response, pescadillo (PES1), has been shown to be upregulated in $p53^{-/-}$ cells and in cancer. In keeping with our results,

Fig. 5. Immunofluorescent staining of FBL, NCL, UTP11L, DDX56 and RPS19 visualizes changes in their nucleolar localization after L-OHP treatment. The localization of the proteins of interest was examined using confocal spinning disc fluorescent microscopy at 1000× magnification.

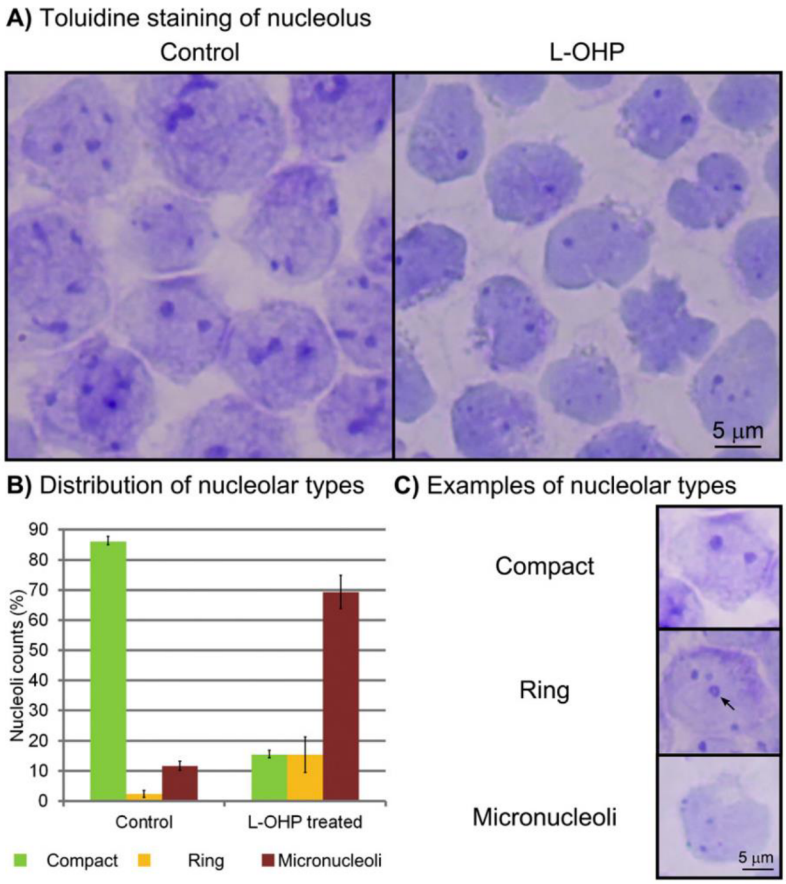

Fig. 6. Fluorescent in-situ hybridization of 47S pre-rRNA (A) and toluidine blue staining of control and L-OHP treated CCRF-CEM cells (B). The distribution of nucleolar types is shown in subfigure C and representative examples of each type are shown in subfigure D. Definitions of single nucleolar types are provided in [87–89].

downregulation of PES1 reportedly leads to cell cycle arrest and apoptosis [79] (Supplementary Table 2).

The activation of nucleolar and ribosomal stress by L-OHP has been already described previously [10,55,56,58] and is described in this paper in more detail. However, nucleolar stress proteins are not often reported in large-scale genomic or proteomic experiments of cellular response to drugs known to induce such a stress e.g. doxorubicin used to induce nucleolar stress in [80] but without its detection in [16,81]. The same situation is in the case of L-OHP, where nucleolar and ribosomal stress were detected in this paper, but in study of Briffa [82] comparing genomic, transcriptomic and proteomic responses of different colorectal cancers was not observed any signs of such stress responses.

Table 2
Proteins exhibiting significant changes in abundance that are involved in DNA damage responses and G2/M arrest. Proteins are shown along with their average fold change, intensity, significance B p-value, and references detailing their involvement in DNA damage responses.

Protein names	Gene names	Ratio L/H	Reference
Proteins involved in DNA damage response			
Glioma tumor suppressor candidate region gene 2 protein	GLTSCR2	0.36	Kim et al. [74]
Non-homologous end-joining factor 1	NHEJ1	0.55	Yano et al. [72]
Pumilio domain-containing protein KIAA0020	KIAA0020	0.81	Chang et al. [75]
Nucleolar and spindle-associated protein 1	NUSAP1	0.85	Kotian et al. [73]
Ribonucleoside-diphosphate reductase subunit M2	RRM2	1.11	Lu et al. [71]
Telomeric repeat-binding factor 2	TERF2	1.39	de Lange et al. [70]
Proteins involved in G2/M arrest			
Centrosomal protein of 41 kDa	CEP41	0.38	Lee et al. [40]
Protein Hook homolog 3	HOOK3	0.39	Ge et al. [39]
Mitotic spindle assembly checkpoint protein MAD1	MAD1L1	0.58	Kruse et al. [38]
Serine/threonine-protein kinase PLK1	PLK1	0.74	Lee et al. [36]
Centromere protein F	CENPF	0.82	Waters et al. [41]
G2/mitotic-specific cyclin-B1	CCNB1	0.87	Menon et al. [35]

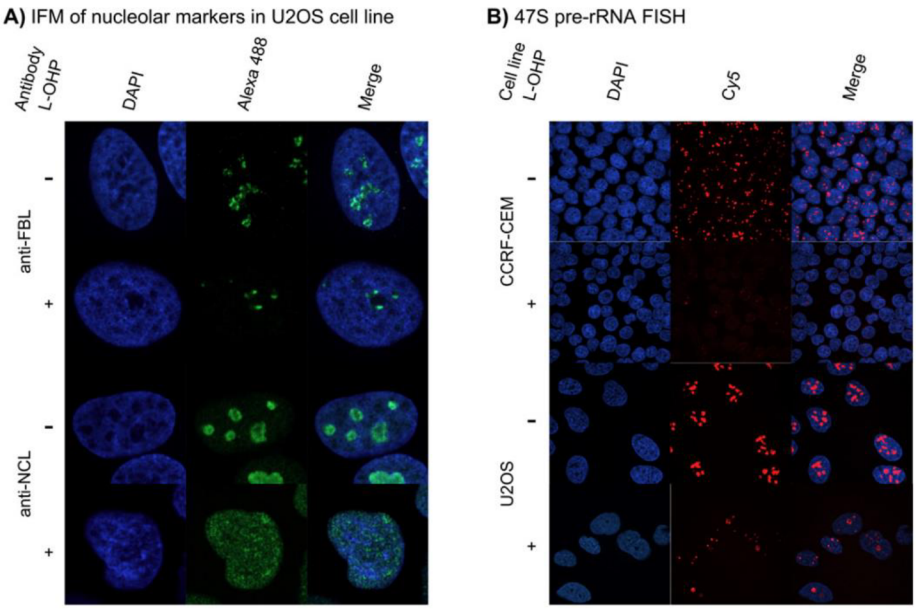

Fig. 7. Nucleolar stress induced by L-OHP in U2OS and HCT116 cell lines.

This is not in strict contradiction with results of this study, because mRNA of nucleolar and ribosomal proteins tested in this study has not changed in expression too and proteomic experiment in [82] was targeted to selected proteins only. However, to address the issue of nucleolar and ribosomal stress, two solid cancer cell lines, osteosarcoma derived U2OS and colorectal cancer derived HCT116, were examined. Whereas U2OS followed the CCRF-CEM in both parameters with shrinking nucleoli and reduction of 47S pre-rRNA, HCT116 cell line responded in opposite manner by increasing of 47S pre-rRNA and activation of protein DDX56 (Fig. 7). Those results show different mechanisms of cellular response in HCT116 and could be the promising background for future comparison of L-OHP cellular responses.

Nucleolar stress is a common stress response induced by a plethora of stressors, e.g. UV irradiation, heat, or chemical stress [83]. Induction of nucleolar stress may play an important role in cancer treatment. This can be illustrated by the wide range of anticancer drugs that cause such stress, including L-OHP, cisplatin [84], doxorubicin [80] and etoposide [85]. Indeed, some authors have suggested that nucleolar stress proteins may be viable targets for anti-cancer drug development [86] because drugs selectively targeting the nucleolus would be unlikely to cause major genotoxic stress and additional mutations. Prior to this work, the effects of L-OHP treatment on nucleolar stress had only received passing attention, notably in Jamieson's investigation into the use of microscopy to monitor nucleolar shrinkage [58]. This shrinkage correlates with observed level of neuropathy in rats or mice, and can be modulated by sequential dosage with paclitaxel and L-OHP.

Interestingly, extensive proteomic profiling of L-OHP treated CCRF-CEM cells did not reveal activation of apoptotic machinery, thus confirming validity of our approach based on treatment of cells with cytotoxic drugs for time corresponding to half-time to induction of apoptosis.

5. Conclusion

We have analysed the proteomic responses of CCRF-CEM cells to L-OHP treatment. The main cellular response to the drug was the activation of DNA damage responses, which triggered nucleolar stress and significantly impaired ribosome biogenesis. With adequate follow-up validation, proteins such as APOA1 and FTH1 that were significantly up-regulated by L-OHP treatment could potentially be used as surrogate biomarkers of therapeutic responses to L-OHP.

Supplementary data to this article can be found online at http://dx.doi.org/10.1016/j.jprot.2017.05.005.

Conflict of interest

The authors declare no conflict of interest.

Acknowledgements

We would like to thank Pavlina Kalabova for help with the verification of MS results. This work was supported by grants LF_2016_019, Ministry of School, Education and Youth (LO1304 and LM2015064) and Technological Agency of the Czech Republic (TE02000058).

MH and PD designed the experiments; TO, DH, GR and PD prepared samples for MS; TO and DH performed MS analysis and data processing; TO, JV and JS performed immunoblotting and staining verification; JBS performed ELISA assays; TO, ZM, JR and PZ performed IFM; ZM performed the FISH; PM performed immunoprecipitation; HS performed RT-PCR; TO, LV, MH and PD wrote the article.

References

[1] R.P. Miller, R.K. Tadagavadi, G. Ramesh, W.B. Reeves, Mechanisms of cisplatin nephrotoxicity, Toxins 2 (2010) 2490–2518, http://dx.doi.org/10.3390/toxins2112490.
[2] M.E. Gore, I. Fryatt, E. Wiltshaw, T. Dawson, B.A. Robinson, A.H. Calvert, Cisplatin/carboplatin cross-resistance in ovarian cancer, Br. J. Cancer 60 (1989) 767–769.
[3] Y. Kidani, M. Noji, T. Tashiro, Antitumor activity of platinum(II) complexes of 1,2-diamino-cyclohexane isomers, Gann 71 (1980) 637–643.
[4] S. Stintzing, Management of Colorectal Cancer, F1000Prime Rep, 6, 2014http://dx.doi.org/10.12703/P6-108.
[5] I. Garrido-Laguna, M. Hidalgo, Pancreatic cancer: from state-of-the-art treatments to promising novel therapies, Nat. Rev. Clin. Oncol. (2015)http://dx.doi.org/10.1038/nrclinonc.2015.53.
[6] S. Dilruba, G.V. Kalayda, Platinum-based drugs: past, present and future, Cancer Chemother. Pharmacol. 77 (2016) 1103–1124, http://dx.doi.org/10.1007/s00280-016-2976-z.
[7] N. Mounier, T. El Gnaoui, H. Tilly, D. Canioni, C. Sebban, R.-O. Casasnovas, R. Delarue, A. Sonet, P. Beaussart, T. Petrella, S. Castaigne, S. Bologna, G. Salles, A. Rahmouni, P.

Gaulard, C. Haioun, Rituximab plus gemcitabine and oxaliplatin in patients with refractory/relapsed diffuse large B-cell lymphoma who are not candidates for high-dose therapy. A phase II lymphoma study association trial, Haematologica 98 (2013) 1726–1731, http://dx.doi.org/10.3324/haematol.2013.090597.
[8] T. Alcindor, N. Beauger, Oxaliplatin: a review in the era of molecularly targeted therapy, Curr. Oncol. 18 (2011) 18–25.
[9] R.K. Mehmood, Review of cisplatin and oxaliplatin in current immunogenic and monoclonal antibody treatments, Oncol. Rev. 8 (2014) 256, http://dx.doi.org/10.4081/oncol.2014.256.
[10] M.J. McKeage, T. Hsu, D. Screnci, G. Haddad, B.C. Baguley, Nucleolar damage correlates with neurotoxicity induced by different platinum drugs, Br. J. Cancer 85 (2001) 1219–1225, http://dx.doi.org/10.1054/bjoc.2001.2024.
[11] M. Stukova, M.D. Hall, S.D. Tsotsoros, J.P. Madigan, N.P. Farrell, M.M. Gottesman, Reduced accumulation of platinum drugs is not observed in drug-resistant ovarian cancer cell lines derived from cisplatin-treated patients, J. Inorg. Biochem. 149 (2015) 45–48, http://dx.doi.org/10.1016/j.jinorgbio.2015.05.003.
[12] L. Li, R. Liu, F. Xu, Y. Zu, Z. Liu, Study on the interactions between anti-cancer drug oxaliplatin and DNA by atomic force microscopy, Micron. Oxf. Engl. 1993 (76) (2015) 46–51, http://dx.doi.org/10.1016/j.micron.2015.05.002.
[13] T. Ochiai, K. Nishimura, T. Watanabe, M. Kitajima, A. Nakatani, T. Sato, K. Kishine, S. Futagawa, S. Mashiko, I. Nagaoka, Mechanism underlying the transient increase of serum iron during FOLFOX/FOLFIRI therapy, Mol. Clin. Oncol. 2 (2014) 968–972, http://dx.doi.org/10.3892/mco.2014.385.
[14] T.J. Preston, J.T. Henderson, G.P. McCallum, P.G. Wells, Base excision repair of reactive oxygen species-initiated 7,8-dihydro-8-oxo-2′-deoxyguanosine inhibits the cytotoxicity of platinum anticancer drugs, Mol. Cancer Ther. 8 (2009) 2015–2026, http://dx.doi.org/10.1158/1535-7163.MCT-08-0929.
[15] S. Ahmad, Platinum-DNA interactions and subsequent cellular processes controlling sensitivity to anticancer platinum complexes, Chem. Biodivers. 7 (2010) 543–566, http://dx.doi.org/10.1002/cbdv.200800340.
[16] J. Tyleckova, R. Hrabakova, K. Mairychova, P. Halada, L. Radova, P. Dzubak, M. Hajduch, S.J. Gadher, H. Kovarova, Cancer cell response to anthracyclines effects: mysteries of the hidden proteins associated with these drugs, Int. J. Mol. Sci. 13 (2012) 15536–15564, http://dx.doi.org/10.3390/ijms131215536.
[17] H. Skalnikova, J. Martinkova, R. Hrabakova, P. Halada, M. Dziechciarkova, M. Hajduch, S.J. Gadher, A. Hammar, D. Enetoft, A. Ekefjard, O. Forsstrom-Olsson, H. Kovarova, Cancer drug-resistance and a look at specific proteins: Rho GDP-dissociation inhibitor 2, Y-box binding protein 1, and HSP70/90 organizing protein in proteomics clinical application, J. Proteome Res. 10 (2011) 404–415, http://dx.doi.org/10.1021/pr100468w.
[18] M. Hajdúch, V. Mihál, J. Minarík, E. Faber, M. Safárová, E. Weigl, P. Antálek, Decreased in vitro chemosensitivity of tumour cells in patients suffering from malignant diseases with poor prognosis, Cytotechnology 19 (1996) 243–245.
[19] J. Cox, M. Mann, MaxQuant enables high peptide identification rates, individualized p.p.b.-range mass accuracies and proteome-wide protein quantification, Nat. Biotechnol. 26 (2008) 1367–1372, http://dx.doi.org/10.1038/nbt.1511.
[20] D.W. Huang, B.T. Sherman, R.A. Lempicki, Systematic and integrative analysis of large gene lists using DAVID bioinformatics resources, Nat. Protoc. 4 (2008) 44–57, http://dx.doi.org/10.1038/nprot.2008.211.
[21] A. Franceschini, D. Szklarczyk, S. Frankild, M. Kuhn, M. Simonovic, A. Roth, J. Lin, P. Minguez, P. Bork, C. von Mering, L.J. Jensen, STRING v9.1: protein-protein interaction networks, with increased coverage and integration, Nucleic Acids Res. 41 (2013) D808–D815, http://dx.doi.org/10.1093/nar/gks1094.
[22] K. Smetana, J. Karban, M. Trneny, To the nucleolar bodies (nucleoli) in cells of the lymphocytic lineage in patients suffering from B - chronic lymphocytic leukemia, Neoplasma 57 (2010) 495–500.
[23] C. Carron, M.-F. O'Donohue, V. Choesmel, M. Faubladier, P.-E. Gleizes, Analysis of two human pre-ribosomal factors, bystin and hTsr1, highlights differences in evolution of ribosome biogenesis between yeast and mammals, Nucleic Acids Res. 39 (2011) 280–291, http://dx.doi.org/10.1093/nar/gkq734.
[24] L. Borkova, S. Gurska, P. Dzubak, R. Burianova, M. Hajduch, J. Sarek, I. Popa, M. Urban, Lupane and 18α-oleanane derivatives substituted in the position 2, their cytotoxicity and influence on cancer cells, Eur. J. Med. Chem. 121 (2016) 120–131, http://dx.doi.org/10.1016/j.ejmech.2016.05.029.
[25] D.C. Dieterich, A.J. Link, J. Graumann, D.A. Tirrell, E.M. Schuman, Selective identification of newly synthesized proteins in mammalian cells using bioorthogonal noncanonical amino acid tagging (BONCAT), Proc. Natl. Acad. Sci. U. S. A. 103 (2006) 9482–9487, http://dx.doi.org/10.1073/pnas.0601637103.
[26] J.A. Vizcaíno, R.G. Côté, A. Csordas, J.A. Dianes, A. Fabregat, J.M. Foster, J. Griss, E. Alpi, M. Birim, J. Contell, G. O'Kelly, A. Schoenegger, D. Ovelleiro, Y. Pérez-Riverol, F. Reisinger, D. Ríos, R. Wang, H. Hermjakob, The PRoteomics IDEntifications (PRIDE) database and associated tools: status in 2013, Nucleic Acids Res. 41 (2013) D1063–D1069, http://dx.doi.org/10.1093/nar/gks1262.
[27] I. Grummt, The nucleolus—guardian of cellular homeostasis and genome integrity, Chromosoma 122 (2013) 487–497, http://dx.doi.org/10.1007/s00412-013-0430-0.
[28] H. Ito, H. Yamaguchi, A. Fujikawa, N. Tanaka, A. Furugen, K. Miyamori, N. Takahashi, J. Ogura, M. Kobayashi, T. Yamada, N. Mano, K. Iseki, A full validated hydrophilic interaction liquid chromatography-tandem mass spectrometric method for the quantification of oxaliplatin in human plasma ultrafiltrates, J. Pharm. Biomed. Anal. 71 (2012) 99–103, http://dx.doi.org/10.1016/j.jpba.2012.08.010.
[29] D.C. Henstridge, M. Whitham, M.A. Febbraio, Chaperoning to the metabolic party: the emerging therapeutic role of heat-shock proteins in obesity and type 2 diabetes, Mol. Metab. 3 (2014) 781–793, http://dx.doi.org/10.1016/j.molmet.2014.08.003.
[30] Y. Duan, S. Huang, J. Yang, P. Niu, Z. Gong, X. Liu, L. Xin, R.W. Currie, T. Wu, HspA1A facilitates DNA repair in human bronchial epithelial cells exposed to benzo[a]pyrene and interacts with casein kinase 2, Cell Stress Chaperones 19 (2014) 271–279, http://dx.doi.org/10.1007/s12192-013-0454-7.
[31] D.S.T. Ong, L. Wang, Y. Zhu, B. Ho, J.L. Ding, The response of ferritin to LPS and acute phase of pseudomonas infection, J. Endotoxin Res. 11 (2005) 267–280, http://dx.doi.org/10.1179/096805105X58698.
[32] D. Finazzi, P. Arosio, Biology of ferritin in mammals: an update on iron storage, oxidative damage and neurodegeneration, Arch. Toxicol. 88 (2014) 1787–1802, http://dx.doi.org/10.1007/s00204-014-1329-0.
[33] E. Stanca, G. Serviddio, F. Bellanti, G. Vendemiale, L. Siculella, A.M. Giudetti, Down-regulation of LPCAT expression increases platelet-activating factor level in cirrhotic rat liver: potential antiinflammatory effect of silybin, Biochim. Biophys. Acta 1832 (2013) 2019–2026, http://dx.doi.org/10.1016/j.bbadis.2013.07.005.
[34] S. William-Faltaos, D. Rouillard, P. Lechat, G. Bastian, Cell cycle arrest by oxaliplatin on cancer cells, Fundam. Clin. Pharmacol. 21 (2007) 165–172, http://dx.doi.org/10.1111/j.1472-8206.2007.00462.x.
[35] V.R. Menon, E.J. Peterson, K. Valerie, N.P. Farrell, L.F. Povirk, Ligand modulation of a dinuclear platinum compound leads to mechanistic differences in cell cycle progression and arrest, Biochem. Pharmacol. 86 (2013) 1708–1720, http://dx.doi.org/10.1016/j.bcp.2013.10.012.
[36] K.S. Lee, D.-Y. Oh, Y.H. Kang, J.-E. Park, Self-regulated mechanism of Plk1 localization to kinetochores: lessons from the Plk1-PBIP1 interaction, Cell Div 3 (2008) 4, http://dx.doi.org/10.1186/1747-1028-3-4.
[37] T. Raemaekers, K. Ribbeck, J. Beaudouin, W. Annaert, M. Van Camp, I. Stockmans, N. Smets, R. Bouillon, J. Ellenberg, G. Carmeliet, NuSAP, a novel microtubule-associated protein involved in mitotic spindle organization, J. Cell Biol. 162 (2003) 1017–1029, http://dx.doi.org/10.1083/jcb.200302129.
[38] T. Kruse, M.S.Y. Larsen, G.G. Sedgwick, J.O. Sigurdsson, W. Streicher, J.V. Olsen, J. Nilsson, A direct role of Mad1 in the spindle assembly checkpoint beyond Mad2 kinetochore recruitment, EMBO Rep. 15 (2014) 282–290, http://dx.doi.org/10.1002/embr.201338101.
[39] X. Ge, C.L. Frank, F. Calderon de Anda, L.-H. Tsai, Hook3 interacts with PCM1 to regulate pericentriolar material assembly and the timing of neurogenesis, Neuron 65 (2010) 191–203, http://dx.doi.org/10.1016/j.neuron.2010.01.011.
[40] J.E. Lee, J.L. Silhavy, M.S. Zaki, J. Schroth, S.L. Bielas, S.E. Marsh, J. Olvera, F. Brancati, M. Iannicelli, K. Ikegami, A.M. Schlossman, B. Merriman, T. Attié-Bitach, C.V. Logan, I.A. Glass, A. Cluckey, C.M. Louie, J.H. Lee, H.R. Raynes, I. Rapin, I.P. Castroviejo, M. Setou, C. Barbot, E. Boltshauser, S.F. Nelson, F. Hildebrandt, C.A. Johnson, D.A. Doherty, E.M. Valente, J.G. Gleeson, CEP41 is mutated in Joubert syndrome and is required for tubulin glutamylation at the cilium, Nat. Genet. 44 (2012) 193–199, http://dx.doi.org/10.1038/ng.1078.
[41] A.M. Waters, R. Asfahani, P. Carroll, L. Bicknell, F. Lescai, A. Bright, E. Chanudet, A. Brooks, S. Christou-Savina, G. Osman, P. Walsh, C. Bacchelli, A. Chapgier, B. Vernay, D.M. Bader, C. Deshpande, M. O'Sullivan, L. Ocaka, H. Stanescu, H.S. Stewart, F. Hildebrandt, E. Otto, C.A. Johnson, K. Szymanska, N. Katsanis, E. Davis, R. Kleta, M. Hubank, S. Doxsey, A. Jackson, E. Stupka, M. Winey, P.L. Beales, The kinetochore protein, CENPF, is mutated in human ciliopathy and microcephaly phenotypes, J. Med. Genet. 52 (2015) 147–156, http://dx.doi.org/10.1136/jmedgenet-2014-10r2691.
[42] P. Noordhuis, A.C. Laan, K. van de Born, N. Losekoot, I. Kathmann, G.J. Peters, Oxaliplatin activity in selected and unselected human ovarian and colorectal cancer cell lines, Biochem. Pharmacol. 76 (2008) 53–61, http://dx.doi.org/10.1016/j.bcp.2008.04.007.
[43] H. Liu, F. Zheng, Q. Cao, B. Ren, L. Zhu, G. Striker, H. Vlassara, Amelioration of oxidant stress by the defensin lysozyme, Am. J. Physiol. Endocrinol. Metab. 290 (2006) E824–E832, http://dx.doi.org/10.1152/ajpendo.00349.2005.
[44] K. Pai, A. Sodhi, Effect of cisplatin, rIFN-Y, LPS and MDP on release of H2O2, O2- and lysozyme from human monocytes in vitro, Indian J. Exp. Biol. 29 (1991) 910–915.
[45] L. Kadaja, S. Laos, T. Maimets, Overexpression of leukocyte marker CD43 causes activation of the tumor suppressor proteins p53 and ARF, Oncogene 23 (2004) 2523–2530, http://dx.doi.org/10.1038/sj.onc.1207359.
[46] D.R. Flower, A.C. North, T.K. Attwood, Structure and sequence relationships in the lipocalins and related proteins, Protein Sci. Publ. Protein Soc. 2 (1993) 753–761, http://dx.doi.org/10.1002/pro.5560020507.
[47] J. Mishra, K. Mori, Q. Ma, C. Kelly, J. Barasch, P. Devarajan, Neutrophil gelatinase-associated lipocalin: a novel early urinary biomarker for cisplatin nephrotoxicity, Am. J. Nephrol. 24 (2004) 307–315, http://dx.doi.org/10.1159/000078452.
[48] M.I. Hassan, A. Waheed, S. Yadav, T.P. Singh, F. Ahmad, Zinc α2-glycoprotein: a multidisciplinary protein, Mol. Cancer Res. 6 (2008) 892–906, http://dx.doi.org/10.1158/1541-7786.MCR-07-2195.
[49] M.I. Hassan, A. Waheed, S. Yadav, T.P. Singh, F. Ahmad, Prolactin inducible protein in cancer, fertility and immunoregulation: structure, function and its clinical implications, Cell. Mol. Life Sci. 66 (2009) 447–459, http://dx.doi.org/10.1007/s00018-008-8463-x.
[50] Q. Quan, Q. Chen, P. Chen, L. Jiang, T. Li, H. Qiu, B. Zhang, Decreased apolipoprotein A-I level indicates poor prognosis in extranodal natural killer/T-cell lymphoma, nasal type, OncoTargets Ther. 9 (2016) 1281–1290, http://dx.doi.org/10.2147/OTT.S96549.
[51] T. Cheng, X. Dai, D.-L. Zhou, Y. Lv, L.-Y. Miao, Correlation of apolipoprotein A-I kinetics with survival and response to first-line platinum-based chemotherapy in advanced non-small cell lung cancer, Med. Oncol. Northwood Lond. Engl. 32 (2015) 407, http://dx.doi.org/10.1007/s12032-014-0407-8.
[52] M. Zamanian-Daryoush, J.A. DiDonato, Apolipoprotein A-I and cancer, Front. Pharmacol. 6 (2015)http://dx.doi.org/10.3389/fphar.2015.00265.
[53] M. Sattari, Y. Pazhang, M. Imani, Calprotectin induces cell death in human prostate cancer cell (LNCaP) through surviving protein alteration, Cell Biol. Int. 38 (2014) 1311–1320, http://dx.doi.org/10.1002/cbin.10328.

[54] E. Nicolas, P. Parisot, C. Pinto-Monteiro, R. de Walque, C. De Vleeschouwer, D.L.J. Lafontaine, Involvement of human ribosomal proteins in nucleolar structure and p53-dependent nucleolar stress, Nat. Commun. 7 (2016) 11390, http://dx.doi.org/10.1038/ncomms11390.
[55] K. Burger, B. Mühl, T. Harasim, M. Rohrmoser, A. Malamoussi, M. Orban, M. Kellner, A. Gruber-Eber, E. Kremmer, M. Hölzel, D. Eick, Chemotherapeutic drugs inhibit ribosome biogenesis at various levels, J. Biol. Chem. 285 (2010) 12416–12425, http://dx.doi.org/10.1074/jbc.M109.074211.
[56] G. Samimi, G. Manorek, R. Castel, J.K. Breaux, T.C. Cheng, C.C. Berry, G. Los, S.B. Howell, cDNA microarray-based identification of genes and pathways associated with oxaliplatin resistance, Cancer Chemother. Pharmacol. 55 (2005) 1–11, http://dx.doi.org/10.1007/s00280-004-0819-9.
[57] M. Horky, G. Wurzer, V. Kotala, M. Anton, B. Vojtesek, J. Vacha, J. Wesierska-Gadek, Segregation of nucleolar components coincides with caspase-3 activation in cisplatin-treated HeLa cells, J. Cell Sci. 114 (2001) 663–670.
[58] S.M.F. Jamieson, J. Liu, T. Hsu, B.C. Baguley, M.J. McKeage, Paclitaxel induces nucleolar enlargement in dorsal root ganglion neurons in vivo reducing oxaliplatin toxicity, Br. J. Cancer 88 (2003) 1942–1947, http://dx.doi.org/10.1038/sj.bjc.6601012.
[59] C.L. Renn, V.A. Carozzi, P. Rhee, D. Gallop, S.G. Dorsey, G. Cavaletti, Multimodal assessment of painful peripheral neuropathy induced by chronic oxaliplatin-based chemotherapy in mice, Mol. Pain 7 (2011) 29, http://dx.doi.org/10.1186/1744-8069-7-29.
[60] K. Wada, M. Sato, N. Araki, M. Kumeta, Y. Hirai, K. Takeyasu, K. Furukawa, T. Horigome, Dynamics of WD-repeat containing proteins in SSU processome components, Biochem. Cell Biol. 92 (2014) 191–199, http://dx.doi.org/10.1139/bcb-2014-0007.
[61] M. Kornprobst, M. Turk, N. Kellner, J. Cheng, D. Flemming, I. Koš-Braun, M. Koš, M. Thoms, O. Berninghausen, R. Beckmann, E. Hurt, Architecture of the 90S pre-ribosome: a structural view on the birth of the eukaryotic ribosome, Cell 166 (2016) 380–393, http://dx.doi.org/10.1016/j.cell.2016.06.014.
[62] M. Kellner, M. Rohrmoser, I. Forné, K. Voss, K. Burger, B. Mühl, A. Gruber-Eber, E. Kremmer, A. Imhof, D. Eick, DEAD-box helicase DDX27 regulates 3′ end formation of ribosomal 47S RNA and stably associates with the PeBoW-complex, Exp. Cell Res. 334 (2015) 146–159, http://dx.doi.org/10.1016/j.yexcr.2015.03.017.
[63] K. Shimoji, J. Jakovljevic, K. Tsuchihashi, Y. Umeki, K. Wan, S. Kawasaki, J. Talkish, J.L. Woolford, K. Mizuta, Ebp2 and Brx1 function cooperatively in 60S ribosomal subunit assembly in *Saccharomyces cerevisiae*, Nucleic Acids Res. 40 (2012) 4574–4588, http://dx.doi.org/10.1093/nar/gks057.
[64] J. Nousbeck, R. Spiegel, A. Ishida-Yamamoto, M. Indelman, A. Shani-Adir, N. Adir, E. Lipkin, S. Bercovici, D. Geiger, M.A. van Steensel, P.M. Steijlen, R. Bergman, A. Bindereif, M. Choder, S. Shalev, E. Sprecher, Alopecia, neurological defects, and endocrinopathy syndrome caused by decreased expression of RBM28, a nucleolar protein associated with ribosome biogenesis, Am. J. Hum. Genet. 82 (2008) 1114–1121, http://dx.doi.org/10.1016/j.ajhg.2008.03.014.
[65] K. Saito, Y. Iizuka, S. Ohta, S. Takahashi, K. Nakamura, H. Saya, K. Yoshida, Y. Kawakami, M. Toda, Functional analysis of a novel glioma antigen, EFTUD1, Neuro-Oncology 16 (2014) 1618–1629, http://dx.doi.org/10.1093/neuonc/nou132.
[66] S. Wu, B. Tutuncuoglu, K. Yan, H. Brown, Y. Zhang, D. Tan, M. Gamalinda, Y. Yuan, Z. Li, J. Jakovljevic, C. Ma, J. Lei, M.-Q. Dong, J.L. Woolford, N. Gao, Diverse roles of assembly factors revealed by structures of late nuclear pre-60S ribosomes, Nature 534 (2016) 133–137, http://dx.doi.org/10.1038/nature17942.
[67] C. Zhang, C. Yin, L. Wang, S. Zhang, Y. Qian, J. Ma, Z. Zhang, Y. Xu, S. Liu, HSPC111 governs breast cancer growth by regulating ribosomal biogenesis, Mol. Cancer Res. 12 (2014) 583–594, http://dx.doi.org/10.1158/1541-7786.MCR-13-0168.
[68] Z. Xu, T.C. Hobman, The helicase activity of DDX56 is required for its role in assembly of infectious West Nile virus particles, Virology 433 (2012) 226–235, http://dx.doi.org/10.1016/j.virol.2012.08.011.
[69] T. Kumazawa, K. Nishimura, N. Katagiri, S. Hashimoto, Y. Hayashi, K. Kimura, Gradual reduction in rRNA transcription triggers p53 acetylation and apoptosis via MYBBP1A, Sci. Rep. 5 (2015)http://dx.doi.org/10.1038/srep10854.
[70] T. de Lange, How shelterin solves the telomere end-protection problem, Cold Spring Harb. Symp. Quant. Biol. 75 (2010) 167–177, http://dx.doi.org/10.1101/sqb.2010.75.017.
[71] A.-G. Lu, H. Feng, P.-X.-Z. Wang, D.-P. Han, X.-H. Chen, M.-H. Zheng, Emerging roles of the ribonucleotide reductase M2 in colorectal cancer and ultraviolet-induced DNA damage repair, World J. Gastroenterol. 18 (2012) 4704–4713, http://dx.doi.org/10.3748/wjg.v18.i34.4704.
[72] K. Yano, K. Morotomi-Yano, N. Adachi, H. Akiyama, Molecular mechanism of protein assembly on DNA double-strand breaks in the non-homologous end-joining pathway, J. Radiat. Res. 50 (2009) 97–108 (Tokyo).
[73] S. Kotian, T. Banerjee, A. Lockhart, K. Huang, U.V. Catalyurek, J.D. Parvin, NUSAP1 influences the DNA damage response by controlling BRCA1 protein levels, Cancer Biol. Ther. 15 (2014) 533–543, http://dx.doi.org/10.4161/cbt.28019.
[74] J.-Y. Kim, K.-O. Seok, Y.-J. Kim, W.K. Bae, S. Lee, J.-H. Park, Involvement of GLTSCR2 in the DNA damage response, Am. J. Pathol. 179 (2011) 1257–1264, http://dx.doi.org/10.1016/j.ajpath.2011.05.041.
[75] H.-Y. Chang, C.-C. Fan, P.-C. Chu, B.-E. Hong, H.J. Lee, M.-S. Chang, hPuf-A/KIAA0020 modulates PARP-1 cleavage upon genotoxic stress, Cancer Res. 71 (2011) 1126–1134, http://dx.doi.org/10.1158/0008-5472.CAN-10-1831.
[76] M. Sokka, K. Rilla, I. Miinalainen, H. Pospiech, J.E. Syväoja, High levels of TopBP1 induce ATR-dependent shut-down of rRNA transcription and nucleolar segregation, Nucleic Acids Res. 43 (2015) 4975–4989, http://dx.doi.org/10.1093/nar/gkv371.
[77] A. James, Y. Wang, H. Raje, R. Rosby, P. DiMario, Nucleolar stress with and without p53, Nucleus 5 (2014) 402–426, http://dx.doi.org/10.4161/nucl.32235.
[78] L. Montanaro, D. Treré, M. Derenzini, Nucleolus, ribosomes, and cancer, Am. J. Pathol. 173 (2008) 301–310, http://dx.doi.org/10.2353/ajpath.2008.070752.
[79] J. Li, L. Yu, H. Zhang, J. Wu, J. Yuan, X. Li, M. Li, Down-regulation of pescadillo inhibits proliferation and tumorigenicity of breast cancer cells, Cancer Sci. 100 (2009) 2255–2260, http://dx.doi.org/10.1111/j.1349-7006.2009.01325.x.
[80] T. Maehama, K. Kawahara, M. Nishio, A. Suzuki, K. Hanada, Nucleolar stress induces ubiquitination-independent proteasomal degradation of PICT1 protein, J. Biol. Chem. 289 (2014) 20802–20812, http://dx.doi.org/10.1074/jbc.M114.571893.
[81] E. Hammer, S. Bien, M.G. Salazar, L. Steil, C. Scharf, P. Hildebrandt, H.W.S. Schroeder, H.K. Kroemer, U. Völker, C.A. Ritter, Proteomic analysis of doxorubicin-induced changes in the proteome of HepG2cells combining 2-D DIGE and LC-MS/MS approaches, Proteomics 10 (2010) 99–114, http://dx.doi.org/10.1002/pmic.200800626.
[82] R. Briffa, I. Um, D. Faratian, Y. Zhou, A.K. Turnbull, S.P. Langdon, D.J. Harrison, Multiscale genomic, transcriptomic and proteomic analysis of colorectal cancer cell lines to identify novel biomarkers, PLoS One 10 (2015), e0144708. http://dx.doi.org/10.1371/journal.pone.0144708.
[83] S. Boulon, B.J. Westman, S. Hutten, F.-M. Boisvert, A.I. Lamond, The nucleolus under stress, Mol. Cell 40 (2010) 216–227, http://dx.doi.org/10.1016/j.molcel.2010.09.024.
[84] P. Jordan, M. Carmo-Fonseca, Cisplatin inhibits synthesis of ribosomal RNA in vivo, Nucleic Acids Res. 26 (1998) 2831–2836, http://dx.doi.org/10.1093/nar/26.12.2831.
[85] M. Pietrzak, S.C. Smith, J.T. Geralds, T. Hagg, C. Gomes, M. Hetman, Nucleolar disruption and apoptosis are distinct neuronal responses to etoposide-induced DNA damage, J. Neurochem. 117 (2011) 1033–1046, http://dx.doi.org/10.1111/j.1471-4159.2011.07279.x.
[86] J.E. Quin, J.R. Devlin, D. Cameron, K.M. Hannan, R.B. Pearson, R.D. Hannan, Targeting the nucleolus for cancer intervention, Biochim. Biophys. Acta 1842 (2014) 802–816, http://dx.doi.org/10.1016/j.bbadis.2013.12.009.
[87] K. Smetana, A. Vlastiborová, I. Iscenko, Studies on micronucleoli of immature human leukemic neutrophils, Neoplasma 20 (1973) 491–498.
[88] N.J. Lane, Spheroidal and ring nucleoli in amphibian oocytes. Patterns of uridine incorporation and fine structural features, J. Cell Biol. 35 (1967) 421–434.
[89] P. Kasík, J. Lejnar, M. Hrobon, K. Smetana, Nucleoli in human pseudostratified columnar epithelium cells. (Microscopic classification of nucleoli), Folia Biol. 23 (1977) 354–358 (Praha).

Appendix 2

Blood Cells, Molecules and Diseases 97 (2022) 102690

Contents lists available at ScienceDirect

Blood Cells, Molecules and Diseases

journal homepage: www.elsevier.com/locate/bcmd

Missense mutation in RPS7 causes Diamond-Blackfan anemia via alteration of erythrocyte metabolism, protein translation and induction of ribosomal stress

Agata Kubickova [a,g,1], Zuzana Maceckova [a,1], Petr Vojta [a], Martin Ondra [a,g], Jana Volejnikova [a,b], Pavla Koralkova [c], Alexandra Jungova [d], Ondřej Jahoda [c], Renata Mojzikova [c], Ivana Hadacova [e], Jaroslav Cermak [f], Monika Horvathova [c], Dagmar Pospisilova [b,*], Marian Hajduch [a,**]

[a] Institute of Molecular and Translational Medicine, Palacky University Olomouc, Hnevotinska 1333/5, 77900 Olomouc, Czech Republic
[b] Department of Paediatrics, Faculty of Medicine and Dentistry, Palacky University and University Hospital Olomouc, I. P. Pavlova 6, 77900 Olomouc, Czech Republic
[c] Department of Biology, Faculty of Medicine and Dentistry, Palacky University Olomouc, Hnevotinska 3, 77515 Olomouc, Czech Republic
[d] Department of Haematooncology, Charles University and University Hospital Pilsen, Alej Svobody 80, 30460 Pilsen-Lochotin, Czech Republic
[e] Department of Haematology, Charles University and University Hospital Motol Prague, V Uvalu 84, 15006 Prague, Czech Republic
[f] Institute of Haematology and Blood Transfusion, U Nemocnice 2094/1, 12820 Prague, Czech Republic
[g] Czech Advanced Technology and Research Institute, Institute of Molecular and Translational Medicine, Palacky University in Olomouc, Hnevotinska 1333/5, 77900 Olomouc, Czech Republic

ARTICLE INFO

Editor: Mohandas Narla

Keywords:
Diamond-Blackfan anemia (DBA)
Ribosomal stress
Wnt pathway
BCCIP
RPS7
c-Myc
CRISPR/Cas9

ABSTRACT

Diamond-Blackfan anemia (DBA) is predominantly underlined by mutations in genes encoding ribosomal proteins (RP); however, its etiology remains unexplained in approximately 25 % of patients.

We previously reported a novel heterozygous *RPS7* mutation hg38 chr2:g.3,580,153G > T p.V134F in one female patient and two asymptomatic family members, in whom mild anemia and increased erythrocyte adenosine deaminase (eADA) activity were detected. We observed that altered erythrocyte metabolism and oxidative stress which may negatively affect the lifespan of erythrocytes distinguishes the patient from her asymptomatic family members. Pathogenicity of the RPS7 p.V134F mutation was extensively validated including molecular defects in protein translational activity and ribosomal stress activation in the cellular model of this variant.

1. Introduction

Diamond-Blackfan anemia (DBA) is a rare congenital red cell aplasia with causative mutations in genes encoding ribosomal proteins (RPs), which involve small ribosomal subunit genes (*RPS19, RPS26, RPS7, RPS24, RPS17, RPS10, RPS15A*) or large ribosomal subunit genes (*RPL5, RPL11* and *RPL35A*) [1–3]. These mutations affect translational efficiency [4], ribosome biogenesis [5] and oncogene signaling [6]. It was also shown that ribosomal insufficiency increases oxidative stress in erythrocytes of DBA patients [7]. Despite intensive research, the etiology of DBA remains unexplained in approximately 25 % of patients.

DBA mostly manifests during the first year after birth, but its phenotype is highly variable from silent carriers over mild (typically macrocytic) anemia to severe transfusion dependency accompanied by short stature with skeletal abnormalities [8], mental retardation [9,10] and increased risk of tumor development [11]. DBA phenotype is mainly attributed to RP haploinsufficiency, but several dominant-negative phenotypes when mutated mRNA is stable were described as well [4,12]. Another rather interesting feature of DBA is incomplete penetrance and variable expressivity. It is common that family members

* Correspondence to: D. Pospisilova, Department of Paediatrics, Faculty of Medicine and Dentistry, Palacky University and University Hospital Olomouc, I. P. Pavlova 6, 77900 Olomouc, Czech Republic.
** Correspondence to: M. Hajduch, Institute of Molecular and Translational Medicine, Palacky University Olomouc, Hnevotinska 1333/5, 77900 Olomouc, Czech Republic.
E mail addresses: dagmar.pospisilova@fnol.cz (D. Pospisilova), marian.hajduch@upol.cz (M. Hajduch).
[1] both authors contributed equally

https://doi.org/10.1016/j.bcmd.2022.102690
Received 29 December 2021; Received in revised form 30 June 2022; Accepted 30 June 2022
Available online 6 July 2022

sharing the same mutation manifest variable severity of phenotype [13]. These observations point towards disease-modifying genes at play. However, up today no such gene has been described.

Using a massive parallel sequencing (MPS) of RP gene panel by selective capture hybridization we found a novel RPS7 p.V134F mutation in three female members of one family showing increased erythrocyte adenosine deaminase (eADA) activity [14]. To assess the causality of RPS7 p.V134F mutation, we developed and extensively analyzed a cellular model of this variant.

2. Patients and methods

2.1. Clinical report

The patient was an 18-year-old female born in term from second uncomplicated pregnancy with a birth weight of 2600 g. She had no congenital malformations and presented with severe anemia during the first month of life. Bone marrow aspirate showed a severe isolated erythroid aplasia and the diagnosis of DBA was established. The patient was transfusion dependent during the first year of life and required irregular red blood cell transfusions until 3 years of age. She was treated with a small dose of prednisolone on alternate days since 3 years of age, responded well to steroid therapy and is currently in remission with hemoglobin (Hb) 101 g/l and mean corpuscular volume (MCV) 112 fl. Her body height is normal.

The patient's mother and older sister are both asymptomatic and their past medical history is insignificant. They harbor no somatic malformations. Normal Hb levels (120 g/l and 127 g/l, respectively) and mild macrocytosis (MCV of 97 fl and 96 fl, respectively) were detected on laboratory examination. Other family members are healthy. Clinical case was partially reported in our previous publications [14,15].

2.2. DNA extraction, RNA extraction and cDNA preparation from patient blood samples

DNA was extracted from peripheral blood by Genomic DNA Whole Blood Kit (Qiagen, Germany) using MagCore HF116 robotic station (RBC Bioscience Corp., Taiwan) according to manufacturer's protocol. RNA isolation was performed from blood samples stored in Tempus Blood RNA Tubes using Tempus Spin RNA Isolation kit (Thermo Fisher Scientific, MA, USA). RNA integrity and concentration were checked by Agilent Bioanalyzer (Agilent Technologies, CA, USA) and Nanodrop ND 1000 (Thermo Scientific, USA).

For reverse transcription, we pre-incubated 3 μg of total RNA with 0.3 μg of Random Primers (Promega, USA) at 70 °C for 5 min, and immediately placed the mixture on ice. Then 6 μl of RevertAid 5× RT buffer (Fermentas, Lithuania), 3 μl of 10 mM deoxyribonucleotide triphosphates (dNTPs), 0.75 μl of 40 U/μl RNAsin ribonuclease inhibitor (Promega, USA), and DEPC treated water (Ambion, USA) up to a final volume of 30 μl were added, and the mixture was incubated for 5 min at room temperature. During the final step, 150 U of RevertAid Moloney Murine Leukemia Virus reverse transcriptase (Fermentas, Lithuania) were added to each tube and the samples were incubated at room temperature for 10 min. Finally, samples were incubated at 42 °C for 60 min and then 70 °C for 10 min.

RPS7 wild-type (RPS7-WT) vs. RPS7 p.V134F (RPS7-mut) allele ratio was estimated using *RPS7* cDNA sequencing. Amplicon for target cDNA *RPS7* was obtained by PCR using primers specifically designed to 5′ and 3′UTR regions of the gene (tctcgcgagatttgggtctctt, ttacaattgaaactctgggaattcaaaat).

2.3. Library preparation and sequencing

2.3.1. RP panel

RP gene panel sequencing was performed as described previously and it revealed *RPS7* hg38 chr2:g.3,580,153G > T mutation, which was subsequently confirmed by Sanger sequencing [14]. DNA was amplified by PCR with the following primers targeting exon 6 of *RPS7* (catttt-gacttaaagaggtgc; cactaaaatccactctcactg). Results from Sanger sequencing were edited and visualized in Unipro UGENE [16].

2.4. Enzyme assays

The activity of enzymes involved in anaerobic glycolysis, oxidative defense and nucleotide metabolism, particularly pyruvate kinase (PK), hexokinase (HK), glucose-6-phosphate dehydrogenase (G6PD) and eADA, was determined according to the methods recommended by the International Committee for Standardization in Haematology [17], with the use of leukocyte- and platelet-free erythrocyte lysates as previously described [18,19]. Briefly, the enzyme reaction was pre-incubated for 10 min at 37 °C, thereafter the substrate was added. Absorbance was measured at 340 nm (for eADA at 265 nm) in 1 min intervals for 20 min at 37 °C (Spectrophotometer Infinite 200 Nanoquant; Tecan, Switzerland) and specific enzyme activity was calculated using the Lambert-Beer law. All chemicals and purified enzymes were purchased from Sigma Aldrich (Germany).

2.5. Measurement of glutathione and ATP

Freshly prepared erythrocyte lysates, extracted with 5 % trichloroacetic acid (Sigma-Aldrich, Germany), were used for the measurements of reduced glutathione (GSH) and ATP levels by high-performance liquid chromatography-mass spectrometry (HPLC-MS) (HPLC Dionex Ultimate 3000 MS, Thermo Scientific, USA; LC/MS/MS System MDS API 3200, Applied Biosystems, USA) as previously published [18,20].

2.6. Oxidative stress and Annexin V binding

Peripheral blood erythrocytes (2×10^7/ml) were incubated with 0.4 mM 2',7'-dichlorofluorescein diacetate (DCF; Sigma-Aldrich, Germany) for 15 min at 37 °C as previously described [20,21]. For positive control, erythrocytes were exposed to 2 mM H_2O_2 for 10 min before DCF labeling. The levels of reactive oxygen species (ROS) were determined based on the DCF-dependent intensity of fluorescence measured by FACS Calibur (FACS Calibur, BD Biosciences, New Jersey, USA).

Annexin V binding to erythrocyte membrane was analyzed using Annexin V/FITC kit (BD Biosciences, New Jersey, USA) following manufacturer's instructions. Fluorescence intensity was also measured by FACS Calibur [21].

2.7. Cell culture and MTS viability assay

U2OS cell line (HTB-96, ATCC, USA) is derived from osteosarcoma, which is one of the most common cancer types of DBA patients, therefore it was chosen for the development of the cellular model for this disease. Cells were maintained in 75 cm^2 plastic tissue culture flasks and cultured in McCoy's 5A Medium w/ L-Glutamine (BE12-688F, Lonza, UK) supplemented by 100 U/ml penicillin, 100 μg/ml streptomycin (D910, Diagnovum, Netherlands) and 10 % fetal calf serum (10270, Gibco, Australia).

Proliferation activity was measured by MTS assay. Cells were seeded by automatic pipettor Multidrop Combi (ThermoFisher Scientific, USA) into 384 well microtiter plates (PerkinElmer, USA) at a density of 800 cells per well. They were incubated for 72 h at 37 °C, in a 5 % CO_2 atmosphere at 100 % humidity. At the end of the incubation period, 5 μl of the MTS solution (G1111, Promega, USA) was added and measurement of the optical density (OD) at 490 nm with an Envision reader (Perkin Elmer, USA) followed after incubation for 1.5 h. Cell survival (CS) was calculated by using the following equation: CS = (mean OD RPS7-mut cell line/mean OD RPS7-WT cell line) × 100 %.

2.8. CRISPR/Cas9 cell line model preparation

CRISPR/Cas9 system was used for genome editing and introduction of mutation in the *RPS7* gene into U2OS cell line. Cas9 endonuclease was directed to create a cut between bases hg38 chr2:g.3,580,178-3,580,179 by synthetic gRNA consisting of specifically designed crRNA and universal tracrRNA. The mutation was then inserted by homology directed repair according to the ssODN donor template. The donor template was designed to prevent the recutting of the edited gene by disrupting the gRNA PAM sequence. Alt-R® CRISPR-Cas9 crRNAs, Alt-R® CRISPR-Cas9 tracrRNA ATTO™ (#1075928), Ultramer DNA Oligo (ssODN template) and Alt-R® S.p HiFi Cas9 nuclease V3 (#1081061) were purchased from Integrated DNA Technologies, USA. crRNA/tracrRNA hybridization and ribonucleoprotein (RNP) complex formation was done according to the manufacturer's instructions. Electroporation of RNP complexes into cells was done by Neon™ Transfection System (1230 V, 10 ms, 4 pulses; Invitrogen™, MPK5000, USA). Monoclonal cell lines were isolated by limiting dilution. The primary screen of monoclonal cell lines, for the desired mutation, was done by comparison of RPS7-WT and RPS7-mut amplicons restriction spectra. Specific restriction site of endonuclease *Pfl*FI (R0595S, New England Biolabs, UK) is invalidated in clonal cell lines carrying RPS7 p.V134F SNV. The candidate cell lines were sequenced by Sanger sequencing of PCR amplicons. This was performed to validate the accuracy of CRISPR/Cas9 insertion of SNV into the genomic locus of the *RPS7* gene. PCR amplification for restriction spectra analysis and Sanger sequencing was carried out by Phusion® High-Fidelity DNA Polymerase (M0530L, New England Biolabs, UK) and specific primers: RPS7_F 5′-ACTGGCAGTTCTGTGATGCTAA-3′ RPS7_R 5′-CAGTCACCCACATGGTTATGTC-3′ (Generi Biotech, Czech Republic).

2.9. RNA isolation from cell lines, mRNA quantification and Sanger sequencing

Total RNA was isolated using a commercially available TRIzol reagent (Invitrogen, USA) following the manufacturer's instructions. Three micrograms of total RNA were reverse transcribed using random primers (C1181, Promega, USA) and RevertAid H Minus Reverse Transcriptase (EP0451, Thermo Scientific™, USA). Two microliters of cDNA reaction were PCR-amplified on a LightCycler® Instrument 480 II/96 (05015278001, Roche, Switzerland) using the Phusion® High-Fidelity DNA Polymerase (M0530L, New England Biolabs, UK) with EvaGreen® dye (#31000-T, Biotium, USA). Sequences of primers used for the evaluation of mRNA levels of RPS7 are: RPS7_F 5'-GTGGGAAGCATGTCGTCTTT-3′, RPS7_R 5′-ATTAACATCCTTGCCCGTGA-3′, GAPDH_F 5'-GAAGATGGTGATGGGATTTC-3′, GAPD_R 5'-GAAGGTGAAGGTCGGAGT-3′ (Generi Biotech, Czech Republic). GAPDH was used as an internal control. Delta-delta Ct values were used to determine relative expression as a fold change. PCR amplification for Sanger sequencing of cDNA was carried out by the same primers but without EvaGreen® dye.

2.10. Cell cycle analysis

RPS7-WT and RPS7-mut cell lines were seeded at a density of 0.5×10^6 cells per 22.1 cm^2 tissue culture dish and after 48 h harvested and collected together with the floating cells. Cell pellets were washed with cold 1 x PBS and fixed in cold 70 % ethanol added dropwise and stored overnight at −20 °C. Afterward, pellets were washed in 1 x citrate buffer, then stained for 15 min in 50 μg/ml propidium iodide (SLBH8362V, Sigma-Aldrich, USA) at 37 °C and treated for another 15 min by 0.5 mg/ml RNAse A (060M7000V, Sigma-Aldrich, USA). In order to stabilize, samples were kept at 4 °C for 1 h prior to measurement by 488 argon laser-equipped flow cytometer (FACSCalibur) and data were analyzed using CellQuest software version 3.3 (both Becton Dickinson, USA).

2.11. BrdU incorporation analysis

Cells were cultivated as previously described and 30 min before harvesting 10 μM 5-bromo-2′-deoxyuridine (125H0932, Sigma-Aldrich, USA) was added for pulse-labeling of newly synthesized DNA. The attached cells were collected together with the floating cells. Cell pellets were washed with cold 1 x PBS and fixed in cold 70 % ethanol added dropwise and stored overnight at −20 °C. Samples were then incubated at room temperature for 30 min in 2 M HCl containing 0.5 % Triton X-100 to denature the DNA. Following neutralization with 0.1 M $Na_2B_4O_7$ (pH = 8.5), the cells were washed with 1 x PBS containing 0.5 % Tween-20 and 0.1 % BSA. Staining with primary anti-BrdU antibody (clone MoBu-1, 11–286-C100, Exbio, Czech Republic) for 30 min at room temperature in the dark followed. Cells were then washed with 1 x PBS containing 0.5 % Tween-20 and 0.1 % BSA and stained with secondary anti-mouse IgG–FITC antibody (F2883, Sigma-Aldrich, USA) for 30 min at room temperature. After another wash with 1 x PBS containing 0.5 % Tween-20 and 0.1 % BSA and incubation with propidium iodide (50 μg/ml, SLBH8362V, Sigma-Aldrich, USA) and RNase A (10 mg/ml, 060M7000V, Sigma-Aldrich, USA) for 30 min at room temperature in the dark, samples were stabilized in 4 °C for 30 min prior measurement by 488 argon laser-equipped flow cytometer (FACSCalibur; Becton Dickinson, USA). Data were analyzed using CellQuest software version 3.3 (Becton Dickinson, USA).

2.12. BrU incorporation analysis

Cells were cultivated as previously described and 30 min before harvesting 1 mM 5-bromouridine (850187, Sigma-Aldrich, USA) was added for pulse-labeling of newly synthesized RNA. The attached cells were collected together with the floating cells. Cell pellets were washed with cold 1 x PBS and fixed in cold 1 x PBS containing 1 % formaldehyde and 0.05 % NP-40 added dropwise at room temperature for 15 min and then stored overnight at 4 °C. Before measurement, cells were firstly washed with 1 % glycine in 1 x PBS, then with 1 x PBS and stained with primary anti-BrdU antibody cross-reacting to BrU (clone MoBu-1, 11–286-C100, Exbio, Czech Reublic) for 45 min at room temperature in the dark. Afterward, samples were washed with 1 x PBS containing 0.1 % NP-40 and 0.1 % BSA and stained with secondary anti-mouse IgG–FITC antibody (F2883, Sigma-Aldrich, USA) for 30 min at room temperature. Then another washing step followed with 1 x PBS containing 0.1 % NP-40 and 0.1 % BSA, fixation in 1 x PBS containing 1 % formaldehyde and 0.05 % NP-40 at room temperature for 15 min with another incubation for 1 h at 4 °C and washing in 1 % glycine in 1 x PBS. Before analysis, samples were incubated with propidium iodide (50 μg/ml, SLBH8362V, Sigma-Aldrich, USA) and RNase A (10 mg/ml, 060M7000V, Sigma-Aldrich, USA) for 30 min at room temperature in the dark and measured by 488 argon laser-equipped flow cytometer (FACSCalibur; Becton Dickinson, USA). Data were analyzed using CellQuest software version 3.3 (Becton Dickinson, USA).

2.13. Protein synthesis analysis

To investigate the inhibition of global protein biosynthesis in RPS7-WT versus RPS7-mut cell lines Click-iT™ AHA Alexa Fluor™ 488 Protein Synthesis HCS Assay kit (C10289, Invitrogen, USA) was used. Cells were seeded at a density of 1.5×10^6 cells per 60 cm^2 tissue culture dish and after 48 h harvested and collected together with the floating cells. After washing with 1 x PBS, the cells were incubated for 1 h in a methionine-free medium to deplete methionine reserves. Then L-azidohomoalanine was added to the methionine-free media in a final concentration 142.9 μM for 1 h. L-azidohomoalanine, an amino acid analog of L-methionine containing an azido moiety, was incorporated into newly synthesized proteins. Afterward, the cells were washed with 1 x PBS, fixed in 1 x PBS containing 4 % formaldehyde for 15 min at room temperature, permeabilized with 0.25 % Triton X-100 in PBS for

15 min and washed in 3 % BSA in 1 x PBS. The cells were then incubated with Click-iT® reaction cocktail for 30 min, at room temperature and protected from light. The cocktail contained AlexaFluor 488 conjugated alkyne in final concentration 19.4 nM which is reactive with azides via a copper-catalyzed click reaction. The resulting fluorescence signal of newly synthesized proteins was measured by 488 argon laser-equipped flow cytometer (FACSCalibur, Becton Dickinson, USA) and data were analyzed using CellQuest software version 3.3 (Becton Dickinson, USA). The antibiotic cycloheximide (01810, Sigma-Aldrich, USA), a known potent inhibitor of protein synthesis, was used as a positive control and added to cells in a methionine-free medium at a final concentration 80 μg/ml for 2 h [22].

2.14. Western blotting

RPS7-WT and RPS7-mut cell lines were seeded and collected under the same conditions as for flow cytometry analysis. Cell pellets were washed with cold 1 x PBS, and lysed in RIPA buffer (50 mM Tris-HCl pH 8.0, 150 mM NaCl, 1 % NP-40, 0.5 % sodium deoxycholate, 0.1 % SDS, 1 mM EDTA and cOmplete™ Protease Inhibitor Cocktail (04693116001, Roche, Switzerland)). Protein concentration was determined by Pierce™ BCA Protein Assay Kit (23225, Thermo Scientific, USA). In total, 30 μg of cellular proteins were denatured in Laemmli buffer (10 % β-mercaptoethanol, 0.06 % bromophenol blue, 47 % glycerol, 12 % SDS, 0.5 M Tris pH 6.8), separated on SDS-polyacrylamide gel electrophoresis and transferred onto nitrocellulose membrane by Trans-Blot® Turbo™ Transfer System (1704150, Bio-Rad, USA). Membranes were incubated with primary antibodies against c-Myc (ab32072, Abcam, UK), cyclin D1 (2978, Cell Signaling Technology, USA), E2F1 (ab179445, Abcam, UK), BCCIP (ab97577, Abcam, UK), MDM2 (ab16895, Abcam, UK), β-catenin (ab32572, Abcam, UK), nucleolin (ab22758, Abcam, UK), p21 (2947, Cell Signaling Technology, USA), p53 (ab1101, Abcam, UK), ubiquitin (3933, Cell Signaling Technology, USA), RPS7 (ab57637, Abcam, UK), β-actin (A2228, Sigma Aldrich, USA) overnight at 4 °C followed by incubation with appropriate peroxidase-linked secondary antibody (A-2304 or A-0545, Sigma Aldrich, USA). Chemiluminescence signals were visualized by the ChemiDoc MP Documentation system (Bio-Rad, USA).

2.15. Immunofluorescence analysis

RPS7-WT and RPS7-mut cell lines were seeded 24 h before the experiment to 96-well plate (CellCarrier-96 Black, Perkin-Elmer, USA) at a density of 1×10^4 cells per well. Grown cells were washed twice with 1 x PBS, fixed by 4 % paraformaldehyde/1 x PBS for 15 min at room temperature and permeabilized by 0.3 % Triton X-100/1 x PBS for 15 min. Afterward, cells were incubated in blocking buffer for 1 h (5 % FCSi, 0.1 % Tween 20, 1 x PBS) and stained with nucleolin antibody (ab22758, Abcam, UK) overnight at 4 °C. Primary antibody was detected with species-specific secondary antibody labeled by Alexa Fluor 488 (Life Technologies, USA) in 5 % FCSi/1 x PBS for 1 h at room temperature. Thereafter cells were washed in 1 x PBS three times and stained with Hoechst 33342 (62249, Thermo Scientific™, USA). Localization and level of nucleolin expression were examined using CV7000 Voyager Cell High throughput cellular imaging and discovery system (Yokogawa, USA) with water objective in 60× magnification. Image quantification was calculated as a corrected spot intensity in the nucleolus using Columbus software version 2.7.1 (Perkin-Elmer, USA).

2.16. rRNA fluorescence in situ hybridization

Cells were seeded and fixed as described above and permeabilized by 70 % ethanol at −20 °C overnight. Cells were washed twice in wash buffer (2 x SSC, 10 % formamide), followed by hybridization at 37 °C for 4 h in hybridization buffer (10 % formamide, 2 x SSC, 0.5 mg/ml tRNA, 10 % dextran sulphate, 250 μg/ml BSA, 10 mM ribonucleoside vanadyl complexes and 0.5 ng/μl 5`ITS1 probe: CCTCGCCCTCCG GGCTCCGTTAATGATC conjugated with cy5). Afterward, samples were washed twice in preheated wash buffer at 37 °C and stained with Hoechst 33342 (62249, Thermo Scientific™, USA). The cells were examined using CV7000 Voyager Cell High throughput cellular imaging and discovery system (Yokogawa, USA). Image quantification was calculated as a corrected spot intensity in the nucleolus by Columbus software version 2.7.1 (Perkin-Elmer, USA).

2.17. Northern blotting

Pre-rRNA species were analyzed by northern blotting. 10 μg of total RNA were mixed with 1 volume of loading buffer (50 % formamide, 0.06 % formaldehyde, 10 % glycerol, 0.05 % bromophenol blue in 1× MOPS buffer) and separated on a 2 % agarose gel in the presence of MOPS buffer (20 mM MOPS, 5 mM sodium acetate, 2 mM EDTA, pH 7.0) containing 2 % formaldehyde, and run in 1 x MOPS buffer at 23 V overnight at 4 °C. RNAs were then transferred to a nylon membrane (Amersham Hybond-N+, GE Healthcare, USA). After fixation by UV-crosslinking, the membranes were pre-hybridized for 1 h at 45 °C in DIG Easy Hyb (DIG Northern Starter Kit, Roche, Switzerland). The digoxigenin-labeled oligodeoxynucleotide probe was then added and incubated overnight at 45 °C. The probes used in this study were: 5ITS1 (5′-CCTCGCCCTCCGGGCTCCGTTAATGATC-3′), ITS2b (5′-CTGCGAGGGAACCCCCAGCCGCGCA-3′), ITS2d/e (5′-GCGCGACGGCGGACGACACCGCGGCGTC-3′) (Generi Biotech, Czech Republic) [23]. For detection of ITS2, probes ITS2b and ITS2d/e were mixed in equal amounts. After probes hybridization took place, the stringency washes followed. Firstly, two times for 5 min at room temperature in 2 x SSC (0.15 M NaCl, 15 mM sodium citrate, pH 7.0) containing 0.1 % SDS and twice for 15 min in 0.25 x SSC with SDS 0.1 %. Before the blocking step, the membranes were briefly washed in washing buffer (0.1 M Maleic acid, 0.15 M NaCl, 0.3 % Tween 20, pH 7.5), then blocked in blocking solution for 30 min and incubated with the anti-digoxigenin-AP antibody (both DIG Northern Starter Kit, Roche, Switzerland) for 1 h at room temperature. Unbound antibodies were removed by two washing steps for 15 min in a washing buffer. Before measurement of the chemiluminescence signal, membranes were equilibrated for 5 min at detection buffer (0.1 M Tris-HCl, 0.1 M NaCl, pH 9.5), then the CDP-Star substrate was added and the signals were acquired by the ChemiDoc MP Documentation system (Bio-Rad, USA).

2.18. Statistical analysis

All data are presented as mean ± SEM from at least three biological replicates. The statistical significance of differences was examined using one-sample *t*-test, $p < 0.05$ was considered statistically significant (GraphPad Prism version 8.0).

3. Results

The Czech and Slovak DBA registry currently includes 62 patients. Previously, causative mutations were identified in 50 out of 62 patients (81 %) in genes encoding for *RPS19*, *RPS26*, *RPL5*, *RPL11* and *RPS17* using massive parallel sequencing [14,15].

A novel nonsynonymous germline heterozygous transversion hg38 chr2:g.3,580,153G > T resulting in amino acid substitution p.V134F was identified by MPS in exon 6 of the *RPS7* gene in one female patient with DBA and in two of her asymptomatic relatives [14]. The mutation was subsequently confirmed by cDNA sequencing (Fig. 1). Ultra-deep cDNA sequencing (average coverage 78,285×) revealed that expression of the mutated allele is in concordance with genotype (proband: 55 % *RPS7-WT* / 45 % RPS7-mut, mother: 58 % *RPS7-WT* / 42 % RPS7-mut, sister: 63 % *RPS7-WT* / 37 % RPS7-mut).

Valine 134 is highly conserved in RPS7 and substitution by phenylalanine in this position is considered possibly damaging by Polyphen2 (score 0.965). In silico protein stability predictors I-Mutant and MUpro

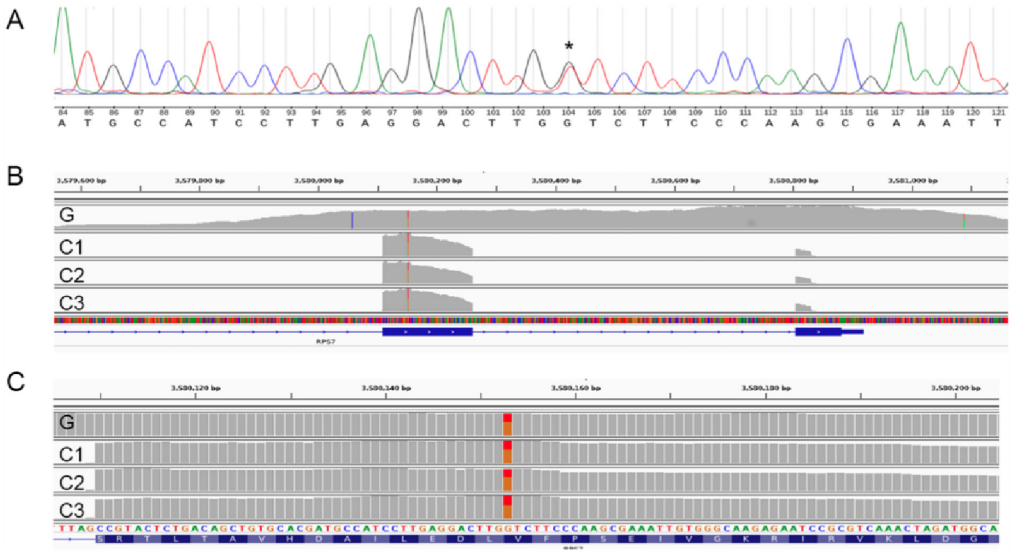

Fig. 1. *RPS7* mutation in the patient with DBA and two of her family members. The confirmation of hg38 chr2:g.3,580,153G > T heterozygous mutation in *RPS7* by Sanger sequencing technique in the patient panel (A). The mutation has been previously identified by MPS sequencing of genomic DNA (G). The mutation was later detected in patient's cDNA C1 as well as in her mother (C2) and sister (C3). Panel (B) visualizes alignments in the last two *RPS7* exons by IGV in comparison of RP panel gene sequencing and cDNA sequencing. Panel (C) shows the position of the mutation in exon 6 of *RPS7* in detail.

evaluated the substitution as decreasing RPS7 protein stability (I-Mutant reliability index 9, MUpro scores were − 0.97 by Neural Network method and − 1 by Support Vector Machine method). Although this variant was reported in a recent update of the Czech and Slovak DBA registry [14], there was no other RPS7 SNV described before and thus we decided to proceed with an extended evaluation of its pathogenicity and underlying disease mechanisms using a genetically modified cellular model.

3.1. Validation of CRISPR/Cas9 cellular model, translational activity, nucleolar morphology, pre-rRNA processing, RPS7 protein stability and TP53 signaling pathway

While the DBA phenotype is usually expressed in erythroid lineage, the ribosomal stress induced by an aberration of RPs is present in many patient's tissues leading to multiple structural, signaling and metabolic abnormalities. For that reason, we selected the U2OS osteosarcoma cell line which is of the same embryonal origin as hematopoietic cells, is frequently used for mechanistic studies in DBA and has been routinely used as a cellular model for ribosomal stress, especially when nucleoli morphology was studied [24–27]. We designed and established cellular model carrying the heterozygous mutation in the *RPS7* gene (genomic coordinates: hg38 chr2:g.3,580,153G > T p.V134F) by CRISPR/Cas9 mediated editing of genomic DNA in the human U2OS cell line. We obtained one monoclonal cell line carrying only the desired non-synonymous variant (Suppl. Fig. 1 A, B). The presence of RPS7 mutation at mRNA level was verified by Sanger sequencing (Suppl. Fig. 2A). Subsequently, we did qRT-PCR to measure the level of total RPS7 mRNA expression. We did not find any significant changes in RPS7 mRNA level in RPS7-mut cell line compared to RPS7-WT cells (Suppl. Fig. 2B).

Overall aberrant protein synthesis is one of the hallmarks of DBA. Therefore we have analyzed cellular uptake of L-azidohomoalanine which was incorporated into newly synthesized proteins instead of methionine. The global protein synthesis was significantly reduced in RPS7-mut cell line compared to the control RPS7-WT cells (13.63 %) (Fig. 3), thus indicating RPS7 V134F leads to ribosome malfunction which is possibly leading to DBA phenotype.

Next, we examined impact of RPS7 V134F variant on cell growth. The proliferation capacity of RPS7-mut cells was reduced by 31.6 % compared with RPS7-WT (Fig. 4A). Furthermore, cell cycle analysis revealed slight G_0/G_1 block in RPS7-mut cells (11.43 %) which was associated with decrease in the cell count in both S phase by 4.46 % ($p < 0.02$) and G_2-M phase by 5.53 % ($p < 0.0003$) compared with RPS7-WT cell line (Fig. 4 B). Moreover, changes in total DNA and RNA synthesis were detected in mutant versus wild-type cells. More specifficaly, we detected mild increase in DNA sythesis (Fig. 4 C), while overall RNA synthesis was decreased by 18.65 % in RPS7–mut cells (Fig. 4 D).

To better understand the phenotype of RPS7-mut cells, we also investigated protein levels deregulated in DBA. Firstly, we focused on the TP53 signaling pathway. This pathway is known to control stress response, cell cycle, apoptosis and plays a major role in ribosomal stress (Fig. 5A). In RPS7-mut cells significant decrease in MDM2 levels (30 %) and a parallel 68 % increase in p21 levels were observed, while p53 levels remained unchanged. Furthermore, other DBA associated pathways were deregulated in RPS7-mut compared to RPS7-WT cellular models. We also observed reduction of c-Myc and E2F1 transcription factors levels together with decrease in cyclin D1 expression (Figs. 4 B, 5 A). Moreover, level of BCCIP protein, directly involved in incorporation of RPS7 to small ribosomal subunit, showed significant 62 % increase in RPS7–mut cells. Recently a new compensatory mechanism, canonical Wnt pathway, for ribosomal stress was described by Dannheisig et al [28]. Therefore, we tested the effect of RPS7 V134F mutation on β-catenin expression. Indeed, β-catenin level was increased by 75 % in RPS7-mut compared to RPS7-WT cell line (Fig. 5 A).

We have also examined the RPS7 protein level in both cellular models and comparable levels were detected (Fig. 5 A). However, important difference in RPS7 p.V134F protein stability was noted (Fig. 5 B). Interestingly, protein p21 also exhibited lower stability in RPS7-mut versus RPS7-WT cell lines (Fig. 5 B). Furthermore, we performed an immunodetection of total ubiquitinylated proteins (Fig. 5 C). An apparent extra band was detected in RPS7-mut compared to RPS7-WT with a molecular weight of approximately 25 kDa corresponding to

the ubiquitinylated form of RPS7 protein. We suppose that altered protein translation and/or incorporation of RPS7 V134F protein into ribosome activates targeted ubiquitinylation and degradation of the protein, which results in decreased cellular concentration and may further aggravate RPS7 deficiency.

Additionally, we performed an indirect immunofluorescence assay with an antibody against the nucleolus marker nucleolin to analyze nucleolar morphology. Nucleolar morphology was not affected in RPS7-mut cells. However, detailed analysis revealed a higher accumulation of this protein in nucleoli of RPS7-mut cells (Fig. 6), although the total amount of nucleolin in the cells was not altered (Fig. 6C).

Finally, we analyzed the maturation of pre-rRNA precursors in nucleolus, which is often affected by mutations in ribosomal proteins [29]. We identified a 10 % accumulation of pre-rRNA precursors containing the ITS1 region in RPS7-mut cells (Fig. 7A, B). To clarify which pre-ribosomal RNA processing step is affected, we performed Northern blotting. Accumulation of 45S, 41S, 30S and 26S pre-rRNAs were observed in RPS7-mut cell line (Fig. 7C). Additionally, we also detected a decrease in the 21S and 21 S-C pre-rRNAs levels in RPS7-mut model (Fig. 7C).

3.2. Erythrocyte metabolism and oxidative stress

Determination of eADA activity is considered as one of the confirmatory tests for DBA [30]. Indeed, we detected increased eADA activity not only in the affected patient but also in both of her asymptomatic family members harboring the same *RPS7* mutation (patient: 4.2 ± 0.8 IU/g Hb; mother: 3.5 ± 0.2 IU/g Hb; sister: 4.6 ± 0.3 IU/g Hb; reference range: 0.8–2.5 IU/g Hb) (Table 1) [14].

We previously reported that the extent of oxidative stress and alterations of erythrocytes' properties may contribute to the high heterogeneity of clinical symptoms in DBA patients [21]. In the following experiments, we, therefore, performed analysis of the anti-oxidative defense of mature erythrocytes and of the activity of their key metabolic enzymes in the patient and her family members harboring the same RPS7 p.V134F mutation but differing in the phenotype. As shown in Fig. 2A, increased levels of ROS were detected only in the patient's erythrocytes (mean fluorescence intensity - MFI: 19.2), but not in erythrocytes of her asymptomatic mother (MFI: 13.7) and sister (MFI: 14.2; mean MFI for controls: 13.4 ± 0.8). Consistently, only the patient showed increased anti-oxidative defense parameters, particularly significantly elevated levels of reduced glutathione (GSH) and significantly increased activity of glucose 6-phosphate dehydrogenase (G6PD) compared to her mother and sister and healthy controls (Table 1), confirming ongoing oxidative stress and stimulated anti-oxidative defense.

The concomitant significant increase in the activity of hexokinase (HK; approximately 3.5×), pyruvate kinase (PK; approximately 2.5×) and in the levels of ATP (approximately 3×) in the patient's red blood cells also differentiated the patient from healthy controls as well as from asymptomatic family members harboring the same mutation (Table 1). These changes in anaerobic glycolysis suggest increased demand for ATP in patients with hypoxia caused by inadequate erythrocyte production.

Despite activated anti-oxidative defense and hyperactivated anaerobic glycolysis, flow cytometry of annexin V binding revealed increased exposure of phosphatidylserines (PS) on the membrane of the patient's erythrocytes (MFI: 1.18) compared to her family members (sister MFI: 0.903; mother MFI: 0.942) and controls (mean MFI 0.84 ± 0.11) (Fig. 2B and C). These results are consistent with our previously published data on alterations of erythocytes' properties in DBA patients (21) and may indicate reduced capacity of patient's erythrocytes to cope with stress.

4. Discussion

Here we present detailed characterization of the first case of a missense mutation in *RPS7* as a cause of DBA in humans. To date, thirty cases of *RPS7* pathogenic mutations clinically associated with DBA have been reported in Ensembl database. However, all of these sequence variations were located at splice sites [29,31–34] (https://www.ensembl.org).

We identified the RPS7 p.V134F substitution in the patient and her mother and sister who have mild symptoms (Fig. 1). To validate the causality of the mutation, we performed a number of functional tests.

As we observed in this study and also reported previously [14,15], the phenotype of family members with identical mutation can be different, including silent carriers. All family members of patients with DBA should therefore be examined, even if asymptomatic and testing of eADA activity (Table 1) could serve as a sensitive screening method for such purpose.

We also showed that the antioxidant defense of patient's erythrocytes (Table 1) is insufficient to cope with increased ROS production (Fig. 2 A), leading to alterations in erythrocytes' membrane properties (Fig. 2 B and C). This may cause enhanced recognition and destruction of patients' red blood cells by reticuloendothelial macrophages in vivo and account for the phenotypic dissimilarity between the patient and her asymptomatic family members harboring the same RPS7 mutation. Profound hypoxia in the patient may further limit the antioxidant buffering capacity in her erythrocytes [35].

The functional assays were carried on a CRISPR-based cellular model with a physiological expression of RPS7 at mRNA and protein levels (Fig. 5A, Supp. Fig. 2 B). We focused on characteristic features commonly linked to DBA, e.g. effect of the SNV on global protein synthesis, proliferation, cell cycle alteration, TP53 signaling pathway, stability and degradation of RPS7 p.V134F protein compared with RPS7-WT, nucleolar morphology and maturation of pre-rRNA precursors [23,29,36–38].

The major hallmark of all ribosomopathies is impaired protein synthesis due to alterations in ribosomal components [36]. Thus our attention was firstly focused on the effect on global protein synthesis because the determination of translational capacity can shed some light on the extent of the negative effect of RPS7 p.V134F. We found that this SNV causes a significant decrease in global protein synthesis ($p<0.01$) and proliferation capacity of mutant cells ($p < 0.001$) (Figs. 3C, 4A). This finding is likely due to the lesser ability of the BCCIP protein to

Table 1
Activity of eADA and selected enzymes of anti-oxidative defense and anaerobic glycolysis (G6PD, PK, and HK) and levels of GSH and ATP in red blood cells. *eADA activity was previously reported by Volejnikova et al., 2020 [14].

	eADA (IU/g Hb)	G6PD (IU/g Hb)	PK (IU/g Hb)	HK (IU/g Hb)	GSH (μM)	ATP (μmol/l)
Reference range	[0.8–2.5]	[5.4–7.0]	[5.12–5.78]	[0.8–1.6]	[1978–2888]	[188–334]
Patient	4.2 ± 0.8*	10.3 ± 0.6	14.8 ± 0.8	4.4 ± 0.05	4356 ± 44	775 ± 96
	P = 5.49E-05	*P* = 7.73E-05	*P* = 1.63E-03	*P* = 7.75E-10	*P* = 2.03E-04	*P* = 3.96E-03
Mother	3.5 ± 0.2*	5.3 ± 0.2	4.9 ± 0.2	0.7 ± 0.02	2125	205 ± 32
	P = 3.56E-07	*NS*	*P* = 4.13E-03	*P* = 3.50E-03		*NS*
Sister	4.6 ± 0.3*	6.5 ± 0.1	6.8 ± 0.5	0.9 ± 0.13	2450 ± 35	251 ± 45
	P = 2.14E-02	*NS*	*P* = 1.63E-03	*NS*	*NS*	*NS*

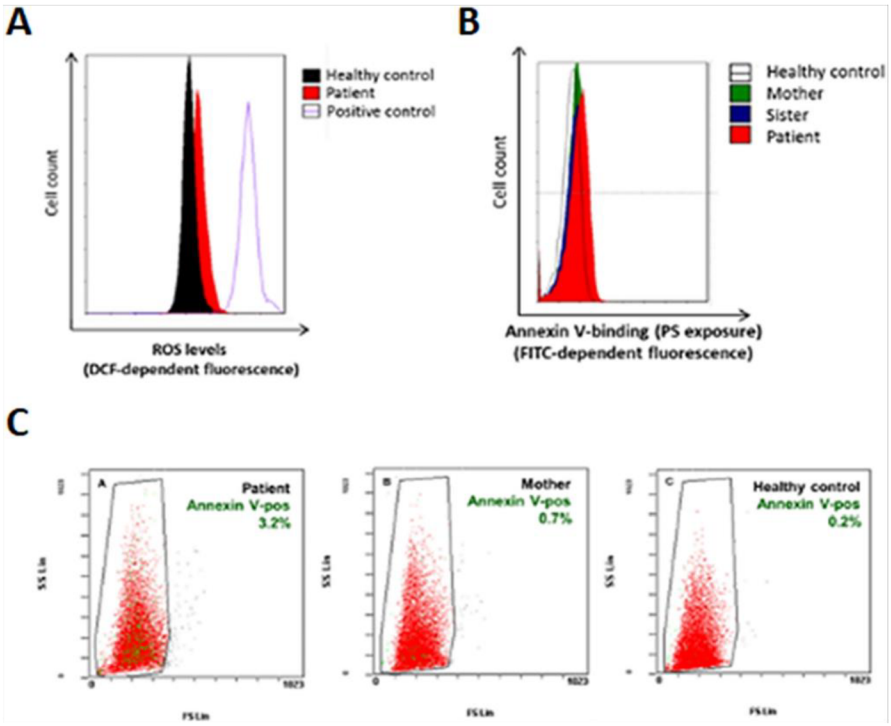

Fig. 2. Determination of ROS levels and Annexin V binding assay. Representative plots and histograms showing elevated levels of ROS (A), increased phosphatidylserine (PS) exposure on erythrocyte membrane (B) and increased percentage of Annexin V-positive erythrocytes (C) in the DBA patient compared to her asymptomatic family member and healthy control. In panel (A), DCF-dependent intensity of fluorescence is proportional to the concentration of ROS; erythrocytes of a healthy control treated with H_2O_2 served as a positive control for induced ROS formation. In panels (B) and (C), increased Annexin V-binding to RBC reflects increased exposure of PS on the erythrocyte membrane.

incorporate RPS7 p.V134F protein into the ribosome as the BCCIP protein specifically binds to the central region (amino acids 59–134) of RPS7 protein [39] (Fig. 5A). RPS7 mutant cell line also demonstrated a slight block in the G_1 phase of the cell cycle most likely caused by decreased protein levels of cyclin D1 and transcription factors c-Myc and E2F1 ($p< 0.05$) (Figs. 4B, 5A). Significantly lower level of c-Myc, a well known global transcription and translation regulator, most probably stands beside the impaired RNA synthesis and modest block in G_1 phase of the cell cycle [40,41] (Figs. 4B, D, 5A). Elevated oxidative stress in patient erythrocytes can be linked to moderately increased DNA synthesis, in the cellular model carrying RPS7 mutation, due to activated DNA repair processes [42] (Figs. 2A, 4C).

As it was previously described, the RPS7 deficiency causes p53-dependent ribosomal stress due to direct interaction with RPL5, RPL11, MDM2 and p53 [43]. Our question was whether a change in single amino acid of RPS7 may impact the TP53 signaling pathway and induce ribosomal stress. Therefore, we examined protein levels of p53 which, remained unchanged in RPS7-mut cell line, while p21 level was significantly increased ($p< 0.000001$). Protein MDM2, a ubiquitin ligase regulating the p53, level was significantly decreased ($p< 0.0004$) (Fig. 5A). We suppose that the higher expression of p21 can be caused by diminished ubiquitination activity of MDM2 and in turn decreased degradation of p53 and other target proteins.

Interestingly, in silico protein stability predictors I-Mutant and MUpro evaluated the p.V134F substitution potentially destabilizing RPS7 protein and this fact was experimentally confirmed (Fig. 5B).

TP53 signaling pathway activation is one of the key attributes of ribosomal stress, while others are linked to nucleolus, where transcription and maturation of ribosomal RNA (rRNA) takes place [44]. As it was previously reported, the haploinsufficiency of RPS7 results in impaired pre-rRNA processing during early stages [29]. Indeed, significantly increased ($p < 0.05$) abundance of pre-rRNA precursors detected by ITS1 probe in the RPS7-mut cell line (Fig. 7B). More specifically, 45S, 41S, 30S and 26S pre-rRNA precursors were accumulated at the expense of later stages pre-rRNA precursors 21S and 21 S-C (Fig. 7C). These findings are consistent with Gazda et al. study [29]. Another interesting finding linked to the maturation of pre-rRNAs is that nucleolin is preferentially located in nucleoli of RPS7-mut cells ($p<0.05$) (Fig. 6). This multifunctional protein is promoting pre-rRNA transcription and acts in the early steps of pre-rRNA processing [44]. Our hypothesis is that higher localization of nucleolin in nucleoli is a compensatory response to insufficient levels of 21S and 21 S-C pre-rRNA precursors. However, a more detailed study of the mechanism involved would certainly shed more light on pathways regulating the maturation of pre-rRNAs in DBA.

To better understand compensatory mechanisms of the ribosomal stress related to RPS7 alteration, we immunodetected the main transcription factor of canonical Wnt pathway, β-catenin. This pathway was recently reported to play an important role in reduction of nucleolar and ribosomal stress by Dannheisig et al. [28]. In case of our CRISPR-based cellular model of RPS7 deficiency, the level of β-catenin was significantly induced ($p< 0.000001$) (Fig. 5A). This finding is in agreement with Dannheisig et al. study [28].

Our results show that SNV in the RPS7 gene cause lower stability of the RPS7 protein and probably its higher presence in ribosome-free form due to negatively affected binding capacity to BCCIP protein, which regulates the localization of RPS7 to ribosomes, under physiological

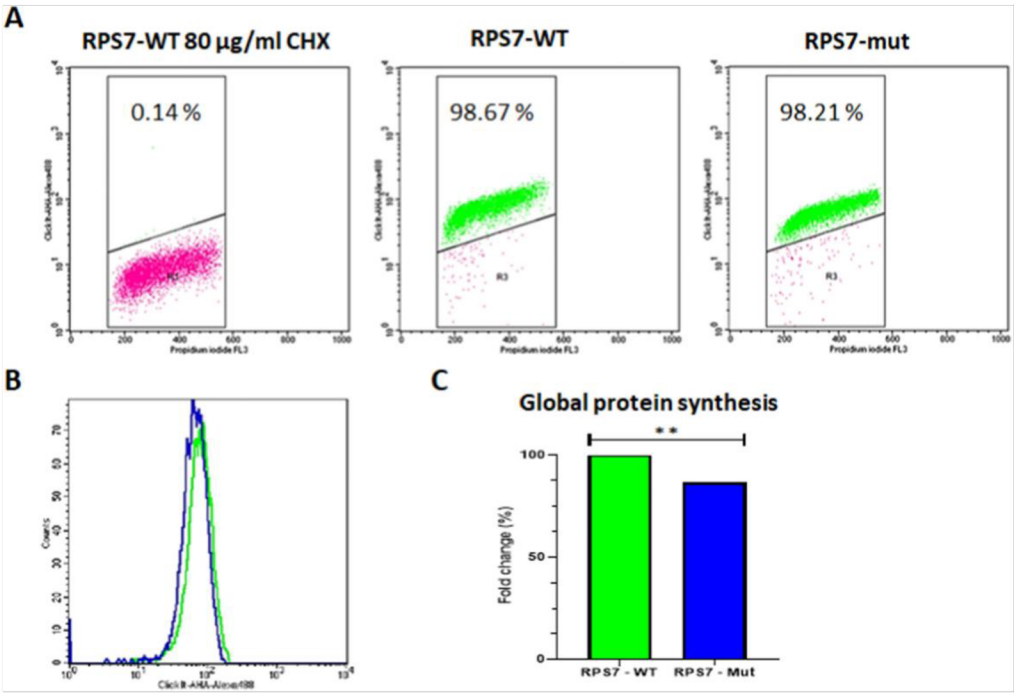

Fig. 3. Analysis of protein synthesis by flow cytometry in RPS7-WT versus RPS7-mut cell lines. (A) The upper gate represents the cell population actively synthesizing proteins. (B, C) The global protein synthesis was determined by the intensity of incorporated L-azidohomoalanine in the cell population actively synthesizing proteins; $n = 3$ biological replicates.

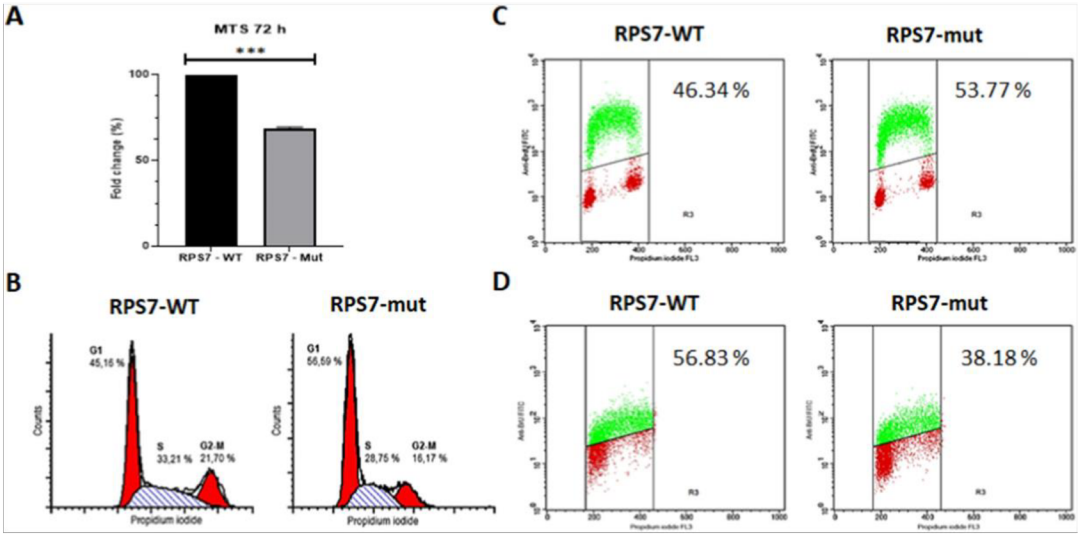

Fig. 4. Results from analysis of cellular proliferation in RPS7-WT versus RPS7-mut cell lines. (A), cell cycle (B), DNA synthesis (C) and RNA synthesis (D); n = 3 biological replicates.

conditions [39]. This leads to ribosomal stress with remarkable impact on protein synthesis, pre-rRNAs maturation and proliferation capacity.

In conclusion, the presented functional tests revealed multiple cellular abnormalities associated with the novel RPS7 p.V134F variant and support pathogenicity of the mutation in DBA. Our case study demonstrates that comprehensive analyses of larger patients cohorts and cellular model systems are needed to further elucidate the pathophysiology of DBA and to better understand disease-modifying conditions,

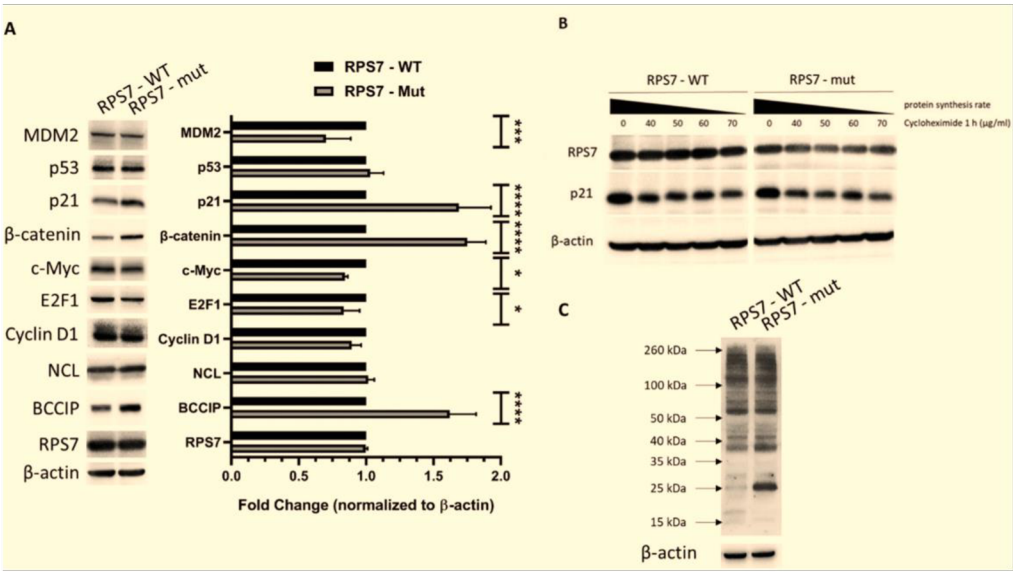

Fig. 5. Alterations in protein expression, stability and ubiquitination in RPS7-WT versus RPS7-mut cell lines. (A) Western blots showing the levels of MDM2, p53, p21, β-catenin, c-Myc, E2F1, cyclin D1, nucleolin, BCCIP, RPS7, β-actin and normalization to β-actin. (B) Stability of RPS7 and p21 proteins after inhibition of translation by increasing concentrations of cycloheximide. (C) Total ubiquitin content.; n = 3 biological replicates.

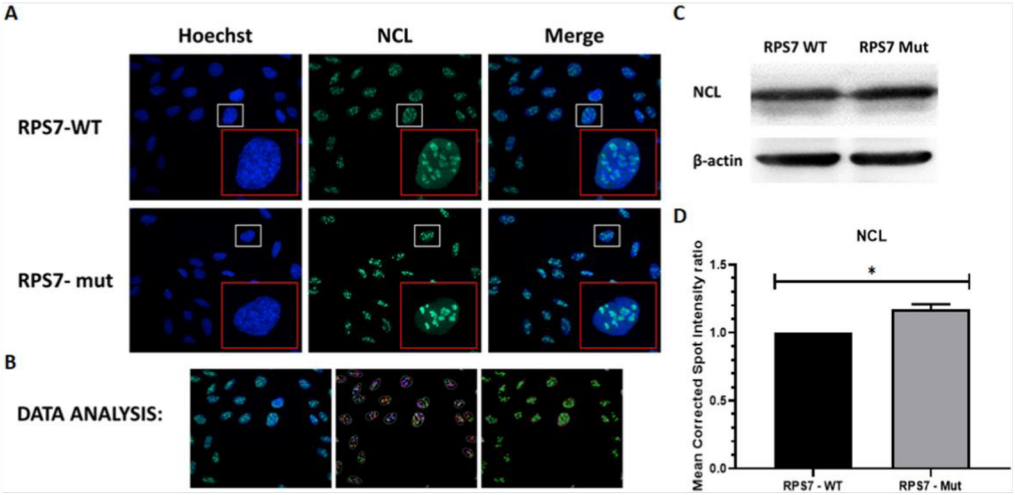

Fig. 6. SNV in RPS7 gene (RPS7-mut) does not increase the total level of nucleolin but causes higher protein accumulation in nucleoli. A) From the left side: cell nuclei stained with Hoechst 33342, localization of nucleolin, merge. (B) Illustration of image analysis using Columbus software. (C) Western blot shows the total levels of nucleolin and β-actin. (D) Statistical analysis of nucleolin amount in nucleoli (mean corrected spot intensity per nucleolus); n = 3 biological replicates.

including oxidative stress, in symptomatic versus asymptomatic carriers.

Supplementary data to this article can be found online at https://doi.org/10.1016/j.bcmd.2022.102690.

CRediT authorship contribution statement

PV performed MPS sequencing, bioinformatics analysis and annotation of genetic variants, AK performed CRISPR/Cas9 cell line model preparation, MTS viability assay, cell cycle analysis, BrdU incorporation analysis, BrU incorporation analysis, protein translational analysis, Western blotting analysis, statistical analysis, ZM performed Northern blotting analysis and rRNA FISH, MO performed mRNA quantification, nucleoli morphology analysis, immunofluorescence analysis, statistical analysis, JV and DP participated in patient management, PV, AK, JV, MO, ZM, MHa, and MHo drafted the manuscript. RM and PK performed enzyme assays and were responsible for GSH, ATP measurements. OJ examined ROS levels and Annexin V binding. MHa, MHo participated in study design, data analysis and interpretation of results. DP and MHa conceived and designed the work and finally revised the manuscript. All authors approved the final manuscript.

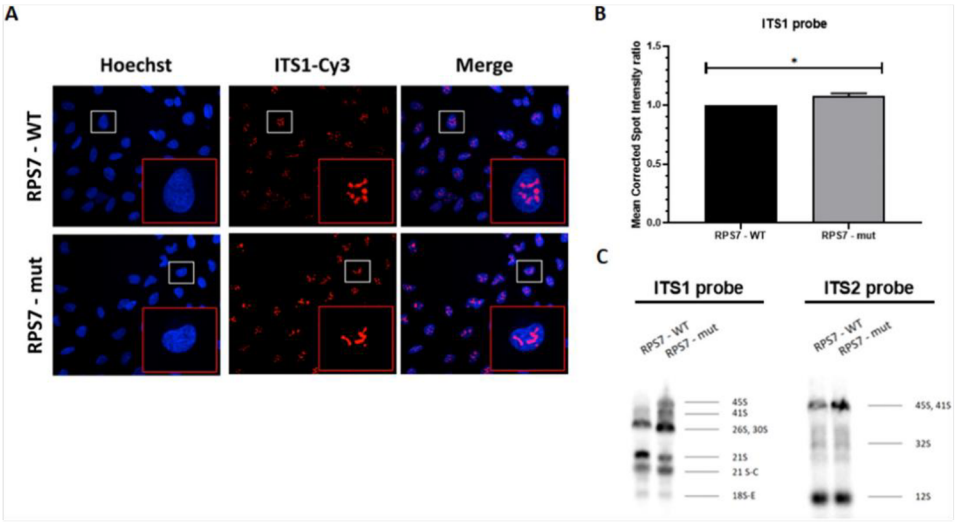

Fig. 7. Detection of pre-ribosomal RNA by FISH and Northern blotting in RPS7-WT versus RPS7-mut cell lines. (A) From the left side: cell nuclei stained with Hoechst 33342, localization of pre-rRNA by ITS1 probe, merge. (B) Statistical analysis of pre-rRNA amount in nucleoli (mean corrected spot intensity per nucleolus). (C) Detection of pre-rRNA species by Northern blotting; n = 3 biological replicates.

Declaration of competing interest

The authors declare that there is no conflict of interest.

Acknowledgments

We thank Renata Burianova for help with flow cytometry data analysis.

Funding

Supported by grants of the Czech Ministry of Health (AZV16-32105A), Czech Ministry of Education, Youth and Sports (8F20005, EATRIS-CZ LM2018133, ACGT-CZ.02.1.01/0.0/0.0/16_026/0008448), Technological Agency of the Czech Republic (PerMed TACR TN 01000013) and Palacky University Olomouc (IGA UP LF_2021_019, IGA UP LF_ 2021_038, and IGA_LF_2021_004).

References

[1] S. Ball, Diamond Blackfan anemia, Hematol. Am. Soc. Hematol. Educ. Prog. 2011 (2011) 487–491, https://doi.org/10.1182/asheducation-2011.1.487.
[2] F. Ikeda, K. Yoshida, T. Toki, T. Uechi, S. Ishida, Y. Nakajima, Y. Sasahara, Y. Okuno, R. Kanezaki, K. Terui, T. Kamio, A. Kobayashi, T. Fujita, A. Sato-Otsubo, Y. Shiraishi, H. Tanaka, K. Chiba, H. Muramatsu, H. Kanno, S. Ohga, A. Ohara, S. Kojima, N. Kenmochi, S. Miyano, S. Ogawa, E. Ito, Exome sequencing identified RPS15A as a novel causative gene for Diamond-Blackfan anemia, Haematologica 102 (2017) e93–e96, https://doi.org/10.3324/haematol.2016.153932.
[3] E. Errichiello, A. Vetro, T. Mina, A. Wischmeijer, E. Berrino, M. Carella, M. Romagnoli, P. Sacchini, T. Venesio, M. Zecca, O. Zuffardi, Whole exome sequencing in the differential diagnosis of Diamond-Blackfan anemia: clinical and molecular study of three patients with novel RPL5 and mosaic RPS19 mutations, Blood Cell Mol. Dis. 64 (2017) 38–44, https://doi.org/10.1016/j.bcmd.2017.03.002.
[4] J. Cmejlova, L. Dolezalova, D. Pospisilova, K. Petrtylova, J. Petrak, R. Cmejla, Translational efficiency in patients with Diamond-Blackfan anemia, Haematologica 91 (2006) 1456–1464.
[5] V.G. Sankaran, R. Ghazvinian, R. Do, P. Thiru, J.-A. Vergilio, A.H. Beggs, C.A. Sieff, S.H. Orkin, D.G. Nathan, E.S. Lander, H.T. Gazda, Exome sequencing identifies GATA1 mutations resulting in diamond-blackfan anemia, J. Clin. Invest. 122 (2012) 2439–2443, https://doi.org/10.1172/JCI63597.
[6] K.W. Gripp, C. Curry, A.H. Olney, C. Sandoval, J. Fisher, J.X. L. Chong, L. Pilchman, R. Sahraoui, D.L. Stabley, K. Sol-Church, Diamond-blackfan anemia with mandibulofacial dystostosis is heterogeneous, including the novel DBA genes TSR2 and RPS28, Am. J. Med. Genet. A 164A (2014) 2240–2249, https://doi.org/10.1002/ajmg.a.36633.
[7] K.A. O'Brien, N.E. Seidel, J. Farrar, A. Vlachos, , Nisc Comparative Sequencing Program, S.M. Anderson, X. An, E. Atsidaftos, H. Malech, R.J. Arceci, S.R. Ellis, J. M. Lipton, D.M. Bodine, Autosomal recessive Diamond-Blackfan anemia: identification of mutations in MCM2 and Flnb, Blood 122 (2013) 589, https://doi.org/10.1182/blood.V122.21.589.589.
[8] P.A. Trainor, A.E. Merrill, Ribosome biogenesis in skeletal development and the pathogenesis of skeletal disorders, Biochim. Biophys. Acta 1842 (2014) 769–778, https://doi.org/10.1016/j.bbadis.2013.11.010.
[9] P. Gustavsson, T.N. Willing, A. van Haeringen, G. Tchernia, I. Dianzani, M. Donnér, G. Elinder, J.I. Henter, P.G. Nilsson, L. Gordon, G. Skeppner, A. Kreuger, N. Dahl, L. van't Veer-Korthof, Diamond-Blackfan anaemia: genetic homogeneity for a gene on chromosome 19q13 restricted to 1.8 Mb, Nat Genet. 16 (1997) 368–371, https://doi.org/10.1038/ng0897-368.
[10] H. Cario, H. Bode, P. Gustavsson, N. Dahl, E. Kohne, A microdeletion syndrome due to a 3-mb deletion on 19q13.2–Diamond-blackfan anemia associated with macrocephaly, hypotonia, and psychomotor retardation, Clin. Genet. 55 (1999) 487–492, https://doi.org/10.1034/j.1399-0004.1999.550616.x.
[11] K.M. Goudarzi, M.S. Lindström, Role of ribosomal protein mutations in tumor development (review), Int. J. Oncol. 48 (2016) 1313–1324, https://doi.org/10.3892/ijo.2016.3387.
[12] N. Danilova, K.M. Sakamoto, S. Lin, Ribosomal protein S19 deficiency in zebrafish leads to developmental abnormalities and defective erythropoiesis through activation of p53 protein family, Blood 112 (2008) 5228–5237, https://doi.org/10.1182/blood-2008-01-132290.
[13] J. Badhai, A.-S. Fröjmark, E.J. Davey, J. Schuster, N. Dahl, Ribosomal protein S19 and S24 insufficiency cause distinct cell cycle defects in Diamond-Blackfan anemia, Biochim. Biophys. Acta 1792 (2009) 1036–1042, https://doi.org/10.1016/j.bbadis.2009.08.002.
[14] J. Volejnikova, P. Vojta, H. Urbankova, R. Mojzíkova, M. Horvathova, I. Hochova, J. Cermak, J. Blatny, M. Sukova, E. Bubanska, J. Feketeova, D. Prochazkova, J. Horakova, M. Hajduch, D. Pospisilova, Czech and slovak diamond-blackfan anemia (DBA) registry update: clinical data and novel causative genetic lesions, Blood Cells Mol. Dis. 81 (2020), 102380, https://doi.org/10.1016/j.bcmd.2019.102380.
[15] D. Pospisilova, J. Cmejlova, B. Ludikova, J. Stary, Z. Cerna, J. Hak, P. Timr, K. Petrtylova, J. Blatny, S. Vokurka, R. Cmejla, The czech National Diamond-Blackfan Anemia Registry: clinical data and ribosomal protein mutations update, Blood Cells Mol. Dis. 48 (2012) 209–218, https://doi.org/10.1016/j.bcmd.2012.02.002.
[16] K. Okonechnikov, O. Golosova, M. Fursov, Unipro UGENE: a unified bioinformatics toolkit, Bioinformatics 28 (2012) 1166–1167, https://doi.org/10.1093/bioinformatics/bts091.
[17] E. Beutler, K.G. Blume, J.C. Kaplan, G.W. Löhr, B. Ramot, W.N. Valentine, International Committee for Standardization in haematology: recommended methods for red-cell enzyme analysis, Br. J. Haematol. 35 (1977) 331–340, https://doi.org/10.1111/j.1365-2141.1977.tb00589.x.
[18] R. Mojzikova, P. Dolezel, J. Pavlicek, P. Mlejnek, D. Pospisilova, V. Divoky, Partial glutathione reductase deficiency as a cause of diverse clinical manifestations in a

family with unstable hemoglobin (Hemoglobin Haná, β63(E7) his-Asn), Blood Cells Mol. Dis. 45 (2010) 219–222, https://doi.org/10.1016/j.bcmd.2010.07.003.
[19] R. Mojzikova, P. Koralkova, D. Holub, Z. Zidova, D. Pospisilova, J. Cermak, Z. Striezencova Laluhova, K. Indrak, M. Sukova, M. Partschova, J. Kucerova, M. Horvathova, V. Divoky, Iron status in patients with pyruvate kinase deficiency: neonatal hyperferritinaemia associated with a novel frameshift deletion in the PKLR gene (p.Arg518fs), and low hepcidin to ferritin ratios, Br. J. Haematol. 165 (2014) 556–563, https://doi.org/10.1111/bjh.12779.
[20] Z. Zidova, K. Kapralova, P. Koralkova, R. Mojzikova, D. Dolezal, V. Divoky, M. Horvathova, DMT1-mutant erythrocytes have shortened life span, accelerated glycolysis and increased oxidative stress, Cell. Physiol. Biochem. 34 (2014) 2221–2231, https://doi.org/10.1159/000369665.
[21] K. Kapralova, O. Jahoda, P. Koralkova, J. Gursky, L. Lanikova, D. Pospisilova, V. Divoky, M. Horvathova, Oxidative DNA damage, inflammatory signature, and altered erythrocytes properties in diamond-blackfan anemia, Int. J. Mol. Sci. 21 (2020), https://doi.org/10.3390/ijms21249652.
[22] T. Schneider-Poetsch, J. Ju, D.E. Eyler, Y. Dang, S. Bhat, W.C. Merrick, R. Green, B. Shen, J.O. Liu, Inhibition of eukaryotic translation elongation by cycloheximide and lactimidomycin, Nat. Chem. Biol. 6 (2010) 209–217, https://doi.org/10.1038/nchembio.304.
[23] C. Carron, M.-F. O'Donohue, V. Choesmel, M. Faubladier, P.-E. Gleizes, Analysis of two human pre-ribosomal factors, bystin and hTsr1, highlights differences in evolution of ribosome biogenesis between yeast and mammals, Nucleic Acids Res. 39 (2011) 280–291, https://doi.org/10.1093/nar/gkq734.
[24] R.A. Idol, S. Robledo, H.-Y. Du, D.L. Crimmins, D.B. Wilson, J.H. Ladenson, M. Bessler, P.J. Mason, Cells depleted for RPS19, a protein associated with diamond blackfan anemia, show defects in 18S ribosomal RNA synthesis and small ribosomal subunit production, Blood Cell Mol. Dis. 39 (2007) 35–43, https://doi.org/10.1016/j.bcmd.2007.02.001.
[25] K. Yang, J. Yang, J. Yi, Nucleolar Stress: hallmarks, sensing mechanism and diseases, Cell Stress 2 (2018) 125–140, https://doi.org/10.15698/cst2018.06.139.
[26] K.Holmberg Olausson, M. Nistér, M.S. Lindström, p53-Dependent and -independent nucleolar stress responses, Cells 1 (2012) 774–798, https://doi.org/10.3390/cells1040774.
[27] P. Moudry, K. Chroma, S. Bursac, S. Volarevic, J. Bartek, RNA-interference screen for p53 regulators unveils a role of WDR75 in ribosome biogenesis, Cell Death Differ. (2021), https://doi.org/10.1038/s41418-021-00882-0.
[28] D.P. Dannheisig, J. Bächle, J. Tasic, M. Keil, A.S. Pfister, The Wnt/β-catenin pathway is activated as a novel nucleolar stress response, J. Mol. Biol. 433 (2021), 166719, https://doi.org/10.1016/j.jmb.2020.11.018.
[29] H.T. Gazda, M.R. Sheen, A. Vlachos, V. Choesmel, M. F. O'Donohue, H. Schneider, N. Darras, C. Hasman, C.A. Sieff, P.E. Newburger, S.E. Ball, E. Niewiadomska, M. Matysiak, J.M. Zaucha, B. Glader, C. Niemeyer, J.J. Meerpohl, F. Atsidaftos, J. M. Lipton, P.-E. Gleizes, A.H. Beggs, Ribosomal protein L5 and L11 mutations are associated with cleft palate and abnormal thumbs in diamond-blackfan anemia patients, Am. J. Hum. Genet. 83 (2008) 769–780, https://doi.org/10.1016/j.ajhg.2008.11.004.
[30] A. Vlachos, S. Ball, N. Dahl, B.P. Alter, S. Sheth, U. Ramenghi, J. Meerpohl, S. Karlsson, J.M. Liu, T. Leblanc, C. Paley, E.M. Kang, E.J. Leder, E. Atsidaftos, A. Shimamura, M. Bessler, B. Glader, J.M. Lipton, Diagnosing and treating Diamond Blackfan anaemia: results of an international clinical consensus conference, Br. J. Haematol. 142 (2008) 859–876, https://doi.org/10.1111/j.1365-2141.2008.07269.x.
[31] G. Gerrard, M. Valgañón, H.E. Foong, D. Kasperaviciute, D. Iskander, L. Game, M. Müller, T.J. Aitman, I. Roberts, J. de la Fuente, L. Foroni, A. Karadimitris, Target enrichment and high-throughput sequencing of 80 ribosomal protein genes to identify mutations associated with diamond-blackfan anaemia, Br. J. Haematol. 162 (2013) 530–536, https://doi.org/10.1111/bjh.12397.
[32] N.S. Smetanina, I.V. Mersiyanova, M.A. Kurnikova, G.S. Ovsyannikova, L. A. Hachatryan, V.O. Bobrynina, M.A. Maschan, G.A. Novichkova, J.M. Lipton, A. A. Maschan, Clinical and genomic heterogeneity of diamond blackfan anemia in the Russian Federation, Pediatr. Blood Cancer 62 (2015) 1597–1600, https://doi.org/10.1002/pbc.25534.
[33] T. Ichimura, K. Yoshida, Y. Okuno, T. Yujiri, K. Nagai, M. Nishi, Y. Shiraishi, H. Ueno, T. Toki, K. Chiba, H. Tanaka, H. Muramatsu, T. Hara, H. Kanno, S. Kojima, S. Miyano, E. Ito, S. Ogawa, S. Ohga, Diagnostic challenge of diamond-blackfan anemia in mothers and children by whole-exome sequencing, Int. J. Hematol. 105 (2017) 515–520, https://doi.org/10.1007/s12185-016-2151-7.
[34] T. Akram, A. Fatima, J. Klar, J. Hoeber, M. Zakaria, M. Tariq, S.M. Baig, J. Schuster, N. Dahl, Aberrant splicing due to a novel RPS7 variant causes diamond-blackfan anemia associated with spontaneous remission and meningocele, Int. J. Hematol. 112 (2020) 894–899, https://doi.org/10.1007/s12185-020-02950-6.
[35] S.C. Rogers, A. Said, D. Corcuera, D. McLaughlin, P. Kell, A. Doctor, Hypoxia limits antioxidant capacity in red blood cells by altering glycolytic pathway dominance, FASEB J. 23 (2009) 3159–3170, https://doi.org/10.1096/fj.09-130666.
[36] R. Cmejla, J. Cmejlova, H. Handrkova, J. Petrak, D. Pospisilova, Ribosomal protein S17 gene (RPS17) is mutated in diamond-blackfan anemia, Hum. Mutat. 28 (2007) 1178–1182, https://doi.org/10.1002/humu.20608.
[37] D. Chen, Z. Zhang, M. Li, W. Wang, Y. Li, E.R. Rayburn, D.L. Hill, H. Wang, R. Zhang, Ribosomal protein S7 as a novel modulator of p53-MDM2 interaction: binding to MDM2, stabilization of p53 protein, and activation of p53 function, Oncogene 26 (2007) 5029–5037, https://doi.org/10.1038/sj.onc.1210327.
[38] Y. Zhu, M.V. Poyurovsky, Y. Li, L. Biderman, J. Stahl, X. Jacq, C. Prives, Ribosomal protein S7 is both a regulator and a substrate of MDM2, Mol. Cell 35 (2009) 316–326, https://doi.org/10.1016/j.molcel.2009.07.014.
[39] Q. Ba, X. Li, C. Huang, J. Li, Y. Fu, P. Chen, J. Duan, M. Hao, Y. Zhang, J. Li, C. Sun, H. Ying, H. Song, R. Zhang, Z. Shen, H. Wang, BCCIPβ modulates the ribosomal and extraribosomal function of S7 through a direct interaction, J. Mol. Cell Biol. 9 (2017) 209–219, https://doi.org/10.1093/jmcb/mjx019.
[40] T.R. Kress, A. Sabò, B. Amati, MYC: connecting selective transcriptional control to global RNA production, Nat. Rev. Cancer 15 (2015) 593–607, https://doi.org/10.1038/nrc3984.
[41] I. Perez-Roger, S.H. Kim, B. Griffiths, A. Sewing, H. Land, Cyclins D1 and D2 mediate myc induced proliferation via sequestration of p27(Kip1) and p21(Cip1), EMBO J. 18 (1999) 5310–5320, https://doi.org/10.1093/emboj/18.19.5310.
[42] R.A. Egler, E. Fernandes, K. Rothermund, S. Sereika, N. de Souza-Pinto, P. Jaruga, M. Dizdaroglu, E.V. Prochownik, Regulation of reactive oxygen species, DNA damage, and c-myc function by peroxiredoxin 1, Oncogene 24 (2005) 8038–8050, https://doi.org/10.1038/sj.onc.1208821.
[43] S. Bursać, M.C. Brdovčak, M. Pfannkuchen, I. Orsolić, L. Golomb, Y. Zhu, C. Katz, L. Daftuar, K. Grabušić, I. Vukelić, V. Filić, M. Oren, C. Prives, S. Volarevic, Mutual protection of ribosomal proteins L5 and L11 from degradation is essential for p53 activation upon ribosomal biogenesis stress, Proc. Natl. Acad. Sci. U. S. A. 109 (2012) 20467–20472, https://doi.org/10.1073/pnas.1218535109.
[44] L.M. Ogawa, S.J. Baserga, Crosstalk between the nucleolus and the DNA damage response, Mol. Biosyst. 13 (2017) 443–455, https://doi.org/10.1039/c6mb00740f, accessed 22.12.2021, https://www.ensembl.org/Homo_sapiens/Gene/Variation_Gene/Table?db=core;g=ENSG00000171863;r=2:3575260-3580920.

Appendix 3

International Journal of
Molecular Sciences

MDPI

Review

Effect of Glucocorticosteroids in Diamond-Blackfan Anaemia: Maybe Not as Elusive as It Seems

Zuzana Macečková [1], Agáta Kubíčková [1,2], Juan Bautista De Sanctis [1,2] and Marian Hajdúch [1,2,*]

[1] Institute of Molecular and Translational Medicine, Palacky University Olomouc, Hnevotinska 1333/5, 77900 Olomouc, Czech Republic; zuzana.maceckova@upol.cz (Z.M.); agata.kubickova@upol.cz (A.K.); juabautista.desanctis@upol.cz (J.B.D.S.)
[2] Czech Advanced Technology and Research Institute, Palacky University Olomouc, Hnevotinska 1333/5, 77900 Olomouc, Czech Republic
* Correspondence: marian.hajduch@upol.cz; Tel.: +420-585632127

Abstract: Diamond-Blackfan anaemia (DBA) is a red blood cell aplasia that in the majority of cases is associated with ribosomal protein (RP) aberrations. However, the mechanism by which this disorder leads to such a specific phenotype remains unclear. Even more elusive is the reason why non-specific agents such as glucocorticosteroids (GCs), also known as glucocorticoids, are an effective therapy for DBA. In this review, we (1) explore why GCs are successful in DBA treatment, (2) discuss the effect of GCs on erythropoiesis, and (3) summarise the GC impact on crucial pathways deregulated in DBA. Furthermore, we show that GCs do not regulate DBA erythropoiesis via a single mechanism but more likely via several interdependent pathways.

Keywords: Diamond-Blackfan anaemia; glucocorticosteroid; erythropoiesis; GATA1; c-myc; mTOR; autophagy

Citation: Macečková, Z.; Kubíčková, A.; De Sanctis, J.B.; Hajdúch, M. Effect of Glucocorticosteroids in Diamond-Blackfan Anaemia: Maybe Not as Elusive as It Seems. *Int. J. Mol. Sci.* **2022**, *23*, 1886. https://doi.org/10.3390/ijms23031886

Academic Editors: Mariano Ostuni and Sarah Ducamp

Received: 26 December 2021
Accepted: 5 February 2022
Published: 8 February 2022

Publisher's Note: MDPI stays neutral with regard to jurisdictional claims in published maps and institutional affiliations.

1. Introduction

Human erythrocytes differ from other cells because of their particular shape, lack of organelles, and transportation of oxygen via haemoglobin. Erythropoiesis is a complex differentiation process in which cells discard several organelles, from mitochondria to the nucleus, and dramatically increase haemoglobin production. These multifaceted changes need to be tightly regulated by numerous factors, and any disruption in signalling during erythropoiesis may lead to anaemia.

Diamond-Blackfan anaemia (DBA) [1] is a rare congenital disease usually diagnosed shortly after birth. Despite normal platelet and neutrophil counts, patients present with macrocytic or normocytic anaemia, reticulocytopenia, and a shortage of erythrocyte precursors [2]. Patients with DBA also manifest physical malformations, mainly craniofacial and upper limb, and growth retardation in approximately 35–50% of cases [3].

The first gene associated with DBA was RPS19 [4]. Interestingly, RPS19 variants account for approximately 25% of all DBA cases [5]. Over the last years, the number of RP genes associated with DBA increased; currently, there are 16 ribosomal protein aberrations linked to the disease, involving both large and small RP genes [6]. Rarely, non-ribosomal protein gene abnormalities were also associated with DBA, for instance in transcription factor GATA1 [7], iron metabolism gene *SLC49A1* [8], and ribosome maturation factor TSR2 [9]. The molecular pathology of approximately 20–50% of cases remains unknown; nonetheless, a number of candidate DBA genes is continually increasing with higher penetration of high-throughput DNA sequencing technologies into the clinic.

The aberration of ribosomal proteins (RPs) results in a decreased number of available ribosomes with a consequent drop in translational activity [10]. A reduced number of ribosomes leads to an imbalance between translated and non-translated mRNA [11]. Furthermore, RP defects may result in ribosomal stress [12], p53 activation [12], altered

mTOR signalling [13], c-Myc [14] deregulation, and other stress-related processes (Figure 1). Deregulation of any of these signal and metabolic pathways may result in anaemia.

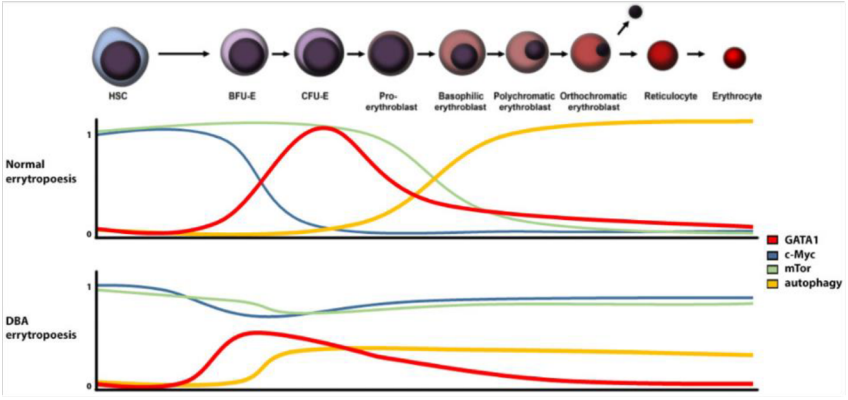

Figure 1. Regulation of relevant signalling proteins and pathways levels in DBA versus normal erythropoiesis (HSC: hematopoietic stem cells, BFU-E: burst-forming unit-erythroid, CFU-E: Colony-forming unit-erythroid).

As for many other rare diseases, therapeutic opportunities in DBA are inadequate. The first-line non-specific therapy usually includes glucocorticosteroids (GCs). However, treatment response is limited, and long-term use is associated with drug resistance and significant side effects [2]. Blood transfusion and iron chelation are usually reserved for GC non-responder [15]. Although some alternative therapies such as L-leucine supplementation to stimulate deficient protein synthesis have been used, the only permanent treatment of DBA is bone marrow transplantation [15]. However, bone marrow replacement is a high-risk procedure reserved for transfusion-dependent individuals. Recently, the approved gene therapy for betta thalassemia is also hope for many other congenital anaemias [16]. For DBA, gene therapy was already successfully tested in mice [17], and its further development is ongoing. Nevertheless, in contrast to thalassemia, where only hematopoietic cells are affected, DBA causes complex signalling and metabolic abnormalities in many other tissues, which will be difficult to correct by currently available gene therapy technologies.

Glucocorticosteroids (GCs) [18] generally improve erythropoiesis [19] and are frequently used for DBA treatment [3]. However, the mechanism by which GCs ameliorate DBA is elusive [19–21]. The present review aims to analyse the possible pathways that may be affected by GCs and improve DBA pathology. This is particularly important in the development of more efficient and targeted DBA therapies without glucocorticoid side effects.

2. Glucocorticosteroids

GCs are stress hormones produced in the adrenal cortex. They regulate diverse cellular functions, including development, homeostasis, metabolism, cognition, and inflammation [22]. GCs are widely used as treatments for a broad range of pathologies, from autoimmune syndromes and allergy to cancer [23]. Although GCs have a wide range of applications, their use is limited by severe adverse effects, especially in long-term or high-dose therapies. Possible side effects include osteoporosis, skin atrophy, diabetes, abdominal obesity, glaucoma, cataracts, avascular necrosis and infection, growth retardation, and hypertension [24].

Approximately 80% of DBA patients respond to initial GC treatment with a starting dose of 2 mg/kg per day for a maximum of 4 weeks to avoid GC toxicity in children [2,25]. The most serious GC adverse effects in infants include immunosuppression and susceptibility to infection, weight gain, growth retardation, osteonecrosis, and Cushingoid features [25].

The majority of GC effects are mediated by the glucocorticoid receptor (GCR). GCR is encoded by the *NR3C1* gene located on chromosome 5 and is a ligand-activated transcription factor. In an inactive form, GCR is predominantly located in the cytoplasm in complex with chaperone proteins and immunophilins [26]. However, its conformation changes upon ligand binding, whereupon it disassociates from the complex and translocates to the nucleolus, where it binds to GCR sequences and initiates the expression of target genes. Interestingly, GCR-mediated expression is tissue specific, and only a small number of genes are activated in all tissues [27]. This is probably caused by tissue-specific DNA methylation [28]. Furthermore, in addition to expression initiation, activated GCR can interact with other proteins. For example, it can modulate the activity of several kinases [29] and regulate GATA1 during erythropoiesis [30].

Moreover, GCR has several isoforms [31] and is highly polymorphic [32]. The genetic variability of GCR can affect body mass index, bone density or coronary artery diseases, probability of developing type II diabetes and GC treatment outcome [33,34]. This also applies in DBA. Surprisingly, the variability of GCR seems to have no or minor impact on GC treatment outcome in DBA [35]. However, it seems to modulate the onset of disease [35]. It has been shown that particular SNPs (rs6196 and rs860457) in GCR result in early onset of DBA, which can be caused by a modified GC response during embryogenesis [35].

3. The Primary Defect in DBA Cells

It is not fully understood how RP aberration causes red blood cell aplasia. A plausible mechanism involves a gap between transcription and translation [11]. The common feature of DBA is a decreased number of available ribosomes, resulting in decreased translational activity [10]. Several mRNAs are particularly affected by DBA ribosome impairment. Among the critically affected complexes are IRES-mediated mRNA and mRNAs with complex 5′ UTR regions [36].

GATA1, the specific erythropoiesis master regulator, is affected in DBA [37]. GATA1 is expressed during the final steps of erythrocyte development. It is responsible for triggering haemoglobin transcription, eliminating organelles and inducing other genes related to the terminal steps of erythropoiesis [38]. Although GATA1 mRNA levels are slightly increased or similar in RP depleted cells or DBA patients compared to controls, protein levels are downregulated [38]. The origin of this phenomenon is related to the complex 5′ UTR region of the gene [38]. GATA1 protein levels are restored and overall erythroid differentiation is improved when GATA1 5′ UTR region is substituted with less complex one [38].

It has been postulated that DBA red blood cells phenotype is induced by GATA1 translation inhibition [37]. GATA1 is expressed when committed cells are in the colony-forming unit-erythroid (CFU-E) stage of red blood cell (RBC) development [39]. At this stage, downregulation of GATA1 protein leads to apoptosis [40], which is consistent with the DBA phenotype. Furthermore, if RBC precursors escape apoptosis at the CFU-E stage, GATA1 decreased signalling may lead to impaired cell responses in later RBC developmental stages. Interestingly, mutations in the GATA1 gene have been described in several DBA-like patients [7,41]. However, although these patients showed impaired erythropoiesis similar to DBA, other typical features, such as physical malformations, were missing [7,41]. Furthermore, arsenic-induced disruption of GATA1 also leads to DBA-like erythropoiesis disruption [42].

Recent findings have suggested that erythropoiesis failure in DBA is more complicated than previously thought. More specifically, it seems that GATA1 impairment plays a crucial role in the DBA phenotype but only in ribosomal proteins of small-(RPS) and not large (RPL) subunit-related disorders [43].

4. GCs and GATA1

Impaired GATA1 protein levels seem to be the primary defect in DBA RBC precursor cells [44]. Therefore, it could be suggested that GCs restore GATA1 translation and related signalling pathways, and consequently increase erythrocyte precursor counts. However,

GCs do not increase GATA1 but deplete it. GCs inhibit GATA1 by transcriptional repression and direct interaction of GCRs with GATA1 [25]. GCs also decrease protein synthesis in cells through mTOR and subsequent S6 kinase inhibition [45]. This reduction affects the levels of HSP70 [46], a chaperone that protects GATA1 from caspase-3 degradation during erythropoiesis [40]. Therefore, GCs do not seem to increase GATA1 levels but instead deplete them.

GCs can promote erythropoiesis by two mechanisms to overcome GATA1 impairment. Firstly, GCs can act before the CFU-E stage and increase the number of CFU-E precursors. Secondly, even though GCs do not rescue GATA1, they can regulate GATA1-related steps in erythropoiesis, as discussed further below.

5. Role of GCs in CFU-E Precursors

Stress erythropoiesis may be caused by blood loss, oxygen deprivation, haemolytic anaemia and long-term stress [47] (Figure 2). This type of erythropoiesis leads to the rapid proliferation of RBC precursors driven by erythropoietin (Epo) and GCs [21]. Because DBA fulfils several criteria, we can hypothesise that stress erythropoiesis plays a crucial role in RBC development in DBA patients.

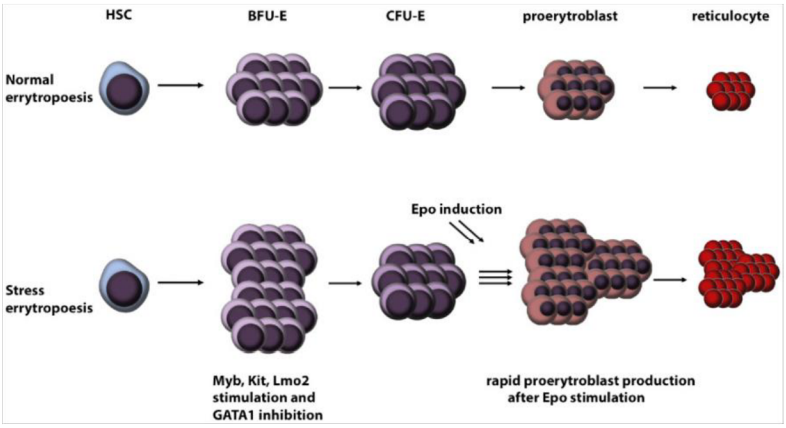

Figure 2. Schematic overview of stress versus normal erythropoiesis. (HSC: hematopoietic stem cells, BFU-E: burst-forming unit-erythroid, CFU-E: colony-forming unit-erythroid, Epo: erythropoietin).

When the body is under stress, cortisol, the intrinsic master GC, induces many physiological responses. One of them is to stimulate the production of Epo [48] in the kidneys [49]. Epo in turn stimulates CFU-E, and its primary target is GATA1 [50]. Due to GATA1 impairment, DBA is one of very few Epo insensitive anaemias [51]. Therefore, we can speculate that Epo induction via stress erythropoiesis probably does not lead to DBA phenotype improvement.

GCs induce stress erythropoiesis also directly by activating GCR [19]. Furthermore, activation of GCR is conditional for stress erythropoiesis [19] and stimulates several transcription factors necessary for burst forming unit-erythroid (BFU-E), CFU-E precursor, cell proliferation, specifically Myb, Kit and Lmo2 [52]. Together with GATA1 inhibition, these transcription factors stimulate the rapid proliferation of BFU-E cells. This induction pathway is specific to BFU-E cells and increases the number of CFU-E precursor cells by up to 10-fold [53]. Thus, an increased number of CFU-E cells are generated, which, after Epo stimulation, undergo rapid differentiation [47]. Hence, stress erythropoiesis results in a significant increase in RBC number originating from one precursor cell.

Furthermore, it seems that stress erythropoiesis impairment plays a crucial role mainly in RPL-related DBA, and its external stimulation by GC treatment may result in restoration of this pathway [43].

6. Regulation of Ribosomal Stress and p53

It has been suggested that apoptosis in DBA RBC precursors is caused by p53 induction via ribosomal stress [54]. However, this hypothesis has been partially refuted since the haploinsufficiency of most RPs does not lead to p53 stimulation via ribosomal stress mechanisms [55]. Even though ribosomal stress and p53 signalling are critical for normal erythropoiesis [56], the activation of p53 in DBA is most likely mediated by impaired metabolism and DNA damage [6,57].

Unfortunately, it is difficult to elucidate the interplay between p53 and GCs. On the one hand, GCs decrease p53 levels [58], whereas on the other hand, increased p53, common in DBA cells, limits proper GCs receptor activation [59]. Moreover, GCs do not only regulate p53 directly but also indirectly by reducing p53 activation signals.

As mentioned above, in addition to ribosomal stress, p53 could be activated by HEM-mediated ROS production [60,61]. Although it has been reported that GCs reduce ROS species [62–64], their overall influence on ROS production is ambiguous [65]. More specifically, it seems that short-term GC usage leads to a reduction in ROS generation, whereas long-term exposure leads to ROS induction [65]. Furthermore, increased ROS levels have been detected in DBA patients regardless of treatment [60]. Therefore, GC-mediated p53 regulation does not seem to reflect ROS levels. Thus, the precise mechanism by which GCs modulate p53 levels in DBA remains mysterious. Nevertheless, we can conclude that GC treatment improves p53 status in DBA [66].

7. Regulation of Enucleation through c-Myc

Enucleation is a critical step in erythropoiesis, in which the cells lose a major part of the nucleus to generate reticulocytes. Inhibition of this process may explain reticulocytopenia in DBA patients [67]. Before enucleation, the nucleolus must be condensed and histones deacetylated.

Protein c-Myc is a master transcription factor that promotes and regulates proliferation, transcription, translation and cellular metabolism with an important role in several cell transduction pathways [68]. GATA1 silences c-Myc expression in RBC precursors [37], which highlights the importance of c-Myc during erythropoiesis. Only a slight increase in c-Myc levels disables enucleation and reticulocyte development by impairing histone deacetylases [68]. Activated c-Myc also induces proerythroblast apoptosis during RBC development [68].

c-Myc is deregulated in DBA in multiple ways. Downregulated GATA1 is probably the central factor leading to upregulation of c-Myc in all DBA erythroid progenitors. Interestingly, some RPs affected in DBA regulate c-Myc on their own, e.g., RPL11 and RPL5. Both these RPs regulate ribosomal stress induction [69] and c-Myc regulation [70] at mRNA and protein levels [14]. Impairment of RPL5 and RPL11 has also been associated with a more severe DBA phenotype [71]. In addition, c-Myc driven lymphomagenesis has been observed in a DBA mouse model [14]. Interestingly, similar or identical mutations of those RPs reported in DBA have also been detected in some cancers [72,73], characterized by p53 deactivation and activation of c-Myc signalling.

GCs transcriptionally repress c-Myc expression [74], leading to cell cycle arrest without apoptosis, which is necessary for proper RBC differentiation [75]. In DBA, GCs may support enucleation during erythropoiesis, and thus prevent reticulocytopenia by downregulating c-Myc.

8. mTOR Pathway and Autophagy

Autophagy is crucial in RBC development [76]. During erythrocyte differentiation, cells discard and/or recycle most subcellular structures, starting from mitochondria to the nucleus. The nucleus is removed through the enucleation step, whereas other organelles are typically removed via autophagy [77]. Autophagy is activated by GATA1 [78] and mTOR [79] mediated induction of autophagy genes transcription. Notably, increased mTOR leads to macrocytic anaemia [80], consistent with the DBA phenotype [81].

mTOR has a dual role in RBC development [82]. Its activity is necessary for proper BFU-E and CFU-E cell proliferation in the primary steps of RBC development. But in later steps of erythropoiesis, it needs to be silenced for autophagy induction. mTOR is known to be activated in DBA cells [13]. Activated mTOR in DBA probably facilitates the increased proliferation of BFU-E and CFU-E cells and in a back-loop manner stimulates deficient protein translation S6-kinase activation and in turn RPS6 phosphorylation [83].

Furthermore, L-leucine, an inductor of mTOR activation, is routinely used as a DBA treatment but with a variable response rate [84,85]. Thus, we suggest induction of mTOR is beneficial for DBA cells, especially during RBC development until the CFU-E stage. On the other hand, constitutive mTOR induction during terminal differentiation may lead to autophagy failure, followed by aberration of the final erythropoiesis steps. We can speculate that this may be the underlying mechanism in DBA because DBA erythroid precursors treated by rapamycin, an mTOR inhibitor, have been shown to increase the proliferation of late erythroid cells in DBA [86].

In DBA, autophagy is increased despite mTOR activation [13]. It seems to be induced by ROS [60], hypoxia [87] or some mTOR-independent pathways [88]. However, mTOR-independent autophagy may not be sufficient for proper RBC development [89]. Therefore, autophagy induction may offer a possible target for future treatment of DBA patients [86].

Inhibition of mTOR by GCs followed by autophagy has been described in several cell types [90–92]. Therefore, a plausible hypothesis is that GCs may also improve erythropoiesis by modulating mTOR, and subsequently autophagy. The other important pathway is inactivation of Akt signalling by GCs in DBA cells [13,93]. Even though GC-induced mTOR inactivation may lead to decreased proliferation of BFU-E and CFU-E cells [82], stress-induced erythropoiesis may compensate for this [39] (Figure 3).

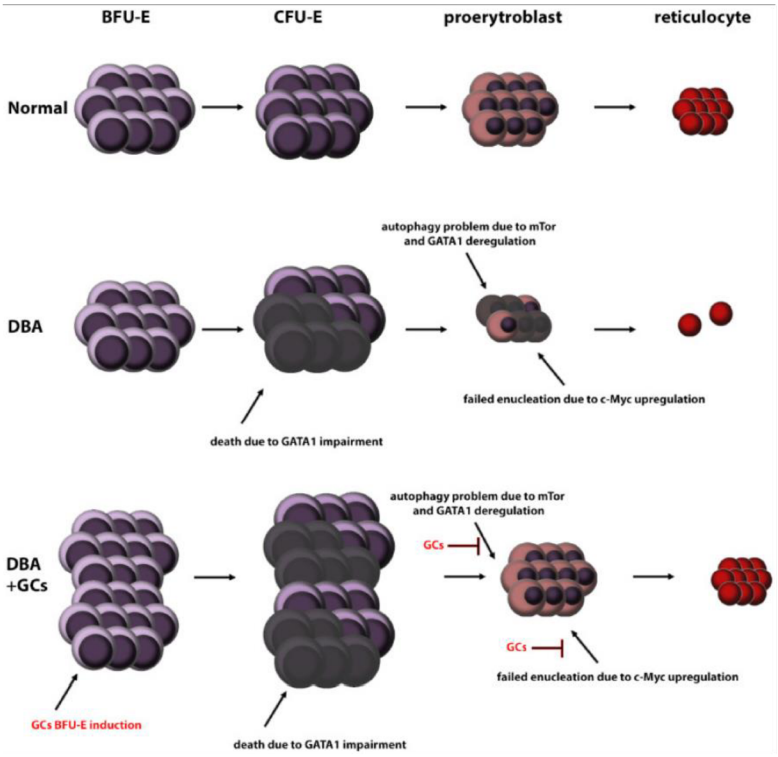

Figure 3. Possible mechanism involved in GC-mediated improvement of DBA erythropoiesis. (HSC: hematopoietic stem cells, BFU-E: burst-forming unit-erythroid, CFU-E: colony-forming unit-erythroid, DBA: Diamond Blackfan anemia, GC: glucocorticosteroids).

9. GC Resistance

GC resistance is common in almost all GC-based therapies [94,95]; DBA is no exception [96]. Multiple mechanisms may induce GC resistance, and these mechanisms may vary among individual patients [97]. GCR polymorphism, alternative splicing and downregulation of GCR expression may also lead to GCR resistance [97], expression of pharmacological multidrug transporters may also be involved [94]. GC resistance in DBA has been shown to be associated with p57 cyclin dependent kinase inhibitor dysregulation [96]. Expression of p57 is directly induced by the GCR responsive element promoter [98]. Therefore, more than one mechanism may play a role to effect GC resistance.

10. Conclusions

GCs have been used to treat DBA for decades, but their mechanism of action remains elusive, and it is difficult to understand them fully due to their pleiotropic effects. We suggest that GCs improve the DBA pathology via at least four relatively independent ways: (i) induction of BFU-E cell proliferation via stress erythropoiesis, (ii) (de)regulation of P53 signalling, (iii) deactivation of c-Myc, and (iv) inhibition of mTOR signalling. Altogether, these four steps result in the induction of BFU-E cell proliferation and terminal differentiation to RBCs.

Although all four pathways seem to be relevant in DBA treatment, to date, only L-leucine modulation of mTOR activity is routinely used as a therapy [84]. Stress erythropoiesis seems to be tightly connected with GCs as stress hormones [19], and there is currently no evidence for other biologically active compounds. Protein p53 [99] and c-Myc [100] inhibitors are tested in cancer clinical trials, but their efficacy in DBA patients or DBA preclinical models is unknown. Thus, further studies are needed to ascertain the role of the above-mentioned GC-dependent pathways in the regulation and pathology of DBA, with the ultimate goal of developing new, more effective, and less toxic therapies for children suffering from this disease.

Author Contributions: Z.M., A.K.—review preparation, J.B.D.S., M.H.—review outline, revision and proofreading. All authors have read and agreed to the published version of the manuscript.

Funding: Supported by grants from the Czech Ministry of Education, Youth and Sports (8F20005, EATRIS-CZ LM2018133, ACGT-CZ.02.1.01/0.0/0.0/16_026/0008448 and NCLG LM2018132), Technological Agency of the Czech Republic (PerMed TACR TN 01000013) and Palacky University Olomouc (IGA UP LF_2021_019, IGA UP LF_2021_038, and IGA_LF_2021_004).

Conflicts of Interest: The authors declare that there is no conflict of interest.

References

1. Bleiber, R.; Eggert, W.; Reichmann, G.; Muhlack, D.; Andres, J. An early childhood erythrocyte phospholipid distribution as further indication of persistence of neonatal erythrocyte characteristics in Diamond-Blackfan anemia. *Folia Haematol.* **1983**, *110*, 71–80.
2. Vlachos, A.; Muir, E. How I treat Diamond-Blackfan anemia. *Blood* **2010**, *116*, 3715–3723. [CrossRef] [PubMed]
3. Vlachos, A.; Ball, S.; Dahl, N.; Alter, B.P.; Sheth, S.; Ramenghi, U.; Meerpohl, J.; Karlsson, S.; Liu, J.M.; Leblanc, T.; et al. Diagnosing and treating Diamond Blackfan anaemia: Results of an international clinical consensus conference. *Br. J. Haematol.* **2008**, *142*, 859–876. [CrossRef] [PubMed]
4. Draptchinskaia, N.; Gustavsson, P.; Andersson, B.; Pettersson, M.; Willig, T.N.; Dianzani, I.; Ball, S.; Tchernia, G.; Klar, J.; Matsson, H.; et al. The gene encoding ribosomal protein S19 is mutated in Diamond-Blackfan anaemia. *Nat. Genet.* **1999**, *21*, 169–175. [CrossRef] [PubMed]
5. Pospisilova, D.; Cmejlova, J.; Ludikova, B.; Stary, J.; Cerna, Z.; Hak, J.; Timr, P.; Petrtylova, K.; Blatny, J.; Vokurka, S.; et al. The Czech National Diamond-Blackfan Anemia Registry: Clinical data and ribosomal protein mutations update. *Blood Cells Mol. Dis.* **2012**, *48*, 209–218. [CrossRef] [PubMed]
6. Danilova, N.; Gazda, H.T. Ribosomopathies: How a common root can cause a tree of pathologies. *Dis. Model. Mech.* **2015**, *8*, 1013–1026. [CrossRef] [PubMed]
7. Klar, J.; Khalfallah, A.; Arzoo, P.S.; Gazda, H.T.; Dahl, N. Recurrent GATA1 mutations in Diamond-Blackfan anaemia. *Br. J. Haematol.* **2014**, *166*, 949–951. [CrossRef] [PubMed]

8. Ulirsch, J.C.; Verboon, J.M.; Kazerounian, S.; Guo, M.H.; Yuan, D.; Ludwig, L.S.; Handsaker, R.E.; Abdulhay, N.J.; Fiorini, C.; Genovese, G.; et al. The Genetic Landscape of Diamond-Blackfan Anemia. *Am. J. Hum. Genet.* **2018**, *103*, 930–947. [CrossRef]
9. Gripp, K.W.; Curry, C.; Olney, A.H.; Sandoval, C.; Fisher, J.; Chong, J.X.; Pilchman, L.; Sahraoui, R.; Stabley, D.L.; Sol-Church, K. Diamond-Blackfan anemia with mandibulofacial dystostosis is heterogeneous, including the novel DBA genes TSR2 and RPS28. *Am. J. Med. Genet. Part A* **2014**, *164*, 2240–2249. [CrossRef]
10. Cmejlova, J.; Dolezalova, L.; Pospisilova, D.; Petrtylova, K.; Petrak, J.; Cmejla, R. Translational efficiency in patients with Diamond-Blackfan anemia. *Haematologica* **2006**, *91*, 1456–1464.
11. Gazda, H.T.; Kho, A.T.; Sanoudou, D.; Zaucha, J.M.; Kohane, I.S.; Sieff, C.A.; Beggs, A.H. Defective ribosomal protein gene expression alters transcription, translation, apoptosis, and oncogenic pathways in Diamond-Blackfan anemia. *Stem Cells* **2006**, *24*, 2034–2044. [CrossRef]
12. Aspesi, A.; Monteleone, V.; Betti, M.; Actis, C.; Morleo, G.; Sculco, M.; Guarrera, S. Author Correction: Lymphoblastoid cell lines from Diamond Blackfan anaemia patients exhibit a full ribosomal stress phenotype that is rescued by gene therapy. *Sci. Rep.* **2018**, *8*, 17227. [CrossRef] [PubMed]
13. Heijnen, H.F.; van Wijk, R.; Pereboom, T.C.; Goos, Y.J.; Seinen, C.W.; van Oirschot, B.A.; van Dooren, R.; Gastou, M.; Giles, R.H.; van Solinge, W.; et al. Ribosomal protein mutations induce autophagy through S6 kinase inhibition of the insulin pathway. *PLoS Genet.* **2014**, *10*, e1004371. [CrossRef]
14. Morgado-Palacin, L.; Varetti, G.; Llanos, S.; Gómez-López, G.; Martinez, D.; Serrano, M. Partial Loss of Rpl11 in Adult Mice Recapitulates Diamond-Blackfan Anemia and Promotes Lymphomagenesis. *Cell Rep.* **2015**, *13*, 712–722. [CrossRef] [PubMed]
15. Bartels, M.; Bierings, M. How I manage children with Diamond-Blackfan anaemia. *Br. J. Haematol.* **2019**, *184*, 123–133. [CrossRef]
16. Harrison, C. First gene therapy for β-thalassemia approved. *Nat. Biotechnol.* **2019**, *37*, 1102–1103. [CrossRef]
17. Liu, Y.; Dahl, M.; Debnath, S.; Rothe, M.; Smith, E.M.; Grahn, T.H.M.; Warsi, S.; Chen, J.; Flygare, J.; Schambach, A.; et al. Successful gene therapy of Diamond-Blackfan anemia in a mouse model and human CD34+ cord blood hematopoietic stem cells using a clinically applicable lentiviral vector. *Haematologica* **2021**. [CrossRef] [PubMed]
18. Barczyk, K.; Ehrchen, J.; Tenbrock, K.; Ahlmann, M.; Kneidl, J.; Viemann, D.; Roth, J. Glucocorticoids promote survival of anti-inflammatory macrophages via stimulation of adenosine receptor A3. *Blood* **2010**, *116*, 446–455. [CrossRef]
19. Bauer, A.; Tronche, F.; Wessely, O.; Kellendonk, C.; Reichardt, H.M.; Steinlein, P.; Schütz, G.; Beug, H. The glucocorticoid receptor is required for stress erythropoiesis. *Genes Dev.* **1999**, *13*, 2996–3002. [CrossRef]
20. Narla, A.; Vlachos, A.; Nathan, D.G. Diamond Blackfan anemia treatment: Past, present, and future. *Semin. Hematol.* **2011**, *48*, 117–123. [CrossRef]
21. Sakamoto, K.M.; Narla, A. Perspective on Diamond-Blackfan anemia: Lessons from a rare congenital bone marrow failure syndrome. *Leukemia* **2018**, *32*, 249–251. [CrossRef] [PubMed]
22. Ramamoorthy, S.; Cidlowski, J.A. Corticosteroids: Mechanisms of Action in Health and Disease. *Rheum. Dis. Clin. N. Am.* **2016**, *42*, 15–31. [CrossRef] [PubMed]
23. Lossignol, D. A little help from steroids in oncology. *J. Transl. Intern. Med.* **2016**, *4*, 52–54. [CrossRef]
24. Schäcke, H.; Döcke, W.D.; Asadullah, K. Mechanisms involved in the side effects of glucocorticoids. *Pharmacol. Ther.* **2002**, *96*, 23–43. [CrossRef]
25. Aljebab, F.; Choonara, I.; Conroy, S. Systematic Review of the Toxicity of Long-Course Oral Corticosteroids in Children. *PLoS ONE* **2017**, *12*, e0170259. [CrossRef]
26. Grad, I.; Picard, D. The glucocorticoid responses are shaped by molecular chaperones. *Mol. Cell. Endocrinol.* **2007**, *275*, 2–12. [CrossRef]
27. Lamberts, S.W.; Huizenga, A.T.; de Lange, P.; de Jong, F.H.; Koper, J.W. Clinical aspects of glucocorticoid sensitivity. *Steroids* **1996**, *61*, 157–160. [CrossRef]
28. John, S.; Sabo, P.J.; Thurman, R.E.; Sung, M.H.; Biddie, S.C.; Johnson, T.A.; Hager, G.L.; Stamatoyannopoulos, J.A. Chromatin accessibility pre-determines glucocorticoid receptor binding patterns. *Nat. Genet.* **2011**, *43*, 264–268. [CrossRef]
29. Samarasinghe, R.A.; Witchell, S.F.; DeFranco, D.B. Cooperativity and complementarity: Synergies in non-classical and classical glucocorticoid signaling. *Cell Cycle* **2012**, *11*, 2819–2827. [CrossRef] [PubMed]
30. Chang, T.J.; Scher, B.M.; Waxman, S.; Scher, W. Inhibition of mouse GATA-1 function by the glucocorticoid receptor: Possible mechanism of steroid inhibition of erythroleukemia cell differentiation. *Mol. Endocrinol.* **1993**, *7*, 528–542. [CrossRef] [PubMed]
31. Lu, N.Z.; Cidlowski, J.A. The origin and functions of multiple human glucocorticoid receptor isoforms. *Ann. N. Y. Acad. Sci.* **2004**, *1024*, 102–123. [CrossRef]
32. Koper, J.W.; van Rossum, E.F.; van den Akker, E.L. Glucocorticoid receptor polymorphisms and haplotypes and their expression in health and disease. *Steroids* **2014**, *92*, 62–73. [CrossRef] [PubMed]
33. Jewell, C.M.; Cidlowski, J.A. Molecular evidence for a link between the N363S glucocorticoid receptor polymorphism and altered gene expression. *J. Clin. Endocrinol. Metab.* **2007**, *92*, 3268–3277. [CrossRef] [PubMed]
34. van Rossum, E.F.; Lamberts, S.W. Polymorphisms in the glucocorticoid receptor gene and their associations with metabolic parameters and body composition. *Recent Prog. Horm. Res.* **2004**, *59*, 333–357. [CrossRef]
35. Lonetti, A.; Indio, V.; Dianzani, I.; Ramenghi, U.; Da Costa, L.; Pospíšilová, D.; Migliaccio, A.R. The Glucocorticoid Receptor Polymorphism Landscape in Patients With Diamond Blackfan Anemia Reveals an Association Between Two Clinically Relevant Single Nucleotide Polymorphisms and Time to Diagnosis. *Front. Physiol.* **2021**, *12*, 745032. [CrossRef]

36. Horos, R.; Ijspeert, H.; Pospisilova, D.; Sendtner, R.; Andrieu-Soler, C.; Taskesen, E.; Nieradka, A.; Cmejla, R.; Sendtner, M.; Touw, I.P.; et al. Ribosomal deficiencies in Diamond-Blackfan anemia impair translation of transcripts essential for differentiation of murine and human erythroblasts. *Blood* **2012**, *119*, 262–272. [CrossRef]
37. Boultwood, J.; Pellagatti, A. Reduced translation of GATA1 in Diamond-Blackfan anemia. *Nat. Med.* **2014**, *20*, 703–704. [CrossRef]
38. Gutiérrez, L.; Caballero, N.; Fernández-Calleja, L.; Karkoulia, E.; Strouboulis, J. Regulation of GATA1 levels in erythropoiesis. *IUBMB Life* **2020**, *72*, 89–105. [CrossRef]
39. Akiyama, M.; Yanagisawa, T.; Yuza, Y.; Yokoi, K.; Ariga, M.; Fujisawa, K.; Hoshi, Y.; Eto, Y. Successful treatment of Diamond-Blackfan anemia with metoclopramide. *Am. J. Hematol.* **2005**, *78*, 295–298. [CrossRef] [PubMed]
40. Ribeil, J.A.; Zermati, Y.; Vandekerckhove, J.; Cathelin, S.; Kersual, J.; Dussiot, M.; Coulon, S.; Moura, I.C.; Zeuner, A.; Kirkegaard-Sørensen, T.; et al. Hsp70 regulates erythropoiesis by preventing caspase-3-mediated cleavage of GATA-1. *Nature* **2007**, *445*, 102–105. [CrossRef]
41. Sankaran, V.G.; Ghazvinian, R.; Do, R.; Thiru, P.; Vergilio, J.A.; Beggs, A.H.; Sieff, C.A.; Orkin, S.H.; Nathan, D.G.; Lander, E.S.; et al. Exome sequencing identifies GATA1 mutations resulting in Diamond-Blackfan anemia. *J. Clin. Investig.* **2012**, *122*, 2439–2443. [CrossRef]
42. Zhou, X.; Medina, S.; Bolt, A.M.; Zhang, H.; Wan, G.; Xu, H.; Lauer, F.T.; Wang, S.C.; Burchiel, S.W.; Liu, K.J. Inhibition of red blood cell development by arsenic-induced disruption of GATA-1. *Sci. Rep.* **2020**, *10*, 19055. [CrossRef] [PubMed]
43. Iskander, D.; Wang, G. Single-cell profiling of human bone marrow progenitors reveals mechanisms of failing erythropoiesis in Diamond-Blackfan anemia. *Sci. Transl. Med.* **2021**, *13*, eabf0113. [CrossRef]
44. Ludwig, L.S.; Gazda, H.T.; Eng, J.C.; Eichhorn, S.W.; Thiru, P.; Ghazvinian, R.; George, T.I.; Gotlib, J.R.; Beggs, A.H.; Sieff, C.A.; et al. Altered translation of GATA1 in Diamond-Blackfan anemia. *Nat. Med.* **2014**, *20*, 748–753. [CrossRef] [PubMed]
45. Long, W.; Wei, L.; Barrett, E.J. Dexamethasone inhibits the stimulation of muscle protein synthesis and PHAS-I and p70 S6-kinase phosphorylation. *Am. J. Physiol. Endocrinol. Metab.* **2001**, *280*, E570–E575. [CrossRef] [PubMed]
46. Yu, J.; Roh, S.; Lee, J.S.; Yang, B.H.; Choi, M.R.; Chai, Y.G.; Kim, S.H. The Effects of Venlafaxine and Dexamethasone on the Expression of HSP70 in Rat C6 Glioma Cells. *Psychiatry Investig.* **2010**, *7*, 43–48. [CrossRef]
47. Paulson, R.F.; Hariharan, S.; Little, J.A. Stress erythropoiesis: Definitions and models for its study. *Exp. Hematol.* **2020**, *89*, 43–54.e42. [CrossRef] [PubMed]
48. Freedman, M.H.; Amato, D.; Saunders, E.F. Haem synthesis in the Diamond-Blackfan syndrome. *Br. J. Haematol.* **1975**, *31*, 515–520. [CrossRef] [PubMed]
49. Malgor, L.A.; Torales, P.R.; Klainer, T.E.; Barrios, L.; Blanc, C.C. Effects of dexamethasone on bone marrow erythropoiesis. *Hormones* **1974**, *5*, 269–277. [CrossRef]
50. Zhao, W.; Kitidis, C.; Fleming, M.D.; Lodish, H.F.; Ghaffari, S. Erythropoietin stimulates phosphorylation and activation of GATA-1 via the PI3-kinase/AKT signaling pathway. *Blood* **2006**, *107*, 907–915. [CrossRef]
51. Sjögren, S.E.; Flygare, J. Progress towards mechanism-based treatment for Diamond-Blackfan anemia. *Sci. World J.* **2012**, *2012*, 184362. [CrossRef] [PubMed]
52. Hattangadi, S.M.; Wong, P.; Zhang, L.; Flygare, J.; Lodish, H.F. From stem cell to red cell: Regulation of erythropoiesis at multiple levels by multiple proteins, RNAs, and chromatin modifications. *Blood* **2011**, *118*, 6258–6268. [CrossRef]
53. Flygare, J.; Rayon Estrada, V.; Shin, C.; Gupta, S.; Lodish, H.F. HIF1alpha synergizes with glucocorticoids to promote BFU-E progenitor self-renewal. *Blood* **2011**, *117*, 3435–3444. [CrossRef]
54. Russo, A.; Russo, G. Ribosomal Proteins Control or Bypass p53 during Nucleolar Stress. *Int. J. Mol. Sci.* **2017**, *18*, 140. [CrossRef]
55. Nicolas, E.; Parisot, P.; Pinto-Monteiro, C.; de Walque, R.; De Vleeschouwer, C.; Lafontaine, D.L. Involvement of human ribosomal proteins in nucleolar structure and p53-dependent nucleolar stress. *Nat. Commun.* **2016**, *7*, 11390. [CrossRef]
56. Le Goff, S.; Boussaid, I.; Floquet, C.; Raimbault, A.; Hatin, I.; Andrieu-Soler, C.; Salma, M.; Leduc, M.; Gautier, E.F.; Guyot, B.; et al. p53 activation during ribosome biogenesis regulates normal erythroid differentiation. *Blood* **2021**, *137*, 89–102. [CrossRef] [PubMed]
57. Danilova, N.; Bibikova, E.; Covey, T.M.; Nathanson, D.; Dimitrova, E.; Konto, Y.; Lindgren, A.; Glader, B.; Radu, C.G.; Sakamoto, K.M.; et al. The role of the DNA damage response in zebrafish and cellular models of Diamond Blackfan anemia. *Dis. Model. Mech.* **2014**, *7*, 895–905. [CrossRef] [PubMed]
58. Li, H.; Qian, W.; Weng, X.; Wu, Z.; Li, H.; Zhuang, Q.; Feng, B.; Bian, Y. Glucocorticoid receptor and sequential P53 activation by dexamethasone mediates apoptosis and cell cycle arrest of osteoblastic MC3T3-E1 cells. *PLoS ONE* **2012**, *7*, e37030. [CrossRef]
59. Sengupta, S.; Vonesch, J.L.; Waltzinger, C.; Zheng, H.; Wasylyk, B. Negative cross-talk between p53 and the glucocorticoid receptor and its role in neuroblastoma cells. *EMBO J.* **2000**, *19*, 6051–6064. [CrossRef]
60. Kapralova, K.; Jahoda, O.; Koralkova, P.; Gursky, J.; Lanikova, L. Oxidative DNA Damage, Inflammatory Signature, and Altered Erythrocytes Properties in Diamond-Blackfan Anemia. *Int. J. Mol. Sci.* **2020**, *21*, 9652. [CrossRef]
61. Rio, S.; Gastou, M.; Karboul, N.; Derman, R.; Suriyun, T.; Manceau, H.; Leblanc, T.; El Benna, J.; Schmitt, C.; Azouzi, S.; et al. Regulation of globin-heme balance in Diamond-Blackfan anemia by HSP70/GATA1. *Blood* **2019**, *133*, 1358–1370. [CrossRef] [PubMed]
62. Sanner, B.M.; Meder, U.; Zidek, W.; Tepel, M. Effects of glucocorticoids on generation of reactive oxygen species in platelets. *Steroids* **2002**, *67*, 715–719. [CrossRef]

63. Gerö, D.; Szabo, C. Glucocorticoids Suppress Mitochondrial Oxidant Production via Upregulation of Uncoupling Protein 2 in Hyperglycemic Endothelial Cells. *PLoS ONE* **2016**, *11*, e0154813. [CrossRef] [PubMed]
64. Dandona, P.; Mohanty, P.; Hamouda, W.; Aljada, A.; Kumbkarni, Y.; Garg, R. Effect of dexamethasone on reactive oxygen species generation by leukocytes and plasma interleukin-10 concentrations: A pharmacodynamic study. *Clin. Pharmacol. Ther.* **1999**, *66*, 58–65. [CrossRef]
65. Chen, L.; Hu, S.L.; Xie, J.; Yan, D.Y.; Weng, S.J.; Tang, J.H.; Wang, B.Z.; Xie, Z.J.; Wu, Z.Y.; Yang, L. Proanthocyanidins-Mediated Nrf2 Activation Ameliorates Glucocorticoid-Induced Oxidative Stress and Mitochondrial Dysfunction in Osteoblasts. *Oxidative Med. Cell. Longev.* **2020**, *2020*, 9102012. [CrossRef] [PubMed]
66. Sjögren, S.E.; Siva, K.; Soneji, S.; George, A.J.; Winkler, M.; Jaako, P.; Wlodarski, M.; Karlsson, S.; Hannan, R.D.; Flygare, J. Glucocorticoids improve erythroid progenitor maintenance and dampen Trp53 response in a mouse model of Diamond-Blackfan anaemia. *Br. J. Haematol.* **2015**, *171*, 517–529. [CrossRef]
67. Naithani, R.; Chandra, J.; Narayan, S.; Singh, V.; Dutta, A.K. Diamond-Blackfan anemia: Clinical features and treatment results in 4 cases. *Hematology* **2006**, *11*, 193–195. [CrossRef]
68. Jayapal, S.R.; Lee, K.L.; Ji, P.; Kaldis, P.; Lim, B.; Lodish, H.F. Down-regulation of Myc is essential for terminal erythroid maturation. *J. Biol. Chem.* **2010**, *285*, 40252–40265. [CrossRef] [PubMed]
69. Sloan, K.E.; Bohnsack, M.T.; Watkins, N.J. The 5S RNP couples p53 homeostasis to ribosome biogenesis and nucleolar stress. *Cell Rep.* **2013**, *5*, 237–247. [CrossRef] [PubMed]
70. Liao, J.M.; Zhou, X.; Gatignol, A.; Lu, H. Ribosomal proteins L5 and L11 co-operatively inactivate c-Myc via RNA-induced silencing complex. *Oncogene* **2014**, *33*, 4916–4923. [CrossRef] [PubMed]
71. Quarello, P.; Garelli, E.; Carando, A.; Brusco, A.; Calabrese, R.; Dufour, C.; Longoni, D.; Misuraca, A.; Vinti, L.; Aspesi, A.; et al. Diamond-Blackfan anemia: Genotype-phenotype correlations in Italian patients with RPL5 and RPL11 mutations. *Haematologica* **2010**, *95*, 206–213. [CrossRef]
72. Oršolić, I.; Bursać, S.; Jurada, D.; Drmić Hofman, I.; Dembić, Z. Cancer-associated mutations in the ribosomal protein L5 gene dysregulate the HDM2/p53-mediated ribosome biogenesis checkpoint. *Oncogene* **2020**, *39*, 3443–3457. [CrossRef]
73. Ajore, R.; Raiser, D.; McConkey, M.; Jöud, M.; Boidol, B.; Mar, B.; Saksena, G.; Weinstock, D.M.; Armstrong, S.; Ellis, S.R.; et al. Deletion of ribosomal protein genes is a common vulnerability in human cancer, especially in concert with TP53 mutations. *EMBO Mol. Med.* **2017**, *9*, 498–507. [CrossRef] [PubMed]
74. Zhou, F.; Medh, R.D.; Thompson, E.B. Glucocorticoid mediated transcriptional repression of c-myc in apoptotic human leukemic CEM cells. *J. Steroid Biochem. Mol. Biol.* **2000**, *73*, 195–202. [CrossRef]
75. Ausserlechner, M.J.; Obexer, P.; Böck, G.; Geley, S.; Kofler, R. Cyclin D3 and c-MYC control glucocorticoid-induced cell cycle arrest but not apoptosis in lymphoblastic leukemia cells. *Cell Death Differ.* **2004**, *11*, 165–174. [CrossRef] [PubMed]
76. Zhang, J.; Wu, K.; Xiao, X.; Liao, J.; Hu, Q.; Chen, H.; Liu, J.; An, X. Autophagy as a regulatory component of erythropoiesis. *Int. J. Mol. Sci.* **2015**, *16*, 4083–4094. [CrossRef]
77. Grosso, R.; Fader, C.M.; Colombo, M.I. Autophagy: A necessary event during erythropoiesis. *Blood Rev.* **2017**, *31*, 300–305. [CrossRef]
78. Kang, Y.A.; Sanalkumar, R.; O'Geen, H.; Linnemann, A.K.; Chang, C.J.; Bouhassira, E.E.; Farnham, P.J.; Keles, S.; Bresnick, E.H. Autophagy driven by a master regulator of hematopoiesis. *Mol. Cell. Biol.* **2012**, *32*, 226–239. [CrossRef]
79. Dunlop, E.A.; Tee, A.R. mTOR and autophagy: A dynamic relationship governed by nutrients and energy. *Semin. Cell Dev. Biol.* **2014**, *36*, 121–129. [CrossRef]
80. Knight, Z.A.; Schmidt, S.F.; Birsoy, K.; Tan, K.; Friedman, J.M. A critical role for mTORC1 in erythropoiesis and anemia. *eLife* **2014**, *3*, e01913. [CrossRef]
81. Yang, Z.; Keel, S.B.; Shimamura, A.; Liu, L.; Gerds, A.T.; Li, H.Y.; Wood, B.L.; Scott, B.L.; Abkowitz, J.L. Delayed globin synthesis leads to excess heme and the macrocytic anemia of Diamond Blackfan anemia and del(5q) myelodysplastic syndrome. *Sci. Transl. Med.* **2016**, *8*, 338ra367. [CrossRef]
82. Liu, Q.; Luo, L.; Ren, C.; Zou, M.; Yang, S.; Cai, B.; Wu, L.; Wang, Y.; Fu, S.; Hua, X.; et al. The opposing roles of the mTOR signaling pathway in different phases of human umbilical cord blood-derived CD34(+) cell erythropoiesis. *Stem Cells* **2020**, *38*, 1492–1505. [CrossRef]
83. Chauvin, C.; Koka, V.; Nouschi, A.; Mieulet, V.; Hoareau-Aveilla, C.; Dreazen, A.; Cagnard, N.; Carpentier, W.; Kiss, T.; Meyuhas, O.; et al. Ribosomal protein S6 kinase activity controls the ribosome biogenesis transcriptional program. *Oncogene* **2014**, *33*, 474–483. [CrossRef] [PubMed]
84. Pospisilova, D.; Cmejlova, J.; Hak, J.; Adam, T.; Cmejla, R. Successful treatment of a Diamond-Blackfan anemia patient with amino acid leucine. *Haematologica* **2007**, *92*, e66–e67. [CrossRef]
85. Payne, E.M.; Virgilio, M.; Narla, A.; Sun, H.; Levine, M.; Paw, B.H.; Berliner, N.; Look, A.T.; Ebert, B.L.; Khanna-Gupta, A. L-Leucine improves the anemia and developmental defects associated with Diamond-Blackfan anemia and del(5q) MDS by activating the mTOR pathway. *Blood* **2012**, *120*, 2214–2224. [CrossRef]
86. Doulatov, S.; Vo, L.T.; Macari, E.R.; Wahlster, L.; Kinney, M.A.; Taylor, A.M.; Barragan, J.; Gupta, M.; McGrath, K.; Lee, H.Y.; et al. Drug discovery for Diamond-Blackfan anemia using reprogrammed hematopoietic progenitors. *Sci. Transl. Med.* **2017**, *9*. [CrossRef] [PubMed]

87. Brumwell, A.; Fell, L.; Obress, L.; Uniacke, J. Hypoxia influences polysome distribution of human ribosomal protein S12 and alternative splicing of ribosomal protein mRNAs. *Rna* **2020**, *26*, 361–371. [CrossRef] [PubMed]
88. Sarkar, S. Regulation of autophagy by mTOR-dependent and mTOR-independent pathways: Autophagy dysfunction in neurodegenerative diseases and therapeutic application of autophagy enhancers. *Biochem. Soc. Trans.* **2013**, *41*, 1103–1130. [CrossRef]
89. Malik, N.; Dunn, K.M.; Cassels, J.; Hay, J.; Estell, C.; Sansom, O.J.; Michie, A.M. mTORC1 activity is essential for erythropoiesis and B cell lineage commitment. *Sci. Rep.* **2019**, *9*, 16917. [CrossRef]
90. Shimizu, N.; Yoshikawa, N.; Ito, N.; Maruyama, T.; Suzuki, Y.; Takeda, S.; Nakae, J.; Tagata, Y.; Nishitani, S.; Takehana, K.; et al. Crosstalk between glucocorticoid receptor and nutritional sensor mTOR in skeletal muscle. *Cell Metab.* **2011**, *13*, 170–182. [CrossRef]
91. Fu, L.; Wu, W.; Sun, X.; Zhang, P. Glucocorticoids Enhanced Osteoclast Autophagy Through the PI3K/Akt/mTOR Signaling Pathway. *Calcif. Tissue Int.* **2020**, *107*, 60–71. [CrossRef]
92. Polman, J.A.; Hunter, R.G.; Speksnijder, N.; van den Oever, J.M.; Korobko, O.B.; McEwen, B.S.; de Kloet, E.R.; Datson, N.A. Glucocorticoids modulate the mTOR pathway in the hippocampus: Differential effects depending on stress history. *Endocrinology* **2012**, *153*, 4317–4327. [CrossRef] [PubMed]
93. Pan, J.M.; Wu, L.G.; Cai, J.W.; Wu, L.T.; Liang, M. Dexamethasone suppresses osteogenesis of osteoblast via the PI3K/Akt signaling pathway in vitro and in vivo. *J. Recept. Signal Transduct.* **2019**, *39*, 80–86. [CrossRef]
94. Kopriva, F.; Dzubak, P.; Potesil, J.; Hajduch, M. The anti-inflammatory effects of inhaled corticosteroids versus anti-leukotrienes on the lymphocyte P-glycoprotein (PGP) expression in asthmatic children. *J. Asthma* **2009**, *46*, 366–370. [CrossRef] [PubMed]
95. Spenerova, M.; Dzubak, P.; Srovnal, J.; Radova, L.; Burianova, R.; Konecny, P.; Salkova, S.; Novak, Z.; Pospisilova, D.; Stary, J.; et al. Combination of prednisolone and low dosed dexamethasone exhibits greater in vitro antileukemic activity than equiactive dose of prednisolone and overcomes prednisolone drug resistance in acute childhood lymphoblastic leukemia. *Biomed. Pap. Med. Fac. Univ. Palacky Olomouc. Czech Repub.* **2014**, *158*, 422–427. [CrossRef]
96. Ashley, R.J.; Yan, H.; Wang, N.; Hale, J.; Dulmovits, B.M.; Papoin, J.; Olive, M.E.; Udeshi, N.D.; Carr, S.A.; Vlachos, A.; et al. Steroid resistance in Diamond Blackfan anemia associates with p57Kip2 dysregulation in erythroid progenitors. *J. Clin. Investig.* **2020**, *130*, 2097–2110. [CrossRef] [PubMed]
97. Adcock, I.M.; Barnes, P.J. Molecular mechanisms of corticosteroid resistance. *Chest* **2008**, *134*, 394–401. [CrossRef] [PubMed]
98. Samuelsson, M.K.; Pazirandeh, A.; Davani, B.; Okret, S. p57Kip2, a glucocorticoid-induced inhibitor of cell cycle progression in HeLa cells. *Mol. Endocrinol.* **1999**, *13*, 1811–1822. [CrossRef] [PubMed]
99. Sanz, G.; Singh, M.; Peuget, S.; Selivanova, G. Inhibition of p53 inhibitors: Progress, challenges and perspectives. *J. Mol. Cell Biol.* **2019**, *11*, 586–599. [CrossRef]
100. Madden, S.K.; de Araujo, A.D. Taking the Myc out of cancer: Toward therapeutic strategies to directly inhibit c-Myc. *Mol. Cancer* **2021**, *20*, 3. [CrossRef]